Some Aspects of Arsenic and Antimony Geochemistry in High Temperature Granitic Melt – Aqueous Fluid System and in Low Temperature Permeable Reactive Barrier – Groundwater System

by

Qiang Guo

A thesis
presented to the University of Waterloo
in fulfilment of the
thesis requirement of the degree of
Doctor of Philosophy
in Earth Sciences

Waterloo, Ontario, Canada, 2008

AUTHOR'S DECLARATION FOR ELECTRONIC SUBMISSION OF A THESIS

I hereby declare that I am the sole author of this thesis. This is a true copy of the thesis, including any required final revisions, as accepted by my examiners. I understand that my thesis may be made electronically available to the public.

Some Aspects of Arsenic and Antimony Geochemistry in High Temperature Granitic Melt – Aqueous Fluid System and in Low Temperature Permeable Reactive Barrier – Groundwater System

Abstract

Arsenic and antimony are important trace elements in magmatic-hydrothermal systems, geothermal systems and epithermal deposits, but their partitioning behavior between melt and aqueous fluid is not well understood. The partitioning of arsenic and antimony between aqueous fluid and granitic melt has been studied in the system SiO_2-Al_2O_3-Na_2O-K_2O-H_2O at 800 °C and 200 MPa. The partition coefficients (± 1σ) of As and Sb between aqueous fluid and melt, are 1.4 ± 0.5 and 0.8 ± 0.5, respectively. The partitioning of As is not affected by aluminum saturation index (ASI) or SiO_2 content of the melt, or by oxygen fugacity under oxidized conditions (f_{O_2} > the nickel-nickel oxide buffer, NNO). The partitioning of Sb is independent of f_{O_2} and SiO_2 content of the melt. However, aluminum saturation index (ASI) does affect Sb partitioning and Sb partition coefficient ($D_{Sb}^{f/m}$) for peralkaline melt (0.1 ± 0.01) is much smaller than that for metaluminous melts (0.8 ± 0.4) and peraluminous melts (1.3 ± 0.7). Thermodynamic calculations show that As(III) is dominant in aqueous fluid at 800 °C and 200 MPa and XPS analysis of run product glass indicate that only As(III) exists in melt, which confirms the finding that f_{O_2} does not affect As partitioning between fluid and melt. XPS analysis of run product glass show that Sb(V) is dominant in melt at oxidized

conditions ($\log f_{O_2}$ > -10). The peralkaline effect only exhibits on Sb partitioning, not on As partitioning at oxidized conditions, which is consistent with the x-ray photoelectron spectroscopy (XPS) measurements that As(III) and Sb(V) are dominant oxidation states in melt under oxidized conditions, because the peralkaline effect is stronger for pentavalent than trivalent cations.

Permeable reactive barriers (PRBs) are an alternative technology to treat mine drainage containing sulfate and heavy metals. Two column experiments were conducted to assess the suitability of an organic carbon (OC) based reactive mixture and an Fe^0-bearing organic carbon (FeOC) based reactive mixture, under controlled groundwater flow conditions. The organic carbon (OC) column showed an initial sulfate reduction rate of 0.4 μmol $g(oc)^{-1}$ d^{-1} and exhausted its capacity to promote sulfate reduction after 30 pore volumes (PVs), or 9 months of flow. The Fe^0-bearing organic carbon (FeOC) column sustained a relative constant sulfate reduction rate of 0.9 μmol $g(oc)^{-1}$ d^{-1} for at least 65 PVs (17 months). The microbial enumerations and isotopic measurements indicate that the sulfate reduction was mediated by sulfate reducing bacteria (SRB). The cathodic production of H_2 by anaerobic corrosion of Fe probably is the cause of the difference in sulfate reduction rates between the two reactive mixtures. Zero-valent iron can be used to provide an electron donor in sulfate reducing PRBs and Fe^0-bearing organic carbon reactive mixture has a potential to improve the performance of organic carbon PRBs. The $\delta^{34}S$ values can be used to determine the extent of sulfate reduction, but the fractionation is not consistent between reactive materials. The $\delta^{13}C$ values indicate that methanogenesis is occurring in the front part of both columns.

Arsenic and antimony in groundwater are great threats to human health. The PRB technology potentially is an efficient and cost-effective approach to remediate organic and inorganic contamination in groundwater. Two column experiments were conducted to assess the rates and capacities of organic carbon (OC) PRB and Fe-bearing organic carbon (FeOC) PRB to remove As and Sb under controlled groundwater flow conditions. The average As removal rate for the OC column was 13 nmole day^{-1} g^{-1} (dry weight of organic carbon) and its removal capacity was 11 μmole g^{-1} (dry weight of organic carbon). The remove rate of the FeOC material was 165 nmole day^{-1} g^{-1} (dry weight of organic carbon) and its minimum removal capacity was 105 μmole g^{-1} (dry weight of organic carbon). Antimony removal rate of the OC material decreases from 8.2 to 1.4 nmole day^{-1} g^{-1} (dry weight of organic carbon) and its removal capacity is 2.4 μmole g^{-1} (dry weight of organic carbon). The minimum removal rate of FeOC material is 13 nmole day^{-1} g^{-1} (dry weight of organic carbon) and its minimum removal capacity is 8.4 μmole g^{-1} (dry weight of organic carbon). The As(III) : [As(III)+As(V)] ratio increased from 1% in the influent to 50% at 5.5 cm from the influent end, and to 80% at 15.5 cm from the influent end of the OC column. X-ray absorption near edge spectroscopy (XANES) shows As(III)-sulfide species on solid samples. These results suggest that As(V) is reduced to As(III) both in pore water and precipitate as As sulfides or coprecipitate with iron sulfides. The arsenic reduction rate suggests that As(V) reduction is mediated by bacterial activity in the OC column and that both abiotic reduction and bacterial reduction could be important in FeOC.

Acknowledgements

I thank my supervisors David Blowes and Robert Linnen for their patience, support and advice through the last seven years. I also thank my committee members, Mario Coniglio, Eric Reardon, Tom Edwards, Linda Nazar, and Dogan Paktunc for spending time on my behalf, and providing valuable insight that has aided the completion of my thesis.

I have spent most time with fellow graduate students. I thank Fred Blain, Laura Groza, Jeff Bain, Matt Lindsay, Blair Gibson, Mandy Moore for their friendship and helpful comments.

There are many people at Waterloo that provided valuable advice or assistance to various aspects of my research. They include William Mark, Ming Zhang, Chris Hanton-Fong and Ralph Dickhout. I also thank Menghua Liu in University of Western Ontario for his help in the electronic microprobe analysis, Mark Biesinger in University of Western Ontario for his assistance in x-ray photoelectron spectroscopy analysis, and Paul Northrup in Brookhaven National Laboratory, Upton, New York, for his help in x-ray adsorption near edge spectroscopy analysis.

Dedication

This thesis is dedicated to my friends in Waterloo, Mei, Ann, Michael, and Gary, and my girlfriend Xu Jia, my sister Guo Yongmei, and my father Guo Tianjin in China. To Mei, Ann, Michael and Gary, because they open their warm homes to me during my difficult times of this long journey; to Xu Jia, because she makes it very easy for me to talk to her; and to my sister and father, because they are always the home in my heart.

TABLE OF CONTENTS

Chapter 1 Introduction

1.1 Background 1

1.2 As Geochemistry 3

1.3 Sb Geochemistry 7

1.4 Objectives 9

1.4.1 As/Sb Partitioning Experiments 9

1.4.2 As/Sb Remediation Experiments 11

1.5 Thesis Organization 12

1.5.1 Thesis Layout 11

1.5.2 Thesis Contents 12

1.6 References 14

Chapter 2 Arsenic and Antimony Partitioning between Aqueous Fluid and Granitic Melt at 800 °C and 2 MPa

2.1 Abstract 21

2.2 Introduction 23

2.3 Experimental Methods 25
2.3.1 Starting Material 25
2.3.2 Experimental Design 27
2.3.3 Analytical Methods 28

2.4 Results 31
2.4.1 Run Products of As Experiments 31
2.4.2 Attainment of Equilibrium 33
2.4.3 Arsenic Partitioning between Melt and Fluid 34
2.4.3.1 Henry's Law 34
2.4.3.2 Effect of ASI of Melt 35
2.4.3.3 Effect of SiO2 Content of Melt 36
2.4.3.4 Effect of Oxygen Fugacity 36
2.4.4 Run Products of Sb Experiments 37
2.4.5 Antimony Partitioning between Melt and Fluid 39
2.4.5.1 Effect of Oxygen Fugacity 39
2.4.5.2 Effect of SiO2 Content of Melt 40
2.4.5.3 Effect of ASI of Melt 40
2.4.6 As and Sb XPS Spectra 41

2.5 Discussions 42
2.5.1 Partitioning Behaviours of As, Sb and P, W, Mo 42
2.5.2 Paralkaline Effect and Partitioning of As and Sb 44
2.5.3 Speciation of As and Sb in Aqueous Fluid and Melt 45

2.6 Application 48

2.7 Acknowledgement 50

2.8 References 50

Chapter 3 Biogeochemistry of Two Types of Permeable Reactive Barriers, Organic Carbon and Iron-Bearing Organic Carbon: Column Experiments

3.1 Abstract 74

3.2 Introduction 76

3.3 Experimental and Analytical Methods 77
3.3.1 Column Design and Experimental Setup 77
3.3.2 Geochemical Analysis 79
3.3.3 Solid Phase Analysis 80
3.3.4 Microbiological Analysis 80
3.3.5 Geochemical Modeling 81

3.4 Results and Discussion 81
3.4.1 Sulfate Reduction and ^{34}S 81
3.4.2 SRB and H_2 84
3.4.3 Methanogenesis and ^{13}C 87
3.4.4 Sulfur Speciation on Solid Surface 89
3.4.5 pH, Eh, Alkalinity, Ca, and Fe 90
3.4.6 Geochemical Modeling 91

3.6 Implications 92

3.7 Conclusions 93

3.8 Acknowledgement 94

3.9 References 94

Chapter 4 Remediation of Arsenic and Antimony Using Two Types of Permeable Reactive Barriers, Organic Carbon and Iron-Bearing Organic Carbon: Column Experiments

4.1 Abstract 116

4.2 Introduction 118

4.3 Experimental and Analytical Methods 120

4.3.1 Column Design and Experimental Setup 120

4.3.2 Geochemical Analysis 120

4.3.3 Solid Phase Analysis 121

4.3.4 Geochemical Modeling 121

4.4 Results and Discussion 122

4.4.1 Arsenic and Antimony Removal 122

4.4.2 Arsenic Speciation 124

4.4.3 Arsenic Removal Mechanisms 126

4.5 Conclusions 128

4.6 Acknowledgement 128

4.7 References 129

Chapter 5 Conclusions

5.1 Conclusions of the three studies 140

5.2 Relationships between the three studies 142

5.3 Recommendation for future research 143

5.4 References 146

List of Appendices

Appendix I Water Chemistry Data 147

Appendix II Isotope, Microbiology, and Saturation Index Data 153

Appendix III Column Flow Data 162

Appendix IV Electron Microprobe Analysis (EMPA) Data 167

List of Tables

Chapter 1

Table 1.1 Physical properties of arsenic and antimony. 19

Table 1.2 Common chemical forms of arsenic and antimony 19

Table 1.3 Major As minerals (Smedley and Kinniburgh, 2002) 20

Table 1.4 Major Sb minerals (Boyle and Jonasson, 1984) 20

Chapter 2

Table 2.1 Normalized compositions of starting synthetic glasses 57

Table 2.2 EPMA analysis of major elements and As in run product glasses 58

Table 2.3 Partition coefficient of As between co-existing aqueous fluid and melt at 800°C and 200 MPa. 59

Table 2.4 Arsenic partition coefficient, ASI and SiO2 of melt, oxygen fugacity, and As in the system. 60

Table 2.5 Arsenic mass and concentration of reduced experiments 60

Table 2.6 EPMA analysis of major elements and Sb in run product glasses 61

Table 2.7 Partition coefficient of Sb between co-existing aqueous fluid and melt at 800°C and 200 MPa. 62

Table 2.8 Antimony partition coefficient, ASI and SiO2 of melt, and oxygen fugacity. 63

Table 2.9 Binding energies, peak full width at half maximum (FWHM), and peak areas for As(3d) XPS spectra 64

Table 2.10 Binding energies and peak full width at half maximum (FWHM) for Sb(3d3/2) XPS spectra 64

Chapter 3

Table 3.1 Composition of Reactive Mixture in Columns 100

Table 3.2 Chemical Composition of Simulated Groundwater (10-3 mol/L) 101

Table 3.3 Sulfur isotopic fractionation of reactive materials. 101

Table 3.4 Carbon isotopic composition of FeOC influent and Port 2 water 102

Table 3.5 Binding energies for S(2p) in various references. 103

Table 3.6 Binding energies, peak full width at half maximum (FWHM), and peak areas for S(2p) XPS spectra. 104

Chapter 4

Table 4.1 Aqueous As speciation of OC column 134

LIST OF ILLUSTRATIONS

Chapter 2

Figure 2.1 Arsenic concentration in system has no effect on As partitioning between granitic melt and fluid at 800 °C and 200 MPa, with $\log f_{O_2}$ ranging from -8.4 to -12.2. The triangles are forward experiments and the squares are reverse experiments. The average value (± 1σ) of As partition coefficients is 1.4 ± 0.5, shown as the dashed line. 65

Figure 2.2 ASI of the melt has no effect on As partitioning between granitic melt and fluid at 800 °C and 200 MPa, with SiO_2 content ranging from 72.24 to 72.96 wt% and $\log f_{O_2}$ from -10.3 to -9.0. The average value (± 1σ) of As partition coefficients is 1.6 ± 0.4, shown as the dashed line. 66

Figure 2.3 SiO_2 content of the melt has no effect on As partitioning between melt and fluid at 800 °C and 200 MPa, with $\log f_{O_2}$ ranging from -9.2 to -8.4. The average value (± 1σ) of As partition coefficients is 1.7 ± 0.6, shown as the dashed line. 67

Figure 2.4 Oxygen fugacity (f_{O_2}) has no effect on As partitioning between granitic melt and fluid at 800 °C and 200 MPa. The triangles are forward experiments and the squares are reverse experiments. The average value (± 1σ) of As partition coefficients is 1.1 ± 0.3, shown as the dashed line. 68

Figure 2.5 Oxygen fugacity (f_{O_2}) has no effect on Sb partitioning between granitic melt and fluid at 800 °C and 200 MPa, with ASI ranging from 0.99 to 1.04. The triangles are forward experiments and the square is a reverse experiment. The average value (± 1σ) of Sb partition coefficients is 0.8 ± 0.5, shown as the dashed line. 69

Figure 2.6 SiO_2 content of the melt has no effect on Sb partitioning between melt and fluid at 800 °C and 200 MPa, with ASI ranging from 0.99 to 1.06. The triangles are forward experiments and the square is a reverse experiment. The average value (± 1σ) of Sb partition coefficients is 0.7 ± 0.4, shown as the dashed line. 70

Figure 2.7 The data show a clear trend that Sb partition coefficient increases with increasing ASI of melt at 800 °C and 200 MPa, with SiO_2 content ranging from 70.84 to 71.80 wt%. All data points are from the forward experiments. 71

Figure 2.8. Figure 2.8. High resolution scan of As(3d) XPS spectra. The thin solid line is the fit curve which only has As(III) components. The spectra show that As(III) is the only species in the two run product glasses. The As $3d_{5/2}$ spectra of As(V) oxide species is at 45.3 eV (Nesbitt et al., 1995). (a) As-2; (b) As-6. Fit curves include As $3d_{5/2}$ (solid line) and As $3d_{3/2}$ (dotted line). 72

Figure 2.9. High resolution scan of Sb($3d_{3/2}$) XPS spectra. The thin solid line is the fit curve. The spectra show that Sb(V) is the only species in the glass sample of (a) Sb-10 and the dominant species in that of (b) Sb-1. 73

Chapter 3

Figure 3.1 Temporal changes in sulfate and sulfide of the OC and FeOC columns. Port 2 is at 5 cm from the bottom of column. The FeOC column removed more sulfate than the OC column. 105

Figure 3.2 3.2 Profiles of sulfate, sulfide, $\delta^{34}S$, and $\delta^{18}O$. The FeOC column removed more sulfate than the OC column through out the column. $\delta^{34}S$ values in the FeOC column increased from bottom to top, but those in the OC column were constant. 106

Figure 3.3 $(\delta^{34}S+10^3)/(\delta^{34}S_0+10^3)$ vs. fraction of remaining SO_4. $\delta^{34}S_0$ and $\delta^{34}S$ are the $\delta^{34}S$ values of the aqueous sulfate of the influent and the samples at different sampling ports, respectively. Best-fit curves are used to calculate instantaneous fractionation factor α (listed in Table 3). 107

Figure 3.4 Profiles of SRB, IRB, APB, and FDA. SRB population of the FeOC column is greater than that of the OC column. IRB population and FDA concentration of the OC column are slightly larger than those of the FeOC column. APB populations in both columns are much smaller than SRB and IRB populations. 108

Figure 3.5 Profiles of $\delta^{13}C$ and alkalinity. From influent to Port 2 (5.5 cm), $\delta^{13}C$ values increases dramatically from -33.2‰ to -7.1‰ in the FeOC column and mildly from -33.2‰ to -22.3‰ in the OC column and continue to increase until Port 6 (15 cm), and DIC decreases in the FeOC column and increases in the OC column. 109

Figure 3.6 Sulfur K-edge XANES spectra. Orpiment, troilite, pyrite, gypsum are reference material. Orpiment and gypsum were analyzed under the same conditions as with the three samples. The spectra of troilite and pyrite are the approximation using the data (corrected

to the peak of element sulfur set to 2472.0) from Vairamurthy (1998). Sample FeOC Port 1 has sulfur species similar to orpiment. Samples FeOC Port 2 and OC Port2 have sulfur species close to troilite and pyrite. 110

Figure 3.7 High resolution scan of S(2p) XPS spectra. (a) OC column Port 2; (b) FeOC column Port 2. Fit curves include 2p3/2 (solid line) and 2p1/2 (dashed line) components. 111

Figure 3.8 Profiles of Fe, Ca, Eh, and pH. Fe concentrations in the OC column were greater than the FeOC column. Ca concentrations decreased in the first 15 cm of the FeOC column, but increased mildly in the same section of the OC column. From 10 cm to the top, pH in the FeOC column is greater than that in the OC column. 112

Figure 3.9 Temporal changes of Eh and pH. pH values of the OC column is smaller than those of the FeOC column, which is caused by anaerobic corrosion of Fe. Eh values decrease from 400 mV in the influent to <200 mV in both columns, which reflects the change from aerobic to anaerobic environments. 113

Figure 3.10 Temporal changes of Fe, Ca, and alkalinity. From the influent to Port 2, the alkalinity and Ca concentrations decrease in the FeOC column. In the OC column, alkalinity increases from the influent to Port 2 and Ca concentrations does not change much after 15 PVs. Fe concentrations are low in both columns. 114

Figure 3.11 Saturation indices (SI) for selected mineral phases for effluent samples from OC and FeOC columns. Both columns are oversaturated with respect to FeS, but undersaturated with respect to gypsum. The SI values for siderite indicate supersaturation in the OC column and in the FeOC column at early time (<17 PVs). 115

Chapter 4

Figure 4.1 Temporal changes in As and Sb of OC and FeOC columns. Arsenic was removed fast and completely in the FeOC column, but only half of As was removed in the OC column after 35 PVs. Antimony was removed in both columns, but the FeOC was more efficient: all Sb was removed before Port 2. 135

Figure 4.2 Profiles of Sb and As of OC and FeOC columns during PV 25-29. Both As and Sb were removed within first 5.5 cm in the FeOC column. In the OC column, only half of As was removed and Sb was detected after 15 to 20 cm. 136

Figure 4.3 Profiles of arsenic aqueous speciation and Eh of OC column. As Eh values dropped from 400 to 0 to 100 mv, As(III) ratio increased from 0 to 80%. 137

Figure 4.4 Arsenic XANES spectra. (a) Spectra of samples and reference materials and the spectra of $NaAsO_2$ is an approximation of the $NaAsO_2$ spectra in Figure 1 of Takahashi et al.(2003). (b) Interpretation of the spectra of FeOC Port 2. Only As(V) species was found in the sample of OC Port 2 and FeOC Port 1, which probably was caused by the As(III) oxidation by x-ray during analysis. As(III) sulfide is the dominant species in the sample of FeOC Port 2. 138

Figure 4.5 Saturation indices (SI) of selected sulfide minerals for the samples of the OC column at PV 25-29. SI values of stibnite were close to 0, indicating that Sb concentrations in pore water were controlled by stibnite. SI values of orpiment were much larger than 0, suggesting that As concentrations in pore water were not controlled by orpiment. 139

Chapter 1

Introduction

1.1 Background

Arsenic and antimony are ubiquitous elements in the Earth's crust, mainly found in sulfide-bearing ore bodies, coal, oil shales and sediments. Arsenic and antimony are important trace elements in magmatic-hydrothermal systems, geothermal systems and their fossil analogs, epithermal deposits. The As concentrations in aqueous vapor and brine inclusions from magmatic-hydrothermal ore deposits, can be hundreds and a few thousands of ppm respectively, and Sb can be tens and a few hundreds of ppm, respectively (Heinrich et al., 1999; Audetat et al., 2000; Muller et al., 2001; Audetat and Pettke, 2003; Beuchat et al., 2004). The highest reported As concentrations in fluid inclusions are 1024 to 7690 ppm in quartz-hosted fluid inclusions of the vein and carbonate replacement Zn-Pb-Cu-Ag deposits in San Cristobal vein Peru (Beuchat et al., 2004).

Arsenic and antimony can be released into groundwater through natural processes such as weathering reactions, biological activity and volcanic emissions, as well as through anthropogenic activities such as mining, combustion of fossil fuels, and the use of arsenical pesticides and wood preservatives, antimonial flame retardants, Pb-Sb alloy in batteries (Smedley and Kinniburgh, 2002; Filella, et al., 2002). In the environment, especially in drinking water, As is a great threat to human health. Arsenic is a teratogen and a carcinogen. It is also chronically toxic at relatively low concentrations (< 100 ppb) (Manning et al. 2002). The WHO guideline value for As in drinking water was

provisionally reduced in 1993 from 50 to 10 μg l^{-1} (WHO, 1993). The US EPA drinking water limit for As was lowered from 50 μg l^{-1} to 10 μg l^{-1} in 2001. The Canadian provisional drinking water limit is 25 ppb. Antimony and its compounds are considered as pollutants of priority interest by EPA (USEPA, 1979) and the European Union (Council of the European Communities, 1976). The EPA drinking water limit for Sb is 6 μg l^{-1} (USEPA, 1999).

Arsenic and antimony are important indicators for the deposits of Cu, Ag, Au, and Zn, and there is a marked coherence between the two elements and gold in practically all types of gold deposits (Boyle and Jonasson, 1973, 1984). They are also the main pollutants during and after the mining of these deposits. Sulfide minerals in mine tailings and waste rocks and geothermal waters are two of the three main sources of As and Sb in the groundwater with high concentrations of the two elements. The other main source is the sedimentary rocks or sediments with high contents of sulfides, mostly pyrite (Smedley and Kinniburgh, 2002; Plant et al., 2003). The knowledge of the partitioning behaviors of As and Sb in high temperature environments will help to understand the concentration and speciation of As and Sb in high temperature hydrothermal and geothermal fluids and to model the ore deposit. It will also help to understand the source and transformations of As and Sb in the groundwater systems.

The geochemistry of As and Sb in the high-temperature hydrothermal systems is also linked with that in the low-temperature groundwater systems by the redox control. In hydrothermal systems, oxygen fugacity could affect As and Sb partitioning if the valence of these two elements in aqueous fluid are different from those in melt. In groundwater

systems, the changes in oxidation states cause As and Sb in sulfides or hydrous iron oxides to release into groundwater, or could cause the dissolved As and Sb to be immobilized in reactive materials. Consequently, a question that needs to be addressed is: does the importance of redox reactions involving As and Sb change with temperature?

1.2 Geochemistry of Arsenic

Arsenic is in group 15 of the periodic table and is usually described as a metalloid (Table 1.1). Arsenic has only one stable isotope, ^{75}As (Table 1.1). In natural environments As mainly exists in –I, -III, 0, III, and V oxidation states (Plant et al., 2003; Table 1.2).

Arsenic is a strongly chalcophile element. There are more than 200 As minerals, including elemental As, arsenides, sulfides, sulfosalts, oxides, arsenates, and arsenites. Major As minerals are given in Table 1.3. Most are sulfide minerals or their alteration products. Arsenopyrite is the most abundant As-bearing mineral but the principal source of As in rocks and ore deposits is arsenian (As-rich) pyrite ($Fe(S,As)_2$) (Boyle and Jonasson, 1973). Arsenic concentrations are very low in major rock-forming silicates, 0.05 – 2.3 mg kg^{-1}., and in carbonates, 1 – 8 mg kg^{-1}. Arsenic concentrations in sulfides range from 5 mg kg^{-1} to ~20 wt% and those in iron oxides can be up to ~3 wt% (Paktunc et al., 2006). In sediment-hosted disseminated gold deposits, arsenopyrite tends to the earliest-formed As-bearing mineral, derived from hydrothermal fluids and typically formed at $T \geq 100°C$ (Arehart et al., 1993). During cooling this is followed by native As in rare locations and thereafter by arsenian pyrite (op. cit.). Realgar and orpiment generally form at the lowest temperatures (op. cit.). This paragenetic sequence can also

be reflected by zonation within sulfide minerals, with arsenopyrite cores zoning out to arsenian pyrite and realgar-orpiment rims and oxides and sulfates are formed at the latest stages of ore mineralization (op. cit.).

The average crustal abundance of arsenic is 1.5 mg kg^{-1} (Plant et al., 2003). Most igneous and metamorphic rocks and carbonate rocks have average As concentrations of 1-10 mg kg^{-1} (Smedley and Kinniburgh, 2002). Arsenic concentrations in sedimentary rocks can be more variable (op. cit.). The highest As concentrations (20 – 200 mg kg^{-1}) are typically found in organic-rich and sulfide-rich shales, sedimentary ironstones, phosphatic rocks, and some coals (Boyle and Jonasson, 1973). Alluvial sands, glacial till, and lake sediments typically contain <1 – 15 mg kg^{-1} As (Smedley and Kinniburgh, 2002). Arsenic concentrations in soil are usually similar to those of sediments except where contaminated by industrial or agricultural activity. Concentrations up to 7 wt% have been found in the tailings of a gold mine (Paktunc et al., 2004).

Concentrations of arsenic in river waters are also low (typically in the range 0.1 – 2.0 μg l^{-1}) (Smedley and Kinniburgh, 2002). High As concentrations are found in some rivers dominated by base flow in arid areas, or in rivers affected by industrial or sewage effluents, or in rivers affected by mine wastes and tailings. Arsenic concentrations in lake waters are typically close to or lower than those of river water. Average As concentrations in open seawater are typically ~1.5 μg l^{-1} (op. cit.). Arsenic concentrations in most groundwaters are <10 μg l^{-1}, but naturally high As groundwaters are found in aquifers in some areas of the world and concentrations occasionally reach the mg l^{-1} level

(op. cit.). Industrially contaminated groundwater can also have high As concentrations but the affected areas are usually localized (op. cit.).

Redox potential (Eh) and pH are the most important factors governing inorganic arsenic speciation at surface water and most groundwater conditions. Under oxidizing conditions, $H_3AsO_4^0$ is dominant where pH < 2, and $H_2AsO_4^-$ is dominant where 2 < pH < 6.9, whereas at higher pH $HAsO_4^{2-}$ is dominant. AsO_4^{3-} may be present in extremely alkaline conditions. Under reducing conditions where the pH is less than ~9.2, $H_3AsO_3^0$ predominates. Native As and orpiment are stable under strongly reducing conditions. Organic As species usually are a minor component in natural waters and the most important ones are dimethylarsinate (DMA, $(CH_3)_2AsO(OH)$) and monomethylarsonate ($CH_3AsO(OH)_2$ or $(CH_3)_3As^+ \cdot CH_2COO^-$; Plant et al, 2002). Arsenic redox reactions in some environments are slow, especially the As(III) oxidation, and As(III) to As(V) ratios often reflect thermodynamic disequilibrium (op. cit.). In the natural environment, the rates of both As(III)-oxidation and As(V)-reduction reactions are controlled by micro-organisms and can be orders of magnitude faster than under abiotic conditions (op. cit.).

Analyses of geothermal reservoir samples show that As is transported mainly as As(III) in geothermal reservoirs at temperature of up to 350 °C whereas As(V) is dominant in oxic low temperature drainages and rivers (Nordstrom et al, 2001; Ballantyne and Moore 1998). Thermodynamic modeling by Heinrich and Eadinton (1986) also predicted that As(III) accounts for the transport of As in hydrothermal systems at temperatures up to 400°C. The dominant As species under most hydrothermal conditions is $H_3AsO_3^0$ (Heinrich and Eadington, 1986; Ballantyne and Moore 1998).

Most high-arsenic natural waters are groundwaters from particular settings such as mineralized, mined and geothermal areas, young alluvial deltaic basins, and inland semi-arid basins (Plant et al., 2003). The high As concentrations of waters in mineralized and mined areas are likely to have been derived from the oxidation and dissolution of sulfides (op. cit.). Geothermal inputs also contribute to high As concentrations of groundwaters in geothermal areas of many parts of the world (op. cit.). Adsorption of As by Fe, Mn, and Al oxides and clays is the most important factor controlling the As concentrations in natural waters. Under aerobic and acidic to near-neutral conditions, As is very strongly adsorbed by the oxides as arsenate (op. cit.). Arsenic can be released by desorption and dissolution of the metal oxides due to a change to reducing conditions. The most common case is the rapid accumulation and burial of sediments, such as young alluvial deltaic basins. Arsenic also desorbs from the oxide surfaces where the pH of groundwaters increases, especially above 8.5, in arid and semi-arid areas as a result of extensive mineral weathering with proton uptake (op. cit.).

1.3 Geochemistry of Antimony

Antimony is in group 15 of the periodic table and is usually described as a metalloid (Table 1.1). Antimony has two isotopes, ^{121}Sb and ^{123}Sb (Table 1.1). In natural environments Sb exists mostly in the 0, III, and V oxidation states (Plant et al., 2003; Table 1.2).

Antimony is a chalcophile element and there are more than 100 Sb-bearing minerals, including elemental Sb, sulfides, sulfosalts, oxides, antimonates, and antimonites. The major Sb minerals are given in Table 1.4. Most are sulfide minerals or their alteration products. The principal source of Sb in ore deposits is arsenopyrite and pyrite (Boyle and Jonasson, 1984). Zack et al. (2005) also found that rutile is the dominant carrier of Sb in metamorphic eclogite. Antimony concentrations are very low in major rock forming silicates and carbonate minerals, < 1 mg kg^{-1} and < 2 mg kg^{-1}, respectively. Antimony is enriched in sulfide minerals (up to 1000s mg kg^{-1} in pyrite, arsenopyrite, galena, and sphalerite) and some iron oxide and hydroxide minerals (5 - 2,440 mg kg^{-1} in goethite).

The abundance of antimony in the Earth's crust is 0.3 mg kg^{-1} (Wedepohl, 1995). Among igneous rocks, the intermediate and felsic extrusive rocks are slightly enriched in Sb (3 - 9 mg kg^{-1}) compared to other igneous rocks (0.4 – 1.2 mg kg^{-1}) (Boyle and Jonasson, 1984). Metamorphic rocks contain Sb similar to the rocks from which they are derived (op. cit.). Among sedimentary rocks shales and argillites contain the most antimony (1.1 – 1.7 mg kg^{-1}) and Sb concentrations in sediments and soils are of the order of a few mg kg^{-1} (op. cit.). Higher concentrations are directly related to Sb-bearing ore deposits, smelting plants, sewage, or fertiliser facilities (Fillela, et al., 2000a). Antimony concentrations are also high (500 mg kg^{-1}) in precipitates form hot springs and boreholes (op. cit.).

Antimony concentrations in river and lake waters are low (typically <1.0 μg l^{-1}) (Fillela, et al., 2000a). The Great Lakes contain 0.2 – 0.5 μg l^{-1} Sb. Concentrations of Sb in oceans is about 0.2 μg l^{-1} (op. cit.) Geothermal waters contain higher Sb concentrations (10s –

100s μg l^{-1}) (op. cit.). Groundwaters tend to have higher concentrations of Sb compared with surface water. Groundwater near sulfide deposits contains up to a few mg l^{-1} of Sb (op. cit.).

Redox potential (Eh) and pH are the most important factors governing inorganic antimony speciation at surface water and most groundwater conditions (Fillela, et al., 2000b). Antimony exists as $Sb(OH)_6^-$ in oxic waters and as $Sb(OH)_3^0$ in anoxic waters (op. cit.). Under reducing conditions, and in the presence of sulfur, stibnite (Sb_2S_3) is formed at low to intermediate pH values (op. cit.). At higher pH values, the SbS_2^- species replaces stibnite (op. cit.). Redox equilibrium is often achieved slowly and thermodynamically unstable species can be stabilised by kinetic factors (op. cit.). Antimony(III) species are found in oxic waters and Sb(V) species in anoxic waters (op. cit.).

In natural hydrothermal fluids Sb mainly exists in +III oxidation state and the main Sb(III) species are considered to be hydroxide and sulfide complexes (Spycher and Reed, 1989). At temperatures greater than 250 °C, $Sb(OH)_3^0$ is predominant over a wide range of pH and appears to be mainly responsible for the hydrothermal transport of Sb (Pokrovski et al, 1996; Zotov et al., 1995, 2003).

Antimony behaviour in natural environments is not well understood. The hydrous oxides of Fe, Mn, and Al adsorb Sb and the adsorption capacities decreases along the sequence MnOOH > $Al(OH)_3$ > FeOOH (Thanabalasingam and Pickering, 1990). Antimony(III) is adsorbed by humic acids following Langmuir-type isotherms (Thanabalasingam and Pickering, 1986).

1.4 Objectives

1.4.1 As/Sb Partition Experiments

Arsenic concentrations are generally low in common silicate minerals (< 2 ppm) and igneous rocks (1 to 6 ppm) (Smedley and Kinniburgh, 2002; Boyle and Jonasson, 1973). Antimony contents in most intrusive igneous rocks also are relatively low in Sb (0.3 to 1.1 ppm), except intermediate and felsic volcanic rocks (3 to 9 ppm) (Boyle and Jonasson, 1984). It is not known how As and Sb are enriched 100s to 1000s times in aqueous fluids compared to their concentrations in the source melts. Arsenic and antimony are considered fluid-mobile, because high concentrations of these elements are observed in hydrothermal vents (black smokers) and sulfide ore deposits (Noll et al., 1996), but the distributions of As and Sb between fluid and melt is not well understood. Thus experimental studies are needed to constrain the partitioning behavior of As and Sb between aqueous fluid and silicate melt under magmatic-hydrothermal conditions.

Arsenic and antimony could exist in +III or +V oxidation states in silicate melts. If the valences of As or Sb in fluid and those in melt are not the same at equilibrium conditions, As and Sb partitioning will be dependent on oxygen fugacity. For example:

$$2H_3AsO_3^{0}{}_{fluid} + O_2 = As_2O_{5\ melt} + 3\ H_2O \qquad (2)$$

The SiO_4 tetrahedron is the basic unit of silicate melt structure and the partitioning behavior of trace elements in melt is inevitably affected by the silica content of melt. Hirschmann and Ghiorso (1994) found that the activity coefficients of Ni, Co and Mn increase with increasing SiO_2 concentration, and that the increase in SiO_2 concentration

of melt causes the partition coefficients of these elements between olivine and melt ($D^{o/m}$) to increase.

Aluminum saturation index (ASI), the molar ratio of Al_2O_3 to ($Na_2O + K_2O$), is another chemical characteristic of melts that strongly influences the geochemical behavior of highly charged cations such as Fe^{3+}, P^{5+}, As^{5+}, Sb^{5+} and Mo^{6+}. Alkalis in molar excess of Al_2O_3 sharply lower the activity coefficients of Fe_2O_3 and P_2O_5 in potassium aluminosilicate melts (Dickenson and Hess,1986; Ellison and Hess, 1988). Thus, ASI might influence the partitioning of As and Sb between fluid and melt.

The objective of the partitioning experiments are: to determine partitioning coefficients of As and Sb between granitic melt and aqueous fluid at 800 °C and 200 MPa, to elucidate the effects of oxygen fugacity, SiO_2 concentration of the melt and the ASI of the melt on the As and Sb partitioning behavior, and to evaluate whether the high concentrations of As and Sb observed in nature can be magmatic in origin.

1.4.2 As/Sb Remediation Experiments

Permeable reactive barriers (PRBs) are a promising alternative technology for the in situ remediation of both organic and inorganic contaminants in groundwater. Zero-valent iron PRBs remove both As(III) and As(V) dissolved in groundwater through precipitation of arsenic sulfides or through adsorption to or co-precipitation with Fe and Mn oxides (Spink, 2001; Bain et al., 2003; Farrell et al., 2001; McRae et al., 1999; Manning et al., 2002; Melitas, et al., 2002; Su and Puls, 2001, 2003). Organic carbon (wood chips, paper mill pulp, municipal compost, etc.) is another widely used medium of PRB to treat acid

mine drainage and heavy metals (Benner et al., 1997, 1999; Ludwig et al., 2002). Organic carbon PRBs remove dissolved sulfate, Fe^{2+} and other metals through enhanced biological sulfate reduction and metal sulfide precipitation (Waybrant et al., 1998, 2002). Organic carbon is less expensive than zero-valent iron. Laboratory and field results show that organic carbon and zero-valent iron mixtures rapidly removed As from groundwater (Spink, 2001; Bain et al., 2003).

Most environmental research on Sb is limited to studies on concentrations and speciation of Sb in environmental, biological, and geochemical samples (Filella et al, 2002). Studies of the interactions between dissolved Sb and solid phases include Pilarski et al., (1995) and Thanabalasingam and Pickering (1990). Very few studies have examined the remediation of antimony pollution in groundwater. Antimony and As are in the same group (group VA) of the periodic table of the elements, and have similar geochemical behaviours in near-surface and surface environments. The two elements are strongly sorbed by Fe, Al and Mn oxides, and precipitate as sparingly soluble sulfide minerals. Many mine drainage waters contain high concentrations of As and Sb (Smedley and Kinniburgh, 2002; Boyle and Jonasson, 1984). However, it is not known whether organic carbon and Fe-bearing organic carbon mixtures will remove both As and Sb. Similarly the relative effectiveness of Fe-bearing organic carbon mixture versus zero-valent iron is not known.

The objectives of this study are: 1) to evaluate the rates and capacities of the mixtures of organic carbon PRB and zero-valent iron PRB to remove dissolved As and Sb from groundwater; 2) to study the speciation of As and Sb in water and in solid phase and to

understand the mechanisms of immobilization of As and Sb; and 3) to study the biogeochemistry of the organic carbon mixture and the Fe-bearing organic carbon mixture.

1.5. Thesis Organization

1.5.1 Thesis Layout

This thesis is composed of three chapters (Chapters 2-4) that address the specific objectives outlined above, and an introductory chapter which presents the background and goals of the overall research. Chapters 2, 3, and 4 are written as independent papers, each with separate abstract, introduction, results, discussion, and conclusions, reflecting the specific nature of the chapter. There is an inherent repetition of the introductory material between Chapter 1 and Chapter 2, 3, and 4. However, the presentation of the thesis in this form is consistent with one of the principal goals of scientific research, to publish the results of the research in a timely fashion and to reach a broad audience in the science community.

1.5.2 Thesis Contents

Arsenic and antimony are important trace elements in magmatic-hydrothermal systems, geothermal systems and epithermal deposits. Experiments are needed to elucidate the partitioning behavior of As and Sb between melt and aqueous fluid. Chapter 2 presents the oxygen fugacity-controlled partitioning experiments of As and Sb between granitic melt and aqueous fluid at 800 °C and 200 MPa. The partition coefficients of As and Sb

are determined as a function of As concentration, oxygen fugacity, SiO_2 content of the melt, and aluminum saturation index (ASI) of the melt. The oxidation states of As and Sb in coexisting melts and fluids and the possible partitioning reactions are also discussed.

Permeable reactive barriers (PRBs) are a promising alternative technology for the in situ remediation of both organic and inorganic contaminants (including As and Sb) in groundwater. In Chapter three the isotopic geochemistry and microbiology of an organic carbon reactive mixture (OC) and an Fe-bearing organic carbon reactive mixture (FeOC) are investigated through two column tests. The rates and capacities of sulfate reduction of the two mixtures are determined. The causes for the enhanced performance of the FeOC mixture and the decline of the OC mixture are discussed. The direct correlation between the extent of the sulfate reduction and the $\delta^{34}S$ values and the link between two methanogenesis pathways and the $\delta^{13}C$ values are described.

The OC PRB and FeOC PRB potentially are efficient and cost-effective approaches to remediate As and Sb contamination in groundwater. Chapter four describes two column experiments designed to assess the rates and capacities of OC mixture and FeOC mixture to remove As and Sb under controlled groundwater flow conditions. The speciation of As and Sb in pore water and on the surface of the solid reactive material is investigated and the reactions involving As and Sb immobilization are discussed.

1.6 References

Arehart, G.B., Chryssoulis, S.L., Kesler, S.E. (1993), Gold and arsenic in iron sulfides from sediment-hosted disseminated gold deposits-implications for depositional processes, Economic Geology, Vol. 88, 171-185.

Audetat A., Gunther D., and Heinrich C. A. (2000), Magmatic-hydrothermal evolution in a fractionating granite: A microchemical study of the Sn-W-F-mineralized Mole Granite (Australia). Geochimica et Cosmochimica Acta, Vol. 64, No. 19, pp. 3373-3393.

Audetat A. and Pettke T. (2003), The magmatic-hydrothermal evolution of two barren granites: A melt and fluid inclusion study of the Rito del Medio and Canada Pinabete plutons in northern New Mexica (USA), Geochimica et Cosmochimica Acta, Vol. 67, No. 1, pp. 97-121.

Bain, J., Spink, L., Blowes, D.W., and Smyth, D. (2003), The removal of arsenic from groundwater using permeable reactive materials, In: Sudbury '03 – Mining and the Environment III, Sudbury, Ontario, Canada.

Ballantyne J.M. and Moore J.N. (1998), Arsenic geochemistry in geothermal systems, Geochimica et Cosmochimica Acta, Vol. 52, pp. 475-483.

Benner, S.G., Blowes, D.W., and Ptacek, C.J. (1997), A full-scale porous reactive wall for prevention of acid mine drainage, Ground Water Monitoring and Remediation, Vol. 17 (4), pp. 99-107.

Beuchat S., Moritz R., and Pettke T. (2004), Fluid evolution in the W-Cu-Zn-Pb San Cristobal vein, Peru: fluid inclusion and stable isotope evidence, Chemical Geology, 210, 201-224.

Boyle, R.W. and Jonasson, I.R. (1973), The geochemistry of arsenic and its use as an indicator element in geochemical prospecting, Journal of Geochemical Exploration, Vol., 2, pp. 251-296.

Boyle, R.W. and Jonasson, I.R. (1984), The geochemistry of antimony and its use as an indicator element in geochemical prospecting, Journal of Geochemical Exploration, Vol., 20, pp. 223-302.

Council of European Communities (1976), Council Directive 76/464/EEC of 4 May 1976 on pollution caused by certain dangerous substances discharged into the aquatic environment of the Community. Official Journal L 129, 18/05/1976, pp. 13-29.

Dickenson M.P., and Hess P.C., The structural role and homogeneous redox equilibria of iron in peraluminous, metaluminous and peralkaline silicate melts, Contributions to Mineralogy and Petrology 92, 207-217.

Ellison A.J. and Hess P.C. (1988), Peraluminous and peralkaline effects upon monazite solubility in high silica liquids, EOS, Vol. 69, 498.

Farrell, J., Wang, J., O'Day, P., and Conklin, M. (2001), Electrochemical and spectroscopic study of arsenate removal from water using zero_valent iron media, Environmental Science and Technology, Vol. 35, pp. 2026-2032.

Filella, M., Belzile, N., and Chen, Y. (2002a), Antimony in the environment: a review focused on natural waters I. Occurrence, Earth-Science Reviews, Vol. 57, pp. 125-176.

Filella, M., Belzile, N., and Chen, Y. (2002b), Antimony in the environment: a review focused on natural waters I. Relevant solution chemistry, Earth-Science Reviews, Vol. 57, pp. 125-176.

Heinrich C.A. and Eadinton P.J. (1986), Thermodynamic predictions of the hydrothermal chemistry of arsenic, and their significance for the paragenetic sequence of some cassiterite-arsenopyrite-base metal sulfide deposits, Economic Geology 81, 511-529.

Heinrich C.A., Günther D., Audétat A., Ulrich T., and Frischknecht R. (1999), Metal fractionation between magmatic brine and vapour, determined by microanalysis of fluid inclusions, Geology 27, 755-758.

Hirschmann M.M., and Ghiorso M.S. (1994), Activities of nickel, cobalt, and manganese silicates in magmatic liquids and applications to olivine/liquid and to silicate/metal partitioning, Geochimica et Cosmochimica Acta 58, 4109-4126.

Ludwig, R.D., McGregor, R.G., Blowes, D.W., Benner, S.G., Mountjoy, K. (2002), A permeable reactive barrier for the treatment of dissolved metals, Ground Water, Vol. 40(1), pp. 59-66.

Manning, B.A., Hunt, M.L., Amrhein, C., and Yarmoff, J.A. (2002), Arsenic(III) and arsenic(V) Reactions with Zero_valent Iron Corrosion Products, Environmental Science and Technology, Vol. 36, pp. 5455-5461.

McRae, C.W.T., Blowes, D.W., and Ptacek, C.J. (1999), In situ removal of arsenic from groundwater using permeable reactive barriers: a laboratory study. Sudbury ’99 - Mining and the Environment II Conference, September 13-17, Sudbury, Ontario, pp. 601-609.

Manning, B.A., Hunt, M.L., Amrhein, C., and Yarmoff, J.A. (2002), Arsenic(III) and arsenic(V) Reactions with Zero_valent Iron Corrosion Products, Environmental Science and Technology, Vol. 36, pp. 5455-5461.

Melitas, N., Wang, J., Conklin, M., O’Day, P., and Farrell, J. (2002), Understanding soluble arsenate removal kinetics by zero_valent iron media, Environmental Science and Technology, Vol. 36, pp. 2074-2081.

Muller B., Frischknecht R., Seward T.M., Heinrich C.A., and Gallegos W.C. (2001), A fluid inclusion reconnaissance study of the Huanuni tin deposit (Bolivia), using LA-ICP-MS micro-analysis, Mineralium Deposita 36, 680-688.

Noll P.D.Jr, Newsom H.E., Leeman W.P., and Ryan J.G. (1996), The role of hydrothermal fluids in the production of subduction zone magmas: Evidence from siderophile and chalcophile trace elements and boron, Geochimica et Cosmochimica Acta, Vol. 60, No. 4, pp. 587-611.

Nordstrom D.K., McCleskey R. B., and Ball J. W. (2001), Processes governing arsenic geochemistry in the thermal waters of Yellowstone National Park. USGS Workshop on Arsenic in the Environment, Denver, CO, Feb. 21-22.

Paktunc D., Kingston D., and Pratt A. (2006), Distribution of gold in pyrite and in products of its transformation resulting from roasting of refractory gold ore, Canadian Mineralogist 44, 218-227.

Pilarski, J., Waller, P., Pickering, W. (1995), Sorption of antimony species by humic acid, Water, Air, Soil Pollution, Vol. 84, pp. 51– 59.

Plant J.A., Kinniburgh, D.G., Smedley, P.L., Fordyce, F.M., and Klinck, B.A. (2003), Arsenic and Selenium, In Treatise on Geochemistry, Eds. Holland, H.D. and Turekian, K.K., Vol. 9, pp. 17-66.

Smedley, P.L. and Kinniburgh, D.G. (2002), A review of the source, behaviour and distribution of arsenic in natural waters, Applied Geochemistry, Vol. 17, pp. 517-568.

Spink, L.E. (2001), B.Sc. thesis, Department of Earth Sciences, University of Waterloo, 56p.

Spycher N.F. and Reed M.H. (1989), As(III) and Sb(III) sulfide complexes: An evaluation of stoichiometry and stability from existing experimental data, Geochimica et Cosmochimica Acta 53, 2185-2194.

Su, C. and Puls R.W. (2001), Arsenate and arsenite removal by zero_valent iron: kinetics, redox Transformation, and Implications for in situ groundwater remediation, Environmental Science and Technology, Vol. 35, pp. 1487-1492.

Su, C. and Puls R.W. (2003), In situ remediation of arsenic in simulated groundwater using zero_valent iron: laboratory column tests on combined effects of phosphate and silicate, Environmental Science and Technology, Vol. 37, pp. 2582-2587.

Thanabalasingam, P. and Pickering, W.F. (1986), Arsenic sorption by humic acids, Environmental Pollution (Series B), Vol. 12, pp. 233-246.

Thanabalasingam, P. and Pickering, W.F. (1990), Specific sorption of antimony(III) by the hydrous oxides of Mn, Fe, and Al, Water, Air, and Soil Pollution, Vol. 49, pp. 175-185.

United States Environmental Protection Agency (1979), Water Related Fate of the 129 Priority Pollutants, vol. 1, USEPA, Washington, DC, USA, EP-440r4-79-029A.

United States Environmental Protection Agency (1999), National Primary Drinking Water Standards, USEPA Office of Water, Washington, DC, USA, Doc. 810-F-94-001.

Waybrant, K.R., Blowes, D.W., and Ptacek, C.J. (1998), Selection of reactive mixtures for use in permeable reactive walls for treatment of mine drainage, Environmental Science and Technology, Vol. 32, pp. 1972-1979

Waybrant, K.R., Ptacek, C.J., and Blowes, D.W. (2002), Treatment of Mine Drainage Using Permeable Reactive Barriers: Column Experiments, Environmental Science and Technology, Vol. 36, pp. 1346-1356

Wedepohl K.H. (1995), The composition of the continental crust, Geochimica et Cosmochimica Acta., Vol. 59, pp. 1217-1232.

WHO (1993), Guidelines for drinking-water quality, Volume 1: Recommendations, 2nd ed, WHO, Geneva.

Zack T., Kronz A., Foley S.F., and Rivers T. (2002), Trace element abundances I rutiles from eclogites and associated garnet mica schists, Chemical Geology 184, 97-122.

Zotov A.V., Kudrin A.V., Levin K.A., Shikina N.D., and Var'yash L.N. (1995), Experimental studies of the solubility and complexing of selected ore elements (Au, Ag, Cu, Mo, As, Sb, Hg) in aqueous solutions. In Fluids in the Crest: Equilibrium an Transport Properties (eds. Shmulovich K.I., Yardley B.W.D., and Gonchar G.G.), pp. 95-137, Chapman and Hall.

Zotov A.V., Shikina N.D., and Akinfiev N.N. (2003), Thermodynamic properties of the Sb(III) hydroxide complex $Sb(OH)_3(aq)$ at hydrothermal conditions, Geochimica et Cosmochimica Acta, Vol. 67, No. 10, pp. 1821-1836.

Table 1.1 Physical properties of arsenic and antimony.

Name	Arsenic	Antimony
Symbol	As	Sb
Atomic number	33	51
Periodic table group	15	15
Atomic mass	74.9216	121.760
Classification	Metalloid	Metalloid
Pauling electronegativity	2.18	2.05
Density (kg m^{-3})	5727	6697
Melting point (°C)	817	904
Boiling point (°C)	614	1860
Natural isotopes and abundance	^{75}As 100%	^{121}Sb 57.21% ^{123}Sb 42.79%

Table 1.2 Common chemical forms of arsenic and antimony

Oxidation state	Major chemical form
As(-III)	Arsine H_3As
As(0)	Native arsenic As
As(III)	Arsenite $H_2AsO_3^-$, H_3AsO_3
As(V)	Arsenate $HAsO_4^{2-}$, $H_2AsO_4^-$
Sb(0)	Native antimony Sb
Sb(III)	Antimonite $Sb(OH)_3$
Sb(V)	Antimonate $Sb(OH)_6^-$

Table 1.3 Major As minerals (Smedley and Kinniburgh, 2002)

Mineral	Composition	Occurrence
Native arsenic	As	Hydrothermal veins
Niccolite	NiAs	Vein deposits and norites
Loellingite	$FeAs_2$	Vein deposits
Realgar	AsS	Vein deposits, hot spring deposits
Orpiment	As_2S_3	Hydrothermal veins, hot spring, volcanic sublimation
Cobaltite	CoAsS	High temperature deposits, metamorphic rocks
Arsenopyrite	FeAsS	Hydrothermal veins, most abundant As mineral
Tennantite	$(Cu, Fe)_{12}As_4S_{13}$	Hydrothermal veins
Enargite	Cu_3AsS_4	Hydrothermal veins
Arsenolite	As_2O_3	Secondary mineral
Claudetite	As_2O_3	Secondary mineral
Scorodite	$FeAsO_4{\cdot}2H_2O$	Secondary mineral
Annabergite	$(Ni,Co)_3(AsO_4)_2{\cdot}8H_2O$	Secondary mineral
Hoernesite	$Mg_3(AsO_4)_2{\cdot}8H_2O$	Secondary mineral, smelter wastes
Pharmacosiderite	$Fe_3(AsO_4)_2(OH)_3{\cdot}5H_2O$	Oxidation products of arsenopyrite & other As minerals

Table 1.4 Major Sb minerals (Boyle and Jonasson, 1984)

Mineral	Composition
Native antimony	Sb
Stibnite	Sb_2S_3
Tetrahedrite	$(Cu, Fe)_{12}Sb_4S_{13}$
Jamesonite	$Pb_4FeSb_6S_{14}$
Boulangerite	$Pb_5Sb_4S_{11}$
Pyrargyrite	Ag_3SbS_3
Senarmontite	Sb_2O_3
Valentinite	Sb_2O_3
Kermesite	Sb_2S_2O
Bindheimite	$Pb_2Sb_2O_6(O,OH)$
Stibiconite	$Sb^{3+}Sb^{5+}{}_2O_6(OH)$

Chapter 2

Arsenic and Antimony Partitioning between Aqueous Fluid and Peralkaline to Peraluminous Granitic Melt at 800 °C and 200 MPa

2.1 Abstract

Arsenic and antimony are important trace elements in magmatic-hydrothermal systems, geothermal systems and epithermal deposits, but their partitioning behavior between melt and aqueous fluid is not well understood. The partitioning of arsenic and antimony between aqueous fluid and granitic melt has been studied in the system SiO_2-Al_2O_3-Na_2O-K_2O-H_2O at 800 °C and 200 MPa. The partition coefficient (± 1σ) of As between aqueous fluid and melt, $D_{As}^{f/m}$, ranges from 0.6 ± 0.2 to 2.3 ± 0.3 with a mean of 1.4 ± 0.5. The value of $D_{As}^{f/m}$ was found to be constant over an ASI range of 0.63 to 1.31 and a SiO_2 concentration of 60.62 wt% to 72.96 wt%. $D_{As}^{f/m}$ is also constant at oxidized conditions, over a $\log f_{O_2}$ range of -12.2 to -8.4 bars (NNO + 1.6 to NNO + 5.4, NNO is nickel-nickel oxide redox buffer). However, at more reduced conditions ($\log f_{O_2}$ close to and less than NNO), an As mineral phase apparently crystallized and $D_{As}^{f/m}$ could not be determined. The partition coefficient (± 1σ) of Sb between aqueous fluid and melt, $D_{Sb}^{f/m}$, ranges from 0.10 ± 0.03 to 1.3 ± 0.2 and the average $D_{Sb}^{f/m}$ for hydrous haplogranite is 0.8 ± 0.5. The fluid-melt partitioning of Sb is independent of f_{O_2} over a $\log f_{O_2}$ range of

–16.8 to –7.9 (NNO – 3.0 to NNO + 5.9), and of the SiO_2 melt concentrations of 55.21 wt% to 72.59 wt%. However, ASI has a strong effect on Sb partitioning and $D_{Sb}^{f/m}$ for peralkaline melt (0.1 ± 0.01) is much smaller than that for metaluminous and peraluminous melts (0.8 ± 0.4).

Thermodynamic calculations show that As(III) is dominant in aqueous fluid at 800 °C and 200 MPa and XPS analysis of run product glass indicate that only As(III) exists in melt, which confirms the finding that f_{O_2} does not affect As partitioning between fluid and melt. Sb(III) is generally considered the dominant oxidation state in fluid and XPS analysis of run product glass show that Sb(V) is dominant in melt under oxidized conditions ($\log f_{O_2}$ > -10). The peralkaline effect only exhibits on Sb partitioning, not on As partitioning at oxidized conditions, which is consistent with the XPS measurements that As(III) and Sb(V) are dominant oxidation states in melt at oxidized conditions, because the peralkaline effect is stronger for pentavalent than trivalent cations.

2.2 Introduction

Arsenic and antimony are important trace elements in magmatic-hydrothermal systems, geothermal systems and their fossil analogs, epithermal deposits. The As concentrations in aqueous vapor and brine inclusions from magmatic-hydrothermal ore deposits, can be hundreds and a few thousand ppm, respectively, and Sb can be tens and a few hundred ppm, respectively (Heinrich et al., 1999; Audetat et al., 2000; Muller et al., 2001; Audetat and Pettke, 2003). S. Beuchat et al. (2004) found 1024 to 7690 ppm As in some quartz-hosted fluid inclusions from vein and carbonate replacement Zn-Pb-Cu-Ag mineralization at the San Cristobal deposit Peru. Mustard et al. (2004) reported 875 ppm Sb in quartz fluid inclusions from the Timbarra gold deposit in New South Wales, Australia. By contrast As concentrations are generally low in common silicate minerals (< 2 ppm) and igneous rocks (1 to 6 ppm) (Smedley and Kinniburgh, 2002; Boyle and Jonasson, 1973). Antimony contents in common silicate minerals are very low (< 1 ppm) and most intrusive igneous rocks are also low in Sb (0.3 to 1.1 ppm), although intermediate and felsic volcano rocks contain slightly higher amounts (3 to 9 ppm) (Boyle and Jonasson, 1984). It is not known how As and Sb are enriched hundreds to thousands times in aqueous fluid compared to their concentrations in the source melt. Arsenic and antimony are considered fluid-mobile, because high concentrations of these elements are observed in hydrothermal vents (black smokers) and sulfide ore deposits (Noll et al., 1996), but the distributions of As and Sb between fluid and melt are not well understood. Thus experimental studies are needed to constrain the partitioning behavior of As and Sb between aqueous fluid and silicate melt at magmatic-hydrothermal

conditions. There is only one study available on As partitioning between aqueous fluid and melt under hydrothermal conditions. Simon et al. (2007) determined the vapour-melt partition coefficients of As at 800 °C and 120 MPa in S-free and S-bearing systems. But no study has been undertaken to probe the possible factors that affect the As partition coefficient between fluid and melt, such as oxygen fugacity and melt composition.

Arsenic and antimony are present in two oxidation states in hydrothermal and geothermal fluids, +III and +V. Analyses of geothermal reservoir samples show that As is transported mainly as As(III) in geothermal reservoirs at temperature of up to 350 °C and As(V) is dominant in oxic low temperature drainages and rivers (Nordstrom et al, 2001; Ballantyne and Moore 1998). Thermodynamic modeling by Heinrich and Eadinton (1986) also predicted that As(III) accounts for the transport of As in hydrothermal systems of temperatures up to 400°C and Sb-bearing hydrothermal fluids mainly contain Sb(III) (Spycher and Reed, 1989). The dominant species under most hydrothermal conditions are $H_3AsO_3^0$ and $Sb(OH)_3^0$ (Heinrich and Eadington, 1986; Ballantyne and Moore 1998; Pokrovski et al, 1996; Zotov et al., 2003). There is little knowledge on the oxidation states of As and Sb in silicate melts. If the valences of As or Sb in fluid and those in melt are the same under equilibrium conditions, As and Sb partitioning will be independent of oxygen fugacity. For example:

$$2H_3AsO_3^0{}_{fluid} = As_2O_{3\ melt} + 3\ H_2O \quad (1)$$

However, if the valences in the fluid and melt are different, then oxygen fugacity of the melt-fluid system will affect As and Sb partitioning between fluid and melt. For example:

$$2H_3AsO_3^0{}_{fluid} + O_2 = As_2O_{5\ melt} + 3\ H_2O \quad (2)$$

The SiO_4 tetrahedron is the basic unit of silicate melt structure and the activity coefficients and the partitioning behavior of trace elements in melt are inevitably affected by the silica content of melt. Hirschmann and Ghiorso (1994) found that the activity coefficients of Ni, Co and Mn increase with increasing SiO_2 concentration and the increase in SiO_2 concentration of melt causes the partition coefficients of these elements between olivine and melt ($D^{ol/m}$) to increase. Aluminum saturation index (ASI), the molar ratio of Al_2O_3 to (Na_2O + K_2O), is another chemical parameters of melt that strongly influence the geochemical behavior of highly charged cations such as Fe^{3+}, P^{5+}, As^{5+}, Sb^{5+} and Mo^{6+}. Alkalis in molar excess of Al_2O_3 sharply lower the activity coefficients of Fe_2O_3 and P_2O_5 in potassium aluminosilicate melts (Dickenson and Hess,1986; Ellison and Hess, 1988). So both SiO_2 and ASI might influence the partitioning of As and Sb between fluid and melt.

This study presents experimental data that determine partitioning coefficients of As and Sb between granitic melt and aqueous fluid at 800 C and 200 MPa, and that describe the effects of oxygen fugacity, SiO_2 concentration of melt and ASI of melt on the As and Sb partitioning behavior.

2.3 Experimental Methods

2.3.1 Starting Material

The starting melt composition is synthetic granitic glass based on the 200 MPa thermal minimum of haplogranite composition (SiO_2 = 78 wt%, ASI or molar (Al_2O_3 / (Na_2O + K_2O)) = 1.0, molar (Na/K) = 1.70; Tuttle and Bowen, 1951). Two series of glass were

made: one consists of five compositions, which has a near-constant ASI (0.99 - 1.01) but the SiO_2 content varies from 58.01 wt% to 73.13 wt%; the other series consists of 6 compositions which have near-constant SiO_2 (74.65 - 76.96 wt%), but the ASI ratio varies from 0.61 to 1.28 (Table 2.1). The glasses were made from spectroscopically pure SiO_2, Al_2O_3, Na_2CO_3, and K_2CO_3. The mixture of oxides and carbonates were heated to 400 °C for 3 hours to decarbonate Na_2CO_3 and K_2CO_3 to Na_2O and K_2O, and then fused at 1200 °C at atmospheric pressure for two or three hours. Then the glasses were quenched and ground to 20 μm powder. The glasses were heated two more times (once at 1200 °C and once at 1500 °C) and reground to ensure the glass powders were homogenous. The As and Sb solutions were made of different concentrations of spectroscopically pure $Na_2HAsO_4{\cdot}7H_2O$ and $C_8H_4K_2Sb_2O_{12}{\cdot}3H_2O$, which have higher water solubilities than As and Sb oxides, and distilled and deionized water.

Two types of experiments were conducted: forward and reverse. The forward experiments started with glass and As or Sb solutions, and the reverse experiments with glasses doped with 3.68 wt% As or 0.45 wt% Sb and distilled and deionized water. The As-bearing or Sb-bearing glasses were made of glass with the haplogranite minimum composition (SiO_2 72.36 wt% and ASI 0.99) and As (~8 wt%) or Sb (~1 wt%) solutions. About 100 mg glass powder and 100 mg As or Sb solution were put into a 5 mm outer diameter 20 mm long gold capsule and reacted at 800 °C and 200 MPa for one week and then quenched. Then the glasses were ground, washed with distilled water to remove As from fluid inclusions in glass, and then dried at 120 °C. The dry glass powder was put into a gold capsule, fused at 800 °C and 200 MPa for another week, and then quenched.

Small chips from both one-week glasses (~30 vol% bubbles) and two-week glasses (~10 vol% bubbles), were analyzed by electron microprobe and the relative errors of As glasses are less than 5% and those of Sb glasses less than 20%.

2.3.2 Experimental Design

All experiments were conducted in cold-seal rapid-quench pressure vessels constructed of Udimet 720®, a Ni-rich alloy that contains Cr, Co, Ti and Mo, and are operated vertically. All experiments were pressurized by water or Ar (at oxidized conditions) to 200 MPa, and then isobarically heated to 800 °C. Temperatures were measured using an external Ni-CrNi thermocouple, calculated against an internal thermocouple, with a total error of ± 5 °C. Pressure was measured by transducers and results were checked against a pressure gauge. The transducers and gauges are factory-calibrated and have an accuracy of better than ± 100 bars. The experiments were quenched from 800 °C to room temperature in a few seconds. The redox conditions were imposed using the filler-rod technique (Matthews et al 2003) and measured using the hydrogen sensor technique (Chou and Eugster, 1976). The oxygen fugacity ranges from about 10^{-18} to 10^{-5} bars (NNO – 4.2 to NNO + 8.8). Both the equipment and the techniques are described in detail in Matthews et al. (2003).

Most experiments contained 15 mg to 20 mg of glass, and 10 mg to 20 mg of a As or Sb solution and a few experiments started with 100 mg glass and 100 mg solution. The starting mixtures were loaded into gold capsules. Most experiments were conducted in 2 mm o.d. 20 mm long gold capsules, and a few were in 5 mm o.d. 30 mm long gold

capsules, both with a wall thickness of 0.127 mm. All capsules were crimped shut, sealed with an arc welder after the capsules had been loaded, weighed, stored in a drying oven at 120 °C for at least two hours, and weighed again to test for leaks. After each experiment, capsules were weighed again to check for any mass change. Any capsules gaining or losing 3 mg mass were rejected. The standard deviation σ of As and Sb concentrations in both glass and solutions were determined as standard error and the relative error was calculated.

The possibility that As or Sb dissolve into Au capsule to form an alloy was tested by the experiments that employed the same procedures and P-T- f_{O_2} conditions as the partition experiments. Solutions with high concentrations of As (8.6 wt%) or Sb (3.0 wt%) were loaded in Au capsules and were reacted at 800 °C and 2000 bars for up to two weeks, at $\log f_{O_2}$ conditions ranging from -17 to -6 (NNO – 3.2 to NNO + 7.8). Pieces of Au from the capsules were analyzed by electron microprobe but the concentrations of As or Sb were below the detection limits (~200 ppm). Gold pieces from most partition experiments (including the reverse experiments and the one that had a run duration of one month) were also analyzed for As and Sb, and no detectable As or Sb were found in these capsules either. Light yellow Au-As alloy was observed from an one-week experiment with As_2O_5 powder in a Au capsule at 800 °C, 2000 bars and $\log f_{O_2}$ about -11. This was undoubtedly because As_2O_5 was in contact with Au. However, for all partition experiments started with As in solution or glass, no As or Sb dissolved into gold at the experiment conditions, therefore alloying is not considered to be a problem.

2.3.3 Analytical Methods

The starting glasses were analyzed for major elements by ICP-AES at Actlabs, Ancaster, Ontario, Canada. The run product glasses as well as most Au capsules were analyzed for Si, Al, K, Na, As, Sb, and Au on a Joel JXA-8600 electron microprobe at the Electron-probe Microanalysis Lab of the Earth Sciences Department, University of Western Ontario. As and Sb were measured with a 25 kV acceleration voltage, 60 nA current, 10 μm beam size and 20 sec counting time (60 to 200 sec for low concentration samples). Major elements Si, Al, K and Na were analyzed separately at 15 kV, 5 nA, 20 μm, 5-20 sec (5 sec for Na and K to minimize the effect of alkali migration). Arsenopyrite, metal Sb, albite, anorthite, and orthoclase were used as standards and PAP correction procedure (Pouchou and Pichoir, 1985) were employed in data reduction.

Arsenic and antimony in solutions were analyzed by hydride generation atomic absorption spectrophotometry (HG-AAS) at PSC Laboratory Inc. After quenching of each experiment, the capsule was cleaned and weighed. The capsules were pierced with a tungsten needle and the aqueous liquid was collected with a 20 μl capillary. The liquid was collected within 24 hours of quenching. Typically 5 to 15 μl of liquid were collected and then diluted to 20 ml to 50 ml. The diluted samples were analyzed for As or Sb by hydride generation atomic absorption spectrophotometry (HG-AAS) method. A few samples were also analyzed using inductively coupled plasma – mass spectroscopy (ICP/MS) at PSC Laboratory Inc. and the difference of the As and Sb concentrations from both methods are within the analytical error of 10%.

The hydrogen sensor technique is based on the reaction:

$$Ag + HCl = AgCl + H_2 \quad (3)$$

The oxygen fugacity was calculated using the chloride concentration of the liquid after quench (Chou and Eugster, 1976). The liquid of hydrogen sensor capsules was recovered with a 20 μl capillary after the capsules were cleaned, weighed, and pierced with a tungsten needle. The liquid was then diluted with 10 ml nanopure water. Some samples were analyzed using mercuric thiocyanate spectrophotometric method (Vogel and Jeffery 1989) at the Environmental Geochemistry Lab of the Department of Earth Sciences, University of Waterloo and some by ion chromatography at the Analytical Lab of the Department of Chemical Engineering, University of Waterloo. The mercuric thiocyanate spectrophotometric method has a relative error of ±6.2% and a detection limit of 0.5 mg/L, using a Pharmacia Novaspec II visible spectrophotometer to measure absorbencies at a wavelength of 460 nm. The ion chromatographic method has a detection limit: 0.014 mg/L and a relative error of 10%.

It was not possible to access x-ray absorption near edge spectroscopy (XANES) analysis. However, it was possible to analyze the run product glasses of some experiments using x-ray photoelectron spectroscopy for oxidation states of As and Sb. XPS analyses were conducted on both glass chip samples (1-2 mm) and glass powder samples (~100 μm). Although XPS is a surface analysis method, the surface feature of the glass powder should indicate the bulk feature of the glass chip, which was confirmed by the results of the analyses on both samples. The XPS analysis was conducted using a Kratos Axis Ultra X-ray photoelectron spectrometer at the Surface Science Centre, University of Western Ontario. The samples were ground to powder (100s microns). XPS

analyzes a surface area of 300 μm × 700 μm and probes the surface of the sample to a depth of 7-10 nanometers. All high-resolution spectra were charge-corrected to the main peak of the carbon 1s spectrum set to 285.0 eV. The data were interpreted using the CASAXPS program, and the background subtraction was carried out using Shirley function (Shirley, 1972).

2.3.4 Error Analysis

Linear regression analysis was performed on all the data but no statistical correlations were able to established with good confidence between As or Sb partition coefficients and As concentration, oxygen fugacity, SiO_2 content, or ASI. This is due to the large analytical error of the low As concentration experiments and/or the lack of enough data points, which was caused by that the experiments were time consuming (at least a month for one data point) and the failure rate for the experiments were very high (about 80%). For experiments with R^2 values of less than 0.3 or those with less than 5 data points, the slope of the trend line is considered to have no significance and only a mean value of the partition coefficient was calculated. The error is the standard deviation, which is also shown on Figures 2.1 to 2.6. An exception is the Sb ASI series, which shows a clear trend; the Sb partition coefficient increases with increasing ASI, with a R squared value of 0.67 (Fig. 2.7).

2.4 Results

2.4.1 Run products of As Experiments

Most run product glasses are vesicular and contain no crystals. Those in which crystals were found under the polarized light microscope or electron microprobe are considered to be failed experiments. The vesicles contain liquid and vapor, no solids were observed. The run product solutions were clear and colorless. The concentrations of the major elements and As of glasses are presented in Table 2.2, and the As concentration is represented as As_2O_3 based on a trivalent oxidation state of As in melt (see text below). The data show that the glasses are homogeneous with respect to all major elements and As. The totals of most glasses range from 91% to 95%, which is consistent with the expected water solubility in the melt (~5-8%) for melt compositions varying from peralkaline to peraluminous (Dingwell et al., 1997). Most glasses with low As concentration (As_2O_3 < 0.6 wt%) became slightly more peraluminous compared to their starting compositions, such as As-4 (ASI changing from 0.99 to 1.07) and As-14 (ASI changing from 0.99 to 1.03), which was also observed by Simon et al. (2007). By contrast, the glasses with high As concentration (As_2O_3 > 2 wt%) became much more peralkaline compared to their starting compositions. For example, the ASI composition of experiment As-1 changed from 0.99 to 0.67, and the ASI of As-11 from 1.01 to 0.84. The change of ASI is probably caused by the equilibration of K and Na between melt and fluid. The As solution was prepared with $Na_2HAsO_4 \cdot 7H_2O$. For the experiments with low As solutions, the Na concentrations are also low, K and Na diffuse from melt into fluid

during experiment and ASI decreases. For the experiments with high As solutions, the high Na concentrations drive Na into melt and cause ASI to increase.

The partition coefficient of As, $D_{As}^{f/m}$, is defined as the ratio of the As concentration in solution to the concentration in glass. $D_{As}^{f/m}$ was calculated with measured concentrations both in the run product solution and in the run product glass.

$$D_{As}^{f/m} = [\mathrm{As}]_{\mathrm{fluid}} / [\mathrm{As}]_{\mathrm{glass}} \quad (4)$$

where $[\mathrm{As}]_{\mathrm{fluid}}$, $[\mathrm{As}]_{\mathrm{glass}}$ are As concentrations in fluid or glass. The uncertainties of $D_{As}^{f/m}$ were calculated using the general error propagation formula:

$$z = x \times y \text{ or } z = x / y \quad (5)$$

$$\frac{\Delta z}{z} = \sqrt{\left(\frac{\Delta x}{x}\right)^2 + \left(\frac{\Delta y}{y}\right)^2} \quad (6)$$

where Δz, Δx, and Δy are standard deviations.

The As concentrations in glass and fluid and $D_{As}^{f/m}$ are presented in Table 2.3. Arsenic concentrations in run product glass range from 0.035 to 5.15 wt%, and those in run product solutions from 0.075 to 5.41wt%. The partition coefficient of As ranges from 0.6 to 2.3 with a mean of 1.4 ± 0.5.

2.4.2 Attainment of Equilibrium

Equilibrium is demonstrated by reverse experiments and the homogeneity of run product glass. Most experiments were forward and a few were reverse. The results of forward and reverse experiments overlap within error limits, which indicates that As and Sb partitioning between melt and aqueous fluid had reached equilibrium. The average values for the reverse experiments are slightly lower than those for the forward

experiments. The partition coefficient is the ratio of As or Sb concentration in fluid to As or Sb concentration in melt. In reverse experiments, this ratio starts at zero and increases until equilibrium is reached, so the partition coefficients measured tend to be equal to or slightly smaller than the equilibrium value. In forward experiments, the ratio of fluid concentration to melt concentration starts from infinity and decreases until equilibrium is reached, so the partition coefficients measured tend to be equal to or slightly greater than the equilibrium value. This explains why partition coefficients of the reverse experiments are slightly lower than those of the forward ones. However, because the two values overlap within error limits, this strongly suggests that they are very close to being equilibrium values.

The homogeneity of As and Sb in run product glass is also an indicator of equilibrium. The partitioning of As or Sb involves diffusion of As or Sb within the aqueous fluid, across the interface between fluid and melt and within the melt. The diffusion with the melt is the slowest step since melt is much more viscous than aqueous fluid. Because most experiments start with As in fluid, if As or Sb is homogeneous in run product glass, it is most likely that the equilibrium has reached. This is confirmed by the distribution of the partition coefficients. The partition coefficients of the experiments with less homogeneous glasses are more scattered than those with homogeneous glasses. The As partition coefficients of the experiments that have a relative error of As concentration in run product glass of greater than 20%, range from 0.74 to 5.90. By contrast, in the experiments where the relative error of As concentration in run product glass is less than 20%, The As partition coefficients range from 0.69 to 2.24. So only the experiments with

the relative error of As concentration in melt of less than 20% are considered to have reached equilibrium.

2.4.3 Arsenic Partitioning between Melt and Fluid

Four series of experiments were designed to study the four different factors that might affect the partitioning behavior of As: 1) As concentration in system, 2) the ASI ratio of the melt, 3) the SiO_2 content of the melt, and 4) oxygen fugacity (Table 2.4).

2.4.3.1 Henry's Law

Whether As behaves by Henry's Law (i.e., partition coefficients for a fixed melt composition are independent of As concentration) in partitioning between fluid and melt was tested with 14 experiments (Table 2.4 and Fig. 2.1). In order to test for Henry's Law, the error is smaller if the partition coefficients are compared to the As concentration in the system instead of to the As concentration in either the fluid or the melt. Out of the 14 experiments, As-6, As-7 and As-10 are the reverse experiments and the rest are the forward ones. Arsenic partition coefficient values of the reversed and the forward experiments are within the same range (Fig. 2.1 and Table 2.4). This indicates that equilibrium is reached from both directions. Arsenic partition coefficient is constant with an average of 1.4 ± 0.5 as arsenic concentration in system varies from 4.6 to 0.043 wt%, although it is more scattered (greater relative error) when As concentration in system is less than 0.5 wt% (Fig. 2.1 and Table 2.4). Arsenic concentration does not affect the As

partitioning between melt and fluid at 800 °C and 200 MPa and thus As partitioning exhibits Henry's law behavior.

2.4.3.2 Effect of ASI of Melt

Four experiments were conducted to study the effect of ASI of melt on As partitioning between melt and fluid (Table 2.4 and Fig. 2.2). These experiments have constant SiO_2 of melt (72.24 wt% to 72.96 wt%), and the $\log f_{O_2}$ is within a narrow range from -10.3 to -9.0 (NNO + 3.5 to NNO + 4.8). As the melt composition varies from peralkaline (ASI = 0.63) to peraluminous (ASI = 1.31), $D_{As}^{f/m}$ stays constant with an average of 1.6. This shows that the ASI ratio of melt does not affect As partitioning between melt and fluid at 800 °C and 200 MPa.

2.4.3.3 Effect of SiO_2 Content of Melt

The effect of the SiO_2 content of the melt was studied with four experiments (Fig. 2.3 and Table 2.4). The $\log f_{O_2}$ of the four experiments is restricted to a narrow range (-9.2 to -8.4, or NNO + 4.6 to NNO + 5.4). The ASI ratio ranges from 0.79 to 1.03, but ASI does not affect As partitioning (see above). Thus the only variable is the SiO_2 content of melt. As melt composition changes from silica poor (SiO_2 = 60.62 wt%) to silica rich (SiO_2 = 72.96 wt%), $D_{As}^{f/m}$ is relatively stable with a mean of 1.7, although its dispersion

is larger at the silica rich end. Thus, within the accuracy of the current data, SiO_2 content of melt has no effect on As partitioning between melt and fluid at 800 °C and 200 MPa.

2.4.3.4 Effect of Oxygen Fugacity

Seven experiments were conducted to study the effect of oxygen fugacity (f_{O_2}) on As partitioning. The SiO_2 content of melt of the seven experiments is within a narrow range (61.28 wt% to 69.98wt) and ASI ratio of melt ranges from 0.58 to 0.84. Discussions above also show that SiO_2 content and ASI ratio do not affect As partitioning. The only variable in these experiments is f_{O_2}. Under oxidized conditions, $\log f_{O_2}$ of -12.2 to -8.4 (NNO + 1.6 to NNO + 5.4), $D_{As}^{f/m}$ is relatively constant, ranging from 0.6 to 1.3 with an average of 1.1 (Fig. 2.4 and Table 2.4). Thus f_{O_2} does not influence As partitioning at $\log f_{O_2}$ > -12.2, 800 °C and 200 MPa.

Five experiments were conducted at conditions near or more reduced than NNO (-12.9 < $\log f_{O_2}$ < -17), but all of them failed because the As mass in run product glass and fluid was much less than the As mass in the starting material (Table 2.5) and As was not found in Au capsule. The bulk As concentrations of the glasses of As-21 and As-23 were below or close to the minimum detection limit of EMPA (100-200 ppm) and the two glasses were dark colored under naked eyes, very different from the colorless run product glass of most experiments. The dark color was a surface feature. Because the sample preparation for EMPA analysis involved grinding, the surface As concentrations of the dark colored area were not measured. Arsenic concentrations in four out of five run product fluid were also close to the detection limit of HG-AAS(1 ppm). This indicates that at 800 °C and 200 MPa and conditions near and more reduced than NNO, an As

phase crystallized either from the melt or the aqueous fluid. However, no As compounds were observed in the quenched glasses possibly due to the small As mass in each experiment (0.2 mg to 1.0 mg), and no precipitate was observed in the capsule either after it was opened.

2.4.4 Run Products of Sb Experiments

The run product glasses of Sb experiments are vesicular and contain no crystals. The vesicles contain liquid and vapor, no solids were observed. The run product solutions are clear and colorless. The major elements and Sb concentrations of glasses are presented in Table 2.6, and the Sb concentration is represented as Sb_2O_5 based on the oxidation state of Sb in melt (see text below). The data show that the glasses are homogeneous with respect to all major elements and Sb. The totals of most glasses range from 91% to 95%, which is consistent with the expected H_2O content in the melt (~5-8%) for melt compositions varying from peralkaline to peraluminous (Dingwell et al., 1997). Most glasses became slightly more peraluminous compared to their starting glasses, such as Sb-1 (ASI changing from 0.99 to 1.03) and Sb-3 (ASI changing from 1.01 to 1.03). Like As glasses, this change of ASI is also caused by the equilibrium of K and Na between melt and fluid. The starting solution has low concentration of K and no Na, K and Na diffuse from melt into fluid during experiment and ASI decreases.

Antimony concentrations in run product solutions were very low (most < 100 ppm). As a result only 20% to 70% Sb mass was recovered after experiments (starting Sb = 100%). It was suspected that dissolved Sb in solution precipitated during quenching. To prove

this, another liquid recovery method was used. The capsules were cleaned and weighed, and then put into a dry oven at 120 °C to inflate the capsule. The inflated capsules were dipped into liquid nitrogen to freeze the liquid inside, and then they were pierced by a tungsten needle and opened using small scissors. The opened capsules were immersed in 50 ml diluted 0.01 m HNO_3 for about 24 hours. The immersion solutions were analyzed, and Sb concentrations in the solution were one order of magnitude higher than former results (100 - 1200 ppm), confirming the precipitation of a Sb phase during quenching. However, the total Sb mass recovered is still less than 80%, which means not all of the Sb precipitate was recovered. Partition coefficients of Sb, $D_{Sb}^{f/m}$, is defined as the ratio of Sb concentration in solution to Sb concentration in glass. Since the measured Sb concentration in fluid was not reliable, $D_{Sb}^{f/m}$ was calculated using mass balance and measured Sb concentrations in glass.

$$D_{Sb}^{f/m} = [Sb]_{fluid}^{calc} / [\mathrm{Sb}]_{\mathrm{glass}} \quad (7)$$

$$[Sb]_{fluid}^{calc} = (\mathrm{Sb}_{\mathrm{starting}} - [\mathrm{Sb}]_{\mathrm{glass}} * \text{glass mass}) / \text{fluid mass} \quad (8)$$

$$\text{glass mass} = \text{starting glass mass} \times (1 + \mathrm{H_2O} \text{ content in glass}) \quad (9)$$

$$\text{fluid mass} = \text{starting fluid mass} - (\text{starting glass mass} \times \mathrm{H_2O} \text{ content in glass}) \quad (10)$$

where $[\mathrm{Sb}]_{\mathrm{glass}}$ is Sb concentration in glass, $[Sb]_{fluid}^{calc}$ is the calculated Sb concentration in fluid, $\mathrm{Sb}_{\mathrm{starting}}$ is the Sb mass in starting material (either fluid or glass), H_2O content in glass is in wt%, estimated from the data of Dingwell et al. (1997). The uncertainties of $D_{Sb}^{f/m}$ were calculated using the general error propagation formula. The Sb concentration in glass and the calculated Sb concentration in fluid and $D_{Sb}^{f/m}$ are presented in Table 2.6. Antimony concentrations in run product glass range from 0.47 to 1.05 wt%, and $D_{Sb}^{f/m}$

from 0.10 to 1.3. The average $D_{Sb}^{f/m}$ is 0.8 ± 0.5 for a melt with 72 wt% SiO_2 and 1.0 ASI at 800°C, 200 MPa and $\log f_{O_2}$ of -7.9 to -16.8 (NNO +5.9 to NNO – 3.0, Table 2.7).

2.4.5 Antimony Partitioning between Melt and Fluid

Three series of experiments were designed to study the three different factors that might affect the partitioning behavior of Sb: 1) the SiO_2 content of the melt, 2) the ASI of the melt, and 3) the oxygen fugacity (Table 2.8).

2.4.5.1 Effect of Oxygen Fugacity

Four experiments, with relatively constant SiO_2 (71-72 wt%) and ASI (0.99-1.04), were conducted to test the effect of oxygen fugacity (f_{O_2}). As $\log f_{O_2}$ increases from –16.8 to –7.9 (NNO – 3.0 to NNO + 5.9), $D_{Sb}^{f/m}$ appears to be constant with an average of 0.8, although the relative error is fairly high (Fig. 2.5 and Table 2.8). Thus, f_{O_2} does not affect Sb partitioning between melt and fluid at 800°C and 200 MPa.

2.4.5.2 Effect of SiO_2 Content of Melt

The effect of SiO_2 was tested by varying SiO_2 concentration of melt and keeping ASI of melt constant. The ASI of melt of the seven experiments in this series is within a narrow range, 0.99 – 1.06. The f_{O_2} of these experiments is variable, but the discussion above shows that it has no significant influence on $D_{Sb}^{f/m}$. $D_{Sb}^{f/m}$ is constant for this series with an average of 0.7 as melt composition changes from silica poor (SiO_2 = 55.21 wt%) to

silica rich (SiO_2 = 72.59 wt%), although it is more dispersed at the silica rich end (Fig. 2.6 and Table 2.8). Thus the SiO_2 content of melt has no effect on Sb partitioning between melt and fluid at 800 °C and 200 MPa. Out of the seven experiments, Sb-1 is the reverse experiment. The $D_{Sb}^{f/m}$ value (0.34) of this experiment is in the same range of the $D_{Sb}^{f/m}$ values of the other experiments, which shows that all of the experiments reached equilibrium.

2.4.5.3 Effect of ASI of Melt

The effect of ASI was studied with six experiments. The oxygen fugacity and SiO_2 content of these experiments are within the narrow ranges, 70.84 to 71.80 wt% and -11.83 to -9.00, respectively (Table 2.8). The data shows a clear trend that as ASI increases from 0.65 to 1.31, $D_{Sb}^{f/m}$ increases from 0.1 to 1.3. $D_{Sb}^{f/m}$ of peralkaline melt (0.1 $\pm$ 0.01) is smaller than that of metaluminous (0.8 $\pm$ 0.6), which is then smaller than that of peraluminous melts (1.3 $\pm$ 0.7). Thus ASI does affect Sb partition coefficient and $D_{Sb}^{f/m}$ values for metaluminous and peraluminous melt are 8 to 13 times greater than that for peralkaline melt.

2.4.6 As and Sb XPS Spectra

The run product glasses of some experiments were analyzed by XPS in order to determine the oxidation states of As and Sb. XPS As(3d) spectra collected from As-2 and As-6 samples are similar. Both have one large peak, which is fitted with a single As($3d_{5/2}$) and its couplet As($3d_{3/2}$) (Fig. 2.8). The As(3d5/2) peaks are attributed to an As(III)

species (bound with oxygen) with binding energies of 44.20 eV and 44.41 eV. This is in agreement with the XPS data of Nesbitt et al. (1995) (Table 2.9). Both As-2 and As-6 were conducted under oxidized conditions with a $\log f_{O_2}$ of -10.1 and -12.2, respectively. The oxidation state of As in melt under NNO and reduced conditions can be expected to be 3+ as well, so As exists as As(III) in melt at 800 °C and 200 MPa regardless of f_{O_2}.

Because of the overlap of Sb($3d_{5/2}$) with O(1s), only Sb($3d_{3/2}$) was used to determine the oxidation states of Sb (Egdell et al., 1999). The spectra of the reference material of this study are similar to Benvenutti et al. (1991) and a binding energy of 540.0 eV was used as the divide between Sb(III) and Sb(V) species. XPS Sb($3d_{3/2}$) spectra collected from Sb-1 and Sb-10 samples are illustrated in Figure 2.9 and Table 2.10. Although there is a Sb(III) component in Sb-1 spectra, Sb(V) is clearly the dominant species in both samples. Both Sb-1 and Sb-10 were conducted under very oxidized conditions with a $\log f_{O_2}$ of -7.9 and -9.5, respectively. Due to the small amount of glass mass and low concentration of Sb in glasses, no Sb($3d_{3/2}$) spectra was collected for reduced experiments Sb-2 and Sb-12. Hence, the oxidation states of Sb in melt under NNO and reduced conditions are unknown.

2.5. Discussion

2.5.1 Partitioning Behaviors of As, Sb and P, W, Mo

Simon et al. (2007) studied the partitioning behavior of As between low-salinity vapor (2 wt% NaCl eq.) and rhyolite melt at 800 °C and 120 MPa in both S-free and S-bearing (pyrrhotite) systems, and determined the vapour-melt partition coefficients of As ($\pm 1\sigma$) of

1.0 ± 0.1 and 2.5 ± 0.3 in the S-free and S-bearing assemblages, respectively. The $D_{As}^{f/m}$ value of this study, 1.4 ± 0.5, is very close to the value of S-free system, despite the differences in pressure and vapor salinity of the two experiments. Many studies have also analyzed the trace element concentrations of natural vapour and liquid-rich aqueous fluid inclusions and melt inclusions of hydrothermal deposits using laser ablation inductively coupled plasma mass spectrometry (LA-ICP-MS). If coexisting primary aqueous fluid inclusions and melt inclusions are found, partition coefficients can be calculated from these natural sample analyses. Audetat et al. (2000a) analyzed trace elements of coexisting melt and fluid inclusions (sample Bism 3.3A) in magmatic topaz of the Mole Granite, Australia, and the calculated values of $D_{As}^{f/m}$ and $D_{Sb}^{f/m}$ from that study are 3.8 and 2.1, respectively. Audetat and Pettke (2003) reported a $D_{As}^{f/m}$ value of 6.7 and a $D_{Sb}^{f/m}$ value of 4.2 for coexisting aqueous fluid and melt inclusions (700 °C 120 MPa and 4.9 wt% NaCl) in quartz of the Rito del Medio pluton, New Mexico. Mustard et al. (2004) measured the average concentrations of trace elements in 25 coexisting aqueous inclusions and 52 melt inclusions of the Timbarra gold deposits, Australia, and a $D_{As}^{f/m}$ value of 1.8 and a $D_{Sb}^{f/m}$ value of 1.2 can be derived from As and Sb data of that study. The larger values of $D_{As}^{f/m}$ and $D_{Sb}^{f/m}$ of the natural system are probably caused by arsenite ion pairing or metal thioarsenites in the aqueous phase (Tossell 2000), which increases the As concentration in fluid in equilibrium with melt. Simon et al. (2007) also suggested the potential existence of an As-S species in the vapour phase. Considering this effect, the results of this study ($D_{As}^{f/m}$ 1.4 ± 0.5, $D_{Sb}^{f/m}$ 0.8 ± 0.5) are in agreement with the measurements from natural samples. It is interesting to note that, although the

$D_{As}^{f/m}$ and $D_{Sb}^{f/m}$ values of natural systems are several times higher than the experimental data of this study, the ratio of the two partition coefficients, $D_{As}^{f/m}$ to $D_{Sb}^{f/m}$ in both natural and experimental systems is consistently between 1.5 and 1.8. Thus there is a consistency of the relative values of $D_{As}^{f/m}$ and $D_{Sb}^{f/m}$ among the data from both experimental studies and the analysis of the natural samples.

Phosphorus, tungsten and molybdenum behave similarly to arsenic and antimony in hydrothermal fluids and melts. They all form oxyanioins in aqueous fluid and bond with oxygen in melt (Keppler, 1994; Wood, 1992; Candela and Holland, 1984; Hess, 1991). London et al. (1988) determined $D_P^{f/m}$ value of 0.9 at 775 °C and 200 MPa between rhyolite obsidian and water. Keppler (1994) measured $D_P^{f/m}$ value of 0.46 at 800 °C and 200 MPa for the thermal minimum haplogranite compositions. Keppler and Wyllie (1991) reported a $D_W^{f/m}$ value of 3.5 for haplogranite melt and water at 750 °C, 200 MPa and NNO buffer conditions. Manning and Henderson (1984) measured a much lower $D_W^{f/m}$ value of 0.1 for the similar system and conditions, but W oxide crystals were found in glass, so this value is not reliable. Kravchuk et al. (1997) determined a $D_W^{f/m}$ that is close to 1 for Ab-Qz melt and 1 m NaCl fluid. Chevychelov and Chevychelova (1997) reported that $D_W^{f/m}$ for granitic melt and water at 920 °C to 950 °C increased from 0.9 to 1.5 as pressure increased from 100 MPa to 500 MPa . Candela and Holland (1984) measured a $D_{Mo}^{f/m}$ value of 2.5 for granitic melt and water at 750 °C and 140 MPa and found $D_{Mo}^{f/m}$ is independent of fluorine and chlorine concentrations of melt. Keppler and Wyllie (1991) measured a $D_{Mo}^{f/m}$ value of 5.5 for haplogranite melt and water at 750 °C, 2 MPa and NNO buffer conditions. Chevychelov and Chevychelova (1997) reported that $D_{Mo}^{f/m}$ for

granitic melt and water at 920 C to 950 C increased from 0.7 to 1.7 as pressure increased from 100 MPa to 500 MPa. Kravchuk et al. (2000) determined $D_{Mo}^{f/m}$ at 800 °C and 150 – 200 MPa is 0.9 for the granite-water system. So for the similar system (granitic melt – H_2O) and at similar conditions (700°C to 950 °C, 100 MPa to 200 MPa), $D_{As}^{f/m}$ values (0.7 to 2.3) and $D_{Sb}^{f/m}$ (0.3 to 1.3) of this study are very similar to $D_{P}^{f/m}$, $D_{W}^{f/m}$ and $D_{Mo}^{f/m}$ values, except for the data Keppler and Wyllie (1991) which is 2 or 3 times higher. These data confirm that the oxyanions of As, Sb, P, W and Mo behave similarly in both melt and aqueous fluid at high pressure and temperature.

2.5.2 Peralkaline Effect and Partitioning of As and Sb

The highly charged cations are stabilized in peralkaline melts compared to peraluminous or metaluminous melts because alkali atoms in excess of aluminum are free to complex with these cations (Hess, 1991). For example, the solubilities of monazite ($LREEPO_4$, light rare earth element phosphates) in peralkaline melts is higher than in metaluminous melt (Elison and Hess, 1988; Montel, 1986). In this study a peralkaline effect is observed on Sb partitioning, but not on As partitioning. The $D_{Sb}^{f/m}$ for melt with ASI of 0.65 is much less than those for melts with ASI of 1.0 to 1.3, which means Sb partitions more favorably towards peralkaline melt than towards peraluminous or metaluminous melts. ASI did not affect As partitioning. The tendency to form alkali-cation complexes is proportional to the charge of the cation, thus the peralkaline effect is stronger for M^{5+} than M^{3+}, where M denotes a cation (Hess, 1991). The ASI experiments for As and Sb were done under oxidized conditions ($\log f_{O_2}$ of -10.3 to -9.0). XPS

analysis also shows that under oxidized conditions the oxidation states of As and Sb in melt are +3 and +5, respectively, so Sb behavior will depend more strongly on alkali concentration than As behavior. Thus XPS analyses are consistent with the results of ASI experiments, and As(III) and Sb(V) are the dominant oxidation states in oxidized hydrous granitic melts.

2.5.3 Speciation of As and Sb in Aqueous Fluid and Melt

Arsenic and antimony have two oxidation states in both melt and hydrothermal fluid, +3 and +5. Studies have shown that As(III) is dominant in geothermal systems up to 400ºC (Heinrich and Eadington, 1986; and Ballantyne and Moore 1998; Nordstrom et al, 2001). To determine the oxidation state of As in fluid at 800ºC and 200 MPa, a thermodynamic calculation was conducted using SUPCRT92 (Johnson et al., 1992) with a database upgraded in 1998 by GEOPIG group and HKF parameters for $H_3AsO_3^0$ from Pokrovski et al. (1996). The equilibrium constants of reactions

$$H_3AsO_4^0 = H_2AsO_4^- + H^+ \quad (11)$$

$$H_2AsO_4^- = HAsO_4^{2-} + H^+ \quad (12)$$

$$H_2O = H^+ + OH^- \quad (13)$$

at 800 ºC and 200 MPa were calculated with log K_{11} = -6.95, log K_{12} = -11.72, and log K_{13} = -12.08. The As solution was made of $Na_2HAsO_4 \cdot 7H_2O$ and H_2O and Na_2HAsO_4 concentrations range from 0.01 $mol \cdot L^{-1}$ to 0.87 $mol \cdot L^{-1}$. The equilibrium calculation shows that ratio of $[H_2AsO_4^{2-}]$ to the total As(V) is from 50% to 100%, and pH from 11.7

to 10.1, as the total As(V) concentration varies from 0.87 mol·L^{-1} to 0.01 mol·L^{-1}. Thus $H_2AsO_4^{2-}$ is the dominant As(V) species. Similar calculations were done for reactions

$$H_3AsO_3^0 = H_2AsO_3^- + H^+ \quad (14)$$

and log K_{14} = 11.84. $H_3AsO_3^0$ is the dominant As(III) species at pH of 11.7 to 10.1. The redox reaction of As in fluid is

$$H_3AsO_3^0 + 0.5\ O_2 = H_2AsO_4^- + H^+ \quad (15)$$

log K_{15} was calculated to be -8.73. Combined with measured oxygen fugacity (10^{-12} to 10^{-8} bar) and calculated pH (10.1 to 11.7), the calculation shows that $H_3AsO_3^0$ / $H_2AsO_4^-$ = 10^5 to 10^{11}, so the oxidation state of As in fluid at 800 ºC and 200 MPa is +3.

The oxidation state of As in melt is not well understood. Verweij (1981) found in xK_2O-$(100-x)SiO_2$-$0.5As_2O_3$ (x, 100 and 0.5 are molar ratios) systems, a small fraction of As(V) is reduced to As (III) at 1300-1600 °C in air, which means very high f_{O_2} (about 0.2 bar). This is consistent with the XPS analysis of the run product glasses that the oxidation state of As in melt is also +3, because f_{O_2} of the experiments in this study is much lower (10^{-12} to 10^{-8} bar). Then the partitioning reaction of As between fluid and melt is

$$2H_3AsO_3^0{}_{\text{fluid}} = As_2O_{3\ \text{melt}} + 3H_2O \quad (16)$$

This confirms the finding that oxygen fugacity does not affect As partitioning between fluid and melt.

It has generally been assumed that only Sb(III) complexes ($Sb(OH)_3$ or Sb sulfide complexes) are important for Sb transport in hydrothermal systems (Spycher and Reed,

1989; Wood, 1989; Williams-Jones and Normand, 1997; Zotov et al., 2003; Pokrovski et al., 2006). This is probably true for f_{O_2} conditions near and more reduced than NNO. However, at f_{O_2} conditions more oxidized than NNO the oxidation state of Sb is not understood and no f_{O_2} controlled experiments has been done to study the Sb(III)/Sb(V) transition at these conditions. Mitsunobu et al. (2006) found that Sb(V) is very stable and Sb(III) is oxidized at more negative Eh than As in surface soil-water system. At low temperature (T < 300°C) and alkaline conditions, Sb(III) in aqueous fluid is easily oxidized to Sb(V) even in the presence of HS^- and the EXAFS measurements show that the polynuclear Sb(V) complexes may be important for Sb transport in hydrothermal systems (Wood, 1989; Sherman et al., 2000). Thus it is possible that Sb(V) is the main oxidation state at oxidized conditions in hydrothermal fluids.

The oxidation states of Sb in silicate melts are not well understood. Klemme et al. (2005) found that at 1250-1500 °C Sb partition coefficients between rutile and silicate melts increase with increasing f_{O_2} and suggested that at higher f_{O_2} ($\log f_{O_2}$ = -0.96) Sb(V) is dominant and at lower f_{O_2} ($\log f_{O_2}$ = -11.3) Sb(III) is dominant. Righter et al. (2001) suggested that Sb exists as Sb(III) in basaltic melt in equilibrium with Fe-Ni-S metal at 1260 °C and Fe-FeO –1.5 to Fe-FeO + 2.5 redox conditions. XPS measurements of this study shows that Sb(V) is the dominant in melt at $\log f_{O_2}$ = -9.5 to -7.9, and the partition experiments show that f_{O_2} does not affect Sb partitioning. This suggests that at 800 °C and 200 MPa there might be two different partitioning reactions: at the oxidized conditions (f_{O_2} > 10),

$$2Sb(OH)_5^{0}{}_{fluid} = Sb_2O_{5\ melt} + 5H_2O \qquad (17)$$

and at f_{O_2} conditions near and more reduced than NNO,

$$2Sb(OH)_3^{0}{}_{fluid} = Sb_2O_{3\ melt} + 3H_2O \quad (18)$$

A Sb(III)/Sb(V) transition might occur at a f_{O_2} condition more oxidized than NNO and more research is needed to elucidate this problem.

2.6 Application

An important problem of the genesis of ore deposits is the source of metals and metalloids. For intrusion-related hydrothermal deposits an important question is: can the ore deposit be explained by magmatic processes? i.e., did the melt contain a sufficient amount of the element to explain the observed concentration of the element in the deposit. Granites contain low concentrations of both As (average 1.2 ppm) (Smedley and Kinniburgh, 2002) and Sb (average 0.36 ppm) (Boyle and Jonasson, 1984), but fluid inclusions from granite-related ore deposits can contain hundreds to thousands ppm As and tens to hundreds ppm Sb (Audetat et al., 2000; Muller et al., 2001; Audetat and T. Pettke, 2003). A question is thus how As and Sb concentrate hundreds to thousands of times?

We believe that the initial As and Sb concentration of magma, crystallization and interaction between melt and aqueous fluid are the three main factors controlling the As/Sb abundance in hydrothermal deposits. Noble et al. (2004) reported that unaltered glassy calc-alkalic volcanic rocks of silicic to intermediate composition from the Julcani district, central Peru contain as much as 65 ppm As and 2.3 ppm Sb, and two Eocene dikes in the Carlin trend, Nevada, also have high contents of As and Sb (34 ppm and 63

ppm, 32 ppm and 6 ppm, respectively), and that these high contents are of magmatic origin, implying that high concentrations of these elements were also present in the parent magmas at depth. Crystallization concentrates incompatible elements in residual melts, and interaction between melt and aqueous fluid drives mobile element from melt to fluid. Arsenic and antimony behave as incompatible elements during magmatic processes (melting and crystallization) in the absence of sulfide or fluid phases (Noll et al, 1996), and major silicate minerals contain 0.1 to 2 ppm As (Smedley and Kinniburgh, 2002) and less than 1 ppm Sb (Boyle and Jonasson, 1984). $D_{As}^{f/m}$ and $D_{Sb}^{f/m}$ values from this study and analysis of natural samples show As and Sb are moderately mobile elements (1< D <10).

If we assume a granite magma initially contained 50 ppm As and 20 ppm Sb at depth, with major silicate minerals containing 2 ppm As and 1 ppm Sb. Based on the mass balances of As and Sb, the residual melt would have 962 ppm As and 381 ppm Sb after 95% crystallization of the melt, assuming that magnetite or pyrrhotite do not crystallize (Simon et al., 2007). If values of $D_{As}^{f/m}$ = 3 and $D_{Sb}^{f/m}$ = 2 as mean values of the partition coefficients from this study and those from analyses of natural samples (Audetat et al., 2000a; Audetat and Pettke, 2003; and Mustard et al. 2004), the coexisting fluid would contain 2886 ppm As and 762 ppm Sb. These concentrations are very comparable to analysis results of natural samples: 2230 ppm As and 740 ppm Sb in the melt inclusions (n = 52), 4200 ppm As and 875 ppm Sb in the fluid inclusions (n = 25) (Mustard et al., 2004); 306 ppm As and 20.6 ppm Sb in the melt inclusions (n = 14), 430 ppm As and 112 ppm Sb in the fluid inclusions (n = 10) (Audetat et al., 2000a).

2.7 Acknowledgements

We thank Menghua Liu and Mark Biesinger very much for their help in EMPA and XPS analysis and interpretation. Ralph Dickhout's help in IC analysis and Fred Blain's helpful comments are appreciated.

2.8 References

Audetat A., Gunther D., and Heinrich C. A. (2000a), Magmatic-hydrothermal evolution in a fractionating granite: A microchemical study of the Sn-W-F-mineralized Mole Granite (Australia). Geochim. Cosmochim. Acta 64, No. 19, pp. 3373-3393.

Audetat A., Gunther D., and Heinrich C. A. (2000b), Causes for large-scale metal zonation around mineralized plutons: fluid inclusion LA-ICP-MS evidence from the Mole Granite, Australia, Economic Geology, Vol. 95, No. 8, pp. 1563-1581.

Audetat A. and Pettke T. (2003), The Magmatic-hydrothermal evolution of two barren granites: A melt and fluid inclusion study of the Rito del Medio and Canada Pinabete plutons in northern New Mexica (USA), Geochim. Cosmochim. Acta 67, No. 1, pp. 97-121.

Bai T.B. and Koster van Groos, A.F. (1999), The distribution of Na, K, Rb, Sr, Al, Ge, Cu, W, Mo, La, and Ce between granitic melts and coexisting aqueous fluids, Geochim. Cosmochim. Acta 63, no.7-8, pp.1117-1131.

Ballantyne J.M. and Moore J.N. (1998), Arsenic geochemistry in geothermal systems, Geochim. Cosmochim. Acta 52, pp. 475-483.

Benvenutti E.V., Gushikem Y., Vasquez A., de Castro S.C., and Zaldivar G.A.P. (1991), X-ray photoelectron spectroscopy and mossbauer spectroscopy study of iron(III) and antimony(V) oxides grafted onto a silica gel surface, Chemical Communications, vol. 19, pp 1325-1327.

Beuchat S., Moritz R., and Pettke T. (2004), Fluid evolution in the W-Cu-Zn-Pb San Cristobal vein, Peru: fluid inclusion and stable isotope evidence, Chemical Geology, 210, 201-224.

Boyle R.W. and Jonasson I.R. (1973), The geochemistry of Arsenic and its use as an indicator element in geochemical prospecting, Journal of Geochemical Exploration, Vol. 2, pp. 251-296.

Boyle R.W. and Jonasson I.R. (1984), The geochemistry of Antimony and its use as an indicator element in geochemical prospecting, Journal of Geochemical Exploration, Vol. 20, pp. 223-302.

Candela P.A. and Holland H.D. (1984), The partitioning of copper and molybdenum between silicate melts and aqueous fluids, Geochim. Cosmochim. Acta 63, 373-380.

Chevychelov V.Yu. and Chevychelova T.K. (1997), Partitioning of Pb, Zn, W, Mo, Cl, and major elements between aqueous fluid and melt in the systems granodiorite (granite, leucogranite) – H2O – NaCl – HCl, N. Jb. Miner. Abh., Vol. 172, pp. 101-115.

Chou I.M. and Eugster H.P. (1976), A sensor for hydrogen fugacities at elevated P and T and applications. EOS Transactions of American Geophysical Union, 57, 340.

Chou I.M. (1987), Oxygen buffer and hydrogen sensor techniques at elevated pressures and temperatures. In Hydrothermal Experimental Techniques, Ulmer, G.C., and Barnes, H.L., Eds., p. 61-99, Wiley, NY.

Dickenson M.P., and Hess P.C., The structural role and homogeneous redox equilibria of iron in peraluminous, metaluminous and peralkaline silicate melts, Contributions to Mineralogy and Petrology 92, 207-217.

Egdell R.G., Rebane J., Walker T.J., and Law D.S.L. (1991), Cometition between initial- and final-state effects in valence- and core-level x-ray photoemission of Sb-doped SnO_2, Physical Review B 59, 1792-1799.

Ellison A.J. and Hess P.C. (1988), Peraluminous and peralkaline effects upon monazite solubility in high silica liquids, EOS, Vol. 69, 498.

Frank M. R., Candela P. A., Piccoli P. M., and Glascock M. D. (2002), Gold solubility, speciation, and partitioning as a function of HCl in the brine-silicate melt-metallic gold system at 800C and 100 MPa. Geochim. Cosmochim. Acta 66, No. 21, pp. 3719-3732.

Fullston D., Fornasiero D., Ralston J. (1999), Oxidation of synthetic and natural samples of enargite and tennantite. 2. X-ray photoelectron spectroscopic study, Langmuir, Vol. 15, pp. 4530-4536.

Heinrich C.A. and Eadinton P.J. (1986), Thermodynamic predictions of the hydrothermal chemistry of arsenic, and their significance for the paragenetic sequence of some cassiterite-arsenopyrite-base metal slfide deposits, Economic Geology 81, 511-529.

Heinrich C.A., Günther D., Audétat A., Ulrich T., and Frischknecht R. (1999), Metal fractionation between magmatic brine and vapor, determined by microanalysis of fluid inclusions, Geology 27, 755-758.

Hess P.C. (1991), The role of high field strength cations in silicate melts, in Physical Chemistry of Magmas, Advances in Physical Geochemistry, Eds. Perchuk, L.L. and Kushiro, I., Vol. 9, pp.152-191.

Hirschmann M.M., and Ghiorso M.S. (1994), Activities of nickel, cobalt, and manganese silicates in magmatic liquids and applications to olivine/liquid and to silicate/metal partitioning, Geochim. Cosmochim. Acta 58, 4109-4126.

Johnson J.W., Oelkers E.H. and Helgeson H.C. (1992) SUPCRT92: A software package for calculating the standard molal thermodynamic properties of minerals, gases, aqueous species and reactions from 1 to 5000 bar and 0 to 1000ºC, Computers & Geosciences., Vol. 18, pp. 899-947.

Keppler H. (1994), Partitioning of phosphorus between melt and fluid in the system haplogranite-H_2O-P_2O_5, Chemical Geology, Vol. 117, pp. 345-353.

Keppler H. and Wyllie P.J. (1991), Partitioning of Cu, Sn, Mo, W, U, and Th between melt and aqueous fluid in the systems haplogranite-H_2O-HCl and haplogranite-H_2O-HF, Contributions to Mineralogy and Petrology, Vol. 109, pp. 139-150.

Khitarov N.I., Malinin S.P., Lebedev Y.B., and Shibayeva N.P. (1982), The distribution of Zn, Cu, Pb, and Mo between a fluid phase and a silicate melt of granitic composition at high temperatures and pressures, Geochemistry International, vol.19, no.4, pp.123-136.

Klemme S., Prowatke S., Hametner K., and Gunther D. (2005), Partitioning of trace elements between rutile and silicate melts: Implications for subduction zones, Geochim. Cosmochim. Acta 69, pp. 2361-2371.

Kravchuk I.F., Malinin S.D., and Dernov-Pegarev V.F. (1997), Tungsten behavior in a silicic fluid-magma system: experimental data, Geochemistry International, Vol. 35, No. 12, pp. 1083-1088.

Kravchuk I.F., Malinin S.D., Senin V.G. and Dernov-Pegarev V.F. (2000), Molybdenum partition between melts of natural and synthetic aluminosilicates and aqueous-salt fluids, Geochemistry International, Vol. 38, No. 2, pp. 157-165.

London D., Hervig R.L. and Morgan VI G.B. (1988), Melt-vapor solubilities and elemental partitioning in peraluminous granite-pegmatite systems: experimental results with Macusani glass at 200 MPa, Contributions to Mineralogy and Petrology, Vol. 99, pp. 360-373.

Manning D.A.C. and Henderson P. (1984), The behaviour of tungsten in granitic melt-vapour systems, Contrib Mineral Petrol, 86, 286-293.

Matthews W., Linnen R.L., and Guo Q. (2003), A filler-rod technique for controlling redox conditions in cold-seal pressure vessels. Am. Mineral. 88, 701-707.

Mitsunobu S., Harada T., and Takahashi Y. (2006), Comparison of Antimony Behavior with that of Arsenic under Various Soil Redox Conditions, Environmental Science and Technology 40, 7270-7276.

Montel J.C. (1986), Experimental determination of the solubility of Ce-monazite in SiO_2-Al_2O_3-K_2O-Na_2O melts at 800 °C, 2 kbar, under H_2O-saturated conditions, Geology, Vol. 14, pp. 659-662.

Muller B., Frischknecht R., Seward T.M., Heinrich C.A., and Gallegos W.C. (2001), A fluid inclusion reconnaissance study of the Huanuni tin deposit (Bolivia), using LA-ICP-MS micro-analysis, Mineralium Deposita 36, 680-688.

Mustard R., Ulrich T. and Mernagh T. (2004), The partitioning of gold and other metals between co-existing silicate melt and CO_2-rich low-salinity aqueous fluid at the magmatic–hydrothermal transition, Geological Society of Australia Abstracts 73, 104.

Nesbitt H.W., Muir I.J., and Pratt A.R. (1995), Oxidation of arsenopyrite by air and air-saturated, distilled water, and implications for mechanism of oxidation. Geochim. Cosmochim. Acta 59, 1773–1786.

Nesbitt H. W., Canning G. W., Bancroft G.M. (1998), XPS study of reductive dissolution of 7Å-birnessite by H_3AsO_3 with constraints on reaction mechanism, Geochim. Cosmochim. Acta 62, pp. 2097-2110.

Noble D.D., Ressel M.W., Lechler P.J. and Connors K.A. (2004), Magmatic As, Sb, Cs, Bi, Tl, and other elements in glassy volcanic rocks of the Julcani District, Peru, and Carlin Trend, Nevada, Boletin de la Sociedad Geologica del Peru, Vol. 97, pp. 29-50.

Noll P.D.Jr, Newsom H.E., Leeman W.P., and Ryan J.G. (1996), The role of hydrothermal fluids in the production of subduction zone magmas: Evidence from siderophile and chalcophile trace elements and boron, Geochim. Cosmochim. Acta 60, No. 4, pp. 587-611.

Nordstrom D.K., McCleskey R. B., and Ball J. W. (2001), Processes governing arsenic geochemistry in the thermal waters of Yellowstone National Park. USGS Workshop on Arsenic in the Environment, Denver, CO, Feb. 21-22.

Ouvrard S., Donato P., Simonnot M.O., Begin S., Ghanbaja J., Alnot M., Duval Y.B., Lhote F., Barres O., Sardin M. (2005), Natural manganese oxide: Combined analytical approach for solid characterization and arsenic retention, Geochim. Cosmochim. Acta. 69, pp. 2715-2724.

Pouchou, J.L., and Pichoir, F. (1985), "PAP" correction procedure for improved quantitative microanalysis. In J.T. Armstrong, Ed., Microbeam analysis, p. 104-106. San Francisco Press, California.

Pokrovski G, Gout R., Schott J. Zotov A., and Harrichoury J. (1996) Thermodynamic properties and stoichiometry of As(III) hydroxide complexes at hydrothermal conditions, Geochim. Cosmochim. Acta 50, No. 5, pp. 737-749.

Pokrovski G.S., Borisova A.Y., Roux J., Hazemann J-L, Petdang A., Tella M., and Testemale D. (2006), Antimony speciation in saline hydrothermal fluids: A combined X-ray absorption fine structure spectroscopy and solubility study, Geochim. Cosmochim. Acta 70, 4196-4214.

Righter K., Hill D., Collins J., Capobianco C.J., and Drake M.J. (2001), Experimental studies of metal-silicate partitioning of Sb, Meteoritics and Planetary Sciences, 36 Suppl. A 5401.

Sherman D.M., Ragnarsdottir K.V., Oelkers E.H. (2000), Antimony transport in hydrothermal solutions: an EXAFS study of antimony(V) complexation in alkaline sulfide and sulfide-chloride brines at temperatures from 25 °C to 300 °C at Psat, Chemical Geology 167, 161-167.

Shirley D.A. (1972), High-Resolution X-Ray Photoemission Spectrum of the Valence Bands of Gold, Physical Review B 5, 4709-4714.

Simon A.C., Pettke T., Candela P.A., Piccoli P.M., and Heinrich C.A. (2007), The partitioning behavior of As and Au in S-free and S-bearing magmatic assemblages, Geochim. Cosmochim. Acta 71, 1764-1782.

Smedley P.L. and Kinniburgh D.G. (2002), A review of the source, behaviour and distribution of arsenic in natural waters, Applied Geochemistry, Vol. 17, pp. 517-568.

Spycher N.F. and Reed M.H. (1989), As(III) and Sb(III) sulfide complexes: An evaluation of stoichiometry and stability from existing experimental data, Geochim. Cosmochim. Acta Acta 53, 2185-2194.

Tossell J.A. (2000), Theoretical studies on metal thioarsenites and thioantimonides: synergistic interactions between transition metals and heavy metalloids, Geochemical Transactions, Vol. 3.

Verweij H. (1981), Raman study of Arsenic-containing potassium silicate glasses, Journal of the American Ceramic Society, Vol. 64, No. 8, pp. 493-498.

Williams-Jones A.E. and Normand C. (1997), Controls of Mineral Parageneses in the system Fe-Sb-S-O, Economic Geology 92, 308-324.

Wood S.A. (1989), Raman spectroscopic determination of the speciation of ore metals in hydrothermal solutions: I. Speciation of antimony in alkaline sulfide solutions at 25 °C, Geochim. Cosmochim. Acta 53, 237-244.

Wood S.A. (1992), Experimental determination of the solubility of WO_3(s) and the thermodynamic properties of H_2WO_4(aq) in the range 300–600 °C at 1 kbar: Calculation of scheelite solubility, Geochim. Cosmochim. Acta 56, 1821-1836.

Zack T., Kronz A., Foley S.F., and Rivers T. (2002), Trace element abundances I rutiles from eclogites and associated garnet mica schists, Chemical Geology 184, 97-122.

Zotov A.V., Kudrin A.V., Levin K.A., Shikina N.D., and Var'yash L.N. (1995), Experimental studies of the solubility and complexing of selected ore elements (Au, Ag, Cu, Mo, As, Sb, Hg) in aqueous solutions. In Fluids in the Crest: Equlibrium an Transport Properties (eds. Shmulovich K.I., Yardley B.W.D., and Gonchar G.G.), pp. 95-137, Chapman and Hall.

Zotov A.V., Shikina N.D., and Akinfiev N.N. (2003), Thermodynamic properties of the Sb(III) hydroxide complex $Sb(OH)_3(aq)$ at hydrothermal conditions, Geochim. Cosmochim. Acta 67, No. 10, pp. 1821-1836.

Table 2.1 Normalized compositions of starting synthetic glasses

SiO_2 wt%	Al_2O_3 wt%	K_2O wt%	Na_2O wt%	Total	ASI[a]
Constant ASI series					
77.09	13.23	5.25	4.42	100.00	0.99
73.65	15.33	5.97	5.05	100.00	1.00
68.73	18.27	7.02	5.99	100.00	1.01
63.63	21.19	8.09	7.10	100.00	1.01
58.01	23.90	9.17	8.05	100.00	1.00
Constant SiO_2 series					
78.11	10.08	6.50	5.31	100.00	0.61
77.45	11.83	5.88	4.84	100.00	0.79
77.18	12.58	5.53	4.72	100.00	0.89
77.13	13.69	5.23	3.96	100.00	1.06
76.82	14.54	4.70	3.94	100.00	1.21
76.99	14.70	4.48	3.83	100.00	1.28

[a] Aluminum saturation index = molar ratio $[Al_2O_3/(K_2O+Na_2O)]$

Table 2.2 EPMA analysis of major elements and As in run product glasses [a]

Run number	Run time (days)	SiO_2 wt% (±1σ)	Al_2O_3 wt% (±1σ)	K_2O wt% (±1σ)	Na_2O wt% (±1σ)	As_2O_3 wt% (±1σ)	Total (±1σ)	ASI of starting glass	ASI of product glass
As-1	7	67.44	10.89	7.47	3.73	4.58	94.10	0.99	0.67
		(0.12)	(0.15)	(0.29)	(0.10)	(0.2)	(0.44)		
As-2	7	63.05	10.68	9.02	3.29	7.06	93.10	0.99	0.58
		(0.22)	(0.04)	(0.39)	(0.02)	(0.64)	(0.84)		
As-3	14	60.62	19.88	7.81	6.32	0.57	95.20	0.99	1.01
		(0.59)	(0.25)	(0.13)	(0.07)	(0.09)	(0.19)		
As-4	14	72.89	12.08	4.25	4.00	0.05	93.26	0.99	1.07
		(0.65)	(0.19)	(0.16)	(0.02)	(0.01)	(0.87)		
As-5	7	69.98	11.50	6.20	3.76	2.46	93.90	0.99	0.81
		(0.26)	(0.06)	(0.22)	(0.13)	(0.16)	(0.54)		
As-6[b]	7	67.35	11.25	6.60	3.62	2.32	91.13	0.67	0.76
		(0.33)	(0.28)	(0.26)	(0.12)	(0.20)	(0.89)		
As-7[b]	7	68.42	11.55	7.68	3.61	2.39	93.66	0.67	0.70
		(0.42)	(0.18)	(0.14)	(0.05)	(0.06)	(0.56)		
As-8	7	72.32	11.13	5.66	4.34	0.53	93.99	0.79	0.79
		(0.38)	(0.08)	(0.15)	(0.04)	(0.04)	(0.40)		
As-9	7	72.96	11.95	5.20	4.16	0.41	94.68	0.89	0.92
		(0.77)	(0.21)	(0.17)	(0.14)	(0.07)	(0.78)		
As-10[b]	7	66.61	11.15	6.59	3.58	3.02	90.95	0.67	0.76
		(0.35)	(0.13)	(0.15)	(0.10)	(0.31)	(0.52)		
As-11	8	61.28	15.33	7.61	5.27	3.20	92.70	1.01	0.84
		(0.26)	(0.13)	(0.17)	(0.08)	(0.39)	(0.47)		
As-12	7	72.24	13.49	4.03	3.38	0.39	93.54	1.28	1.31
		(0.29)	(0.13)	(0.22)	(0.06)	(0.04)	(0.19)		
As-13	7	72.38	9.25	5.82	4.71	0.48	92.65	0.61	0.63
		(0.97)	(0.22)	(0.47)	(0.06)	(0.07)	(0.79)		
As-14	10	68.79	13.88	5.14	4.62	0.42	92.84	1.00	1.03
		(0.36)	(0.38)	(0.32)	(0.07)	(0.10)	(0.41)		

[a] Each element was analyzed 5 to 15 times for each sample.
[b] Reverse experiments.

Table 2.3 Partition coefficient of As between co-existing aqueous fluid and melt at 800°C and 200 MPa.

Run number	As in fluid (±1σ) wt%		As in glass (±1σ) wt%		$D_{As}^{f/m}$	(±1σ)
As-1	4.877	(0.487)	3.471	(0.154)	1.41	(0.15)
As-2	5.413	(0.541)	5.152	(0.116)	1.05	(0.14)
As-3	0.467	(0.047)	0.430	(0.066)	1.09	(0.26)
As-4	0.075	(0.008)	0.035	(0.007)	2.14	(0.32)
As-5	2.483	(0.248)	1.860	(0.120)	1.33	(0.17)
As-6[a]	1.880	(0.188)	1.755	(0.149)	1.07	(0.18)
As-7[a]	2.394	(0.239)	1.809	(0.048)	1.32	(0.15)
As-8	0.477	(0.048)	0.400	(0.032)	1.19	(0.18)
As-9	0.727	(0.073)	0.312	(0.052)	2.33	(0.27)
As-10[a]	1.577	(0.158)	2.286	(0.231)	0.69	(0.20)
As-11	1.471	(0.147)	2.421	(0.297)	0.61	(0.22)
As-12	0.444	(0.044)	0.298	(0.032)	1.49	(0.21)
As-13	0.540	(0.054)	0.364	(0.054)	1.48	(0.25)
As-14	0.705	(0.071)	0.314	(0.078)	2.25	(0.38)

[a] Reverse experiments.

Table 2.4 Arsenic partition coefficient, ASI and SiO_2 of melt, oxygen fugacity, and As in the system.[a]

Run number	$D_{As}^{f/m}$	ASI	SiO_2 wt%	$\log f_{O_2}$ (bar)	As in system [b] wt%
ASI series					
As-13	1.48	0.63	72.38	-10.3	0.412
As-8	1.19	0.79	72.32	-9.0	0.423
As-9	2.33	0.92	72.96	-9.1	0.417
As-12	1.49	1.31	72.24	-9.8	0.387
SiO_2 series					
As-8	1.19	0.79	72.32	-9.0	0.423
As-9	2.33	0.92	72.96	-9.1	0.417
As-14	2.25	1.03	68.79	-8.4	0.393
As-3	1.09	1.01	60.62	-9.2	0.407
f_{O_2} series					
As-5	1.33	0.81	69.98	-8.4	1.904
As-10	0.69	0.76	66.61	-9.4	1.861
As-2	1.05	0.58	63.05	-10.1	4.623
As-1	1.41	0.67	67.44	-10.5	2.741
As-11	0.61	0.84	61.28	-12.0	2.169
As-6	1.07	0.76	67.35	-12.2	1.817
As-7	1.32	0.70	68.42	-12.2	1.820
Henry's Law series (includes all of above plus As-4)					
As-4	2.14	1.07	72.89	-9.27	0.043

[a] Some experiments are listed repeatedly in different series.
[b] As in system = As mass / (melt mass + fluid mass)

Table 2.5 Arsenic mass and concentration of reduced experiments

Exp ID	As bf exp (mg)	As aft exp (mg)	As in glass (wt%)	As in fluid (wt%)	Log fO2
As-21	0.17	0.00	BD[a]	0.001	-17.0
As-22	0.17	0.04	0.173	0.007	-15.1
As-23	0.17	0.01	0.035	0.002	-15.0
As-24	0.18	0.03	0.130	0.001	-13.8
As-25	0.93	0.20	0.904	0.689	-12.9

[a] below the minimum detection limit.

Table 2.6 EPMA analysis of major elements and Sb in run product glasses

Run number	Run time (days)	SiO_2 wt% (±1σ)	Al_2O_3 wt% (±1σ)	Na_2O wt% (±1σ)	K_2O wt% (±1σ)	Sb_2O_5 wt% (±1σ)	Total (±1σ)	Final ASI
Sb-1	7	72.59	12.63	4.29	4.77	0.62	94.91	1.03
		0.49	0.04	0.11	0.29	0.02	0.41	
Sb-2	7	71.57	11.98	4.32	4.13	0.89	92.90	1.04
		0.24	0.12	0.22	0.14	0.19	0.34	
Sb-3	14	63.98	16.40	5.47	5.99	1.16	93.01	1.06
		0.13	0.11	0.20	0.14	0.20	0.37	
Sb-4	14	71.85	10.80	4.78	4.69	1.12	93.24	0.84
		0.34	0.09	0.31	0.07	0.10	0.45	
Sb-5	14	71.79	11.92	4.43	4.25	0.74	93.14	1.00
		0.41	0.19	0.18	0.06	0.13	0.58	
Sb-6	14	59.25	19.23	7.10	6.65	1.08	93.31	1.02
		0.24	0.15	0.17	0.09	0.14	0.30	
Sb-7	14	71.58	12.99	3.44	3.92	0.59	92.52	1.31
		0.61	0.17	0.13	0.01	0.02	0.70	
Sb-8	14	71.57	13.07	3.45	4.08	0.91	93.08	1.30
		0.41	0.18	0.17	0.07	0.12	0.35	
Sb-9	14	55.21	21.84	7.49	7.63	1.09	93.26	1.06
		0.14	0.05	0.31	0.11	0.02	0.50	
Sb-10	14	70.84	8.93	4.96	5.12	1.36	91.22	0.65
		0.36	0.16	0.11	0.11	0.04	0.56	
Sb-11	14	71.13	9.05	5.08	5.22	1.39	91.88	0.65
		0.24	0.10	0.35	0.09	0.04	0.45	
Sb-12	11	71.20	11.98	4.34	4.54	1.17	93.23	0.99
		0.19	0.06	0.30	0.04	0.21	0.38	

Table 2.7 Partition coefficient of Sb between co-existing aqueous fluid and melt at 800°C and 200 MPa.

Run number	Sb in glass (±1σ) wt%		Calc. Sb in fluid* wt%	$D_{Sb}^{f/m}$ (±1σ)	
Sb-1	0.468	(0.018)	0.160	0.34	(0.01)
Sb-2	0.731	(0.143)	0.188	0.26	(0.05)
Sb-3	0.873	(0.148)	0.329	0.38	(0.06)
Sb-4	0.846	(0.074)	0.319	0.38	(0.03)
Sb-5	0.559	(0.095)	0.679	1.21	(0.21)
Sb-6	0.815	(0.104)	0.433	0.53	(0.07)
Sb-7	0.443	0.014	0.802	1.81	0.06
Sb-8	0.688	(0.083)	0.531	0.77	(0.09)
Sb-9	0.824	(0.012)	0.400	0.49	(0.01)
Sb-10	1.026	(0.031)	0.113	0.11	(0.00)
Sb-11	1.050	(0.028)	0.107	0.10	(0.00)
Sb-12	0.881	(0.158)	1.107	1.26	(0.23)

* Calc. Sb in fluid = ($Sb_{starting}$ – Sb in glass * glass mass) / fluid mass

Table 2.8 Antimony partition coefficient, ASI and SiO_2 of melt, and oxygen fugacity.

Run number	$D_{Sb}^{f/m}$	ASI	SiO2 wt%	$\log f_{O_2}$
f_{O_2} series				
Sb-1	0.34	1.03	72.59	-7.9
Sb-5	1.21	1.00	71.79	-9.6
Sb-12	1.26	0.99	71.20	-16.5
Sb-2	0.26	1.04	71.57	-16.8
SiO_2 series				
Sb-1	0.34	1.03	72.59	-7.9
Sb-5	1.21	1.00	71.79	-9.6
Sb-2	0.26	1.04	71.57	-16.8
Sb-12	1.26	0.99	71.20	-16.5
Sb-3	0.38	1.06	63.98	-10.5
Sb-6	0.53	1.02	59.25	-9.3
Sb-9	0.49	1.06	55.21	-10.1
ASI series				
Sb-10	0.11	0.65	70.84	-9.5
Sb-11	0.10	0.65	71.13	-9.5
Sb-4	0.38	0.89	71.80	-9.0
Sb-5	1.21	1.00	71.79	-9.6
Sb-8	0.77	1.30	71.57	-9.7
Sb-7	1.81	1.31	71.58	-11.83

Note: some experiments are listed repeatedly in different series.

Table 2.9 Binding energies, peak full width at half maximum (FWHM), and peak areas for As(3d) XPS spectra

BE (eV)[a]	FWHM (eV)	Species
As-2		
44.20	1.79	As(III)
As-6		
44.41	1.79	As(III)
References[b]		
44.54	0.95	As(III)
45.28	0.95	As(V)

[a] Binding energy is the peak locations of $As3d_{5/2}$ and were charge corrected to the main peak of the carbon 1s spectrum set to 285.0 eV.
[b] Nesbitt et al. (1995)

Table 2.10 Binding energies and peak full width at half maximum (FWHM) for $Sb(3d_{3/2})$ XPS spectra

BE (eV)[a]	FWHM (eV)	Species
Sb-10		
540.36	1.30	Sb(V)
Sb-1		
540.79	1.40	Sb(V)
539.71	1.40	Sb(III)
Reference material		
539.83	1.06	Sb_2O_3
540.20	1.40	$KSbO_3$
539.9	2.0	Sb_2O_3 [b]
540.9	2.0	Sb_2O_5 [b]

[a] Binding energy is the peak locations of $Sb3d_{3/2}$ and were charge corrected to the main peak of the carbon 1s spectrum set to 285.0 eV.
[b] Benvenutti et al. (1991)

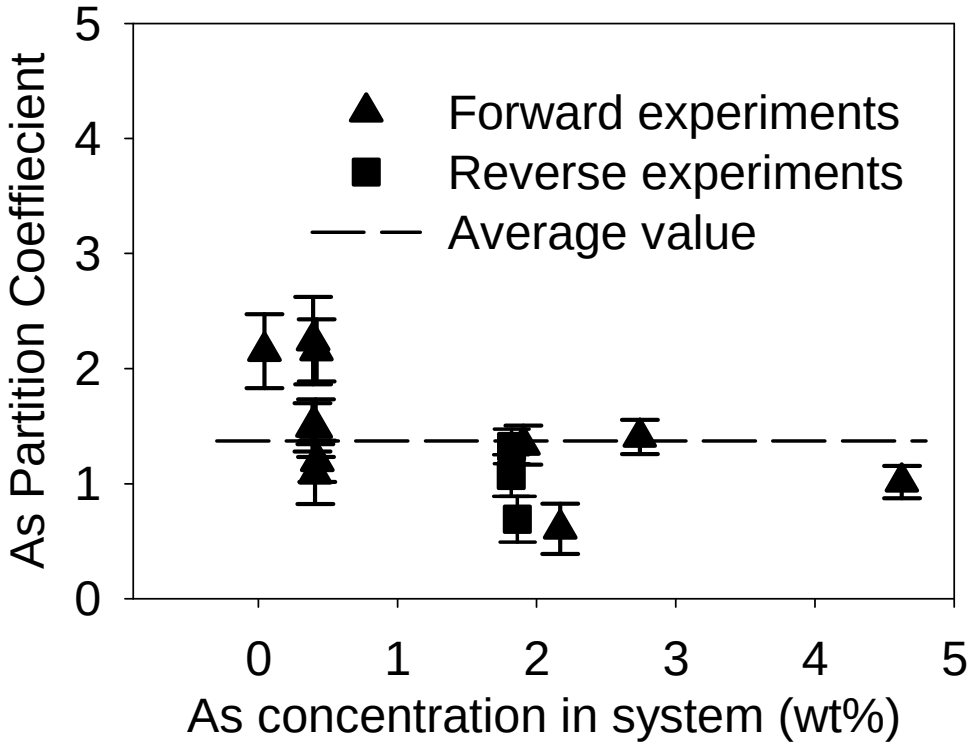

Figure 2.1 Arsenic concentration in system has no effect on As partitioning between granitic melt and fluid at 800 °C and 200 MPa, with $\log f_{O_2}$ ranging from -8.4 to -12.2. The triangles are forward experiments and the squares are reverse experiments. The average value ($\pm 1\sigma$) of As partition coefficients is 1.4 ± 0.5, shown as the dashed line.

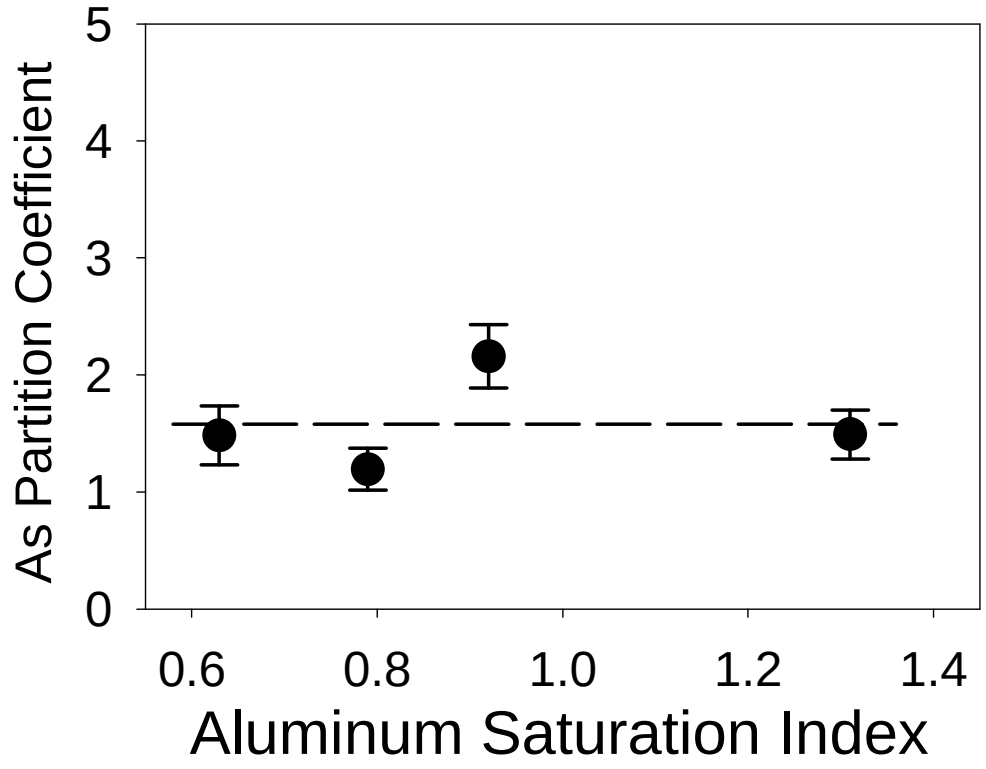

Figure 2.2 ASI of the melt has no effect on As partitioning between granitic melt and fluid at 800 °C and 200 MPa, with SiO_2 content ranging from 72.24 to 72.96 wt% and $\log f_{O_2}$ from -10.3 to -9.0. The average value (± 1σ) of As partition coefficients is 1.6 ± 0.4, shown as the dashed line.

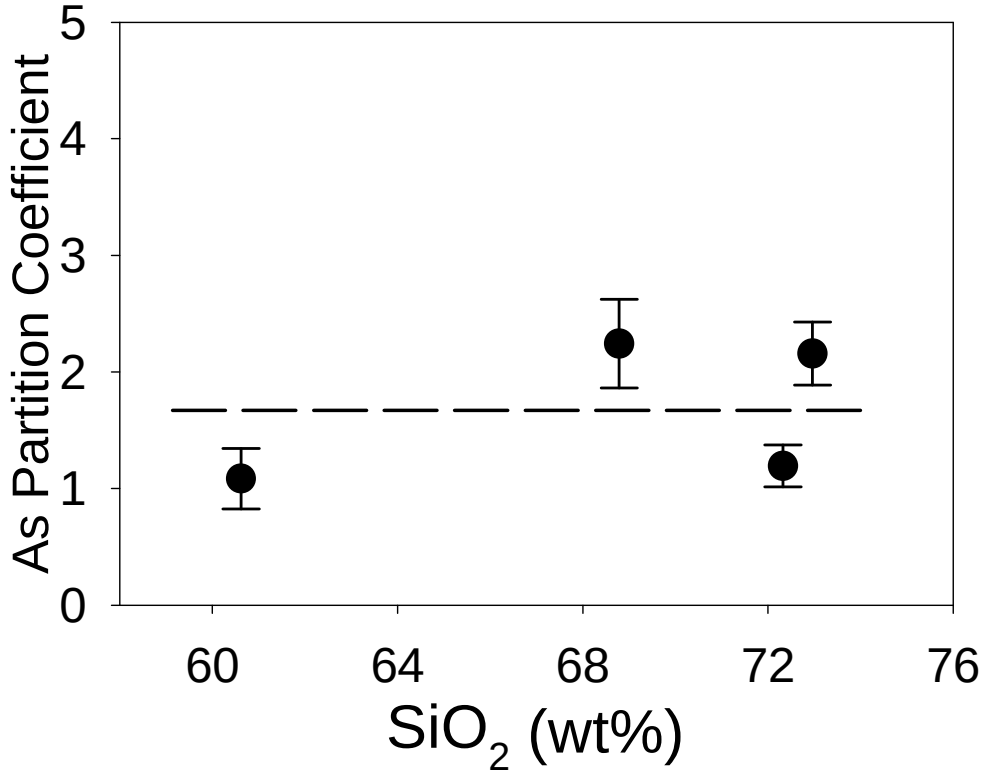

Figure 2.3 SiO_2 content of the melt has no effect on As partitioning between melt and fluid at 800 °C and 200 MPa, with $\log f_{O_2}$ ranging from -9.2 to -8.4. The average value ($\pm 1\sigma$) of As partition coefficients is 1.7 ± 0.6, shown as the dashed line.

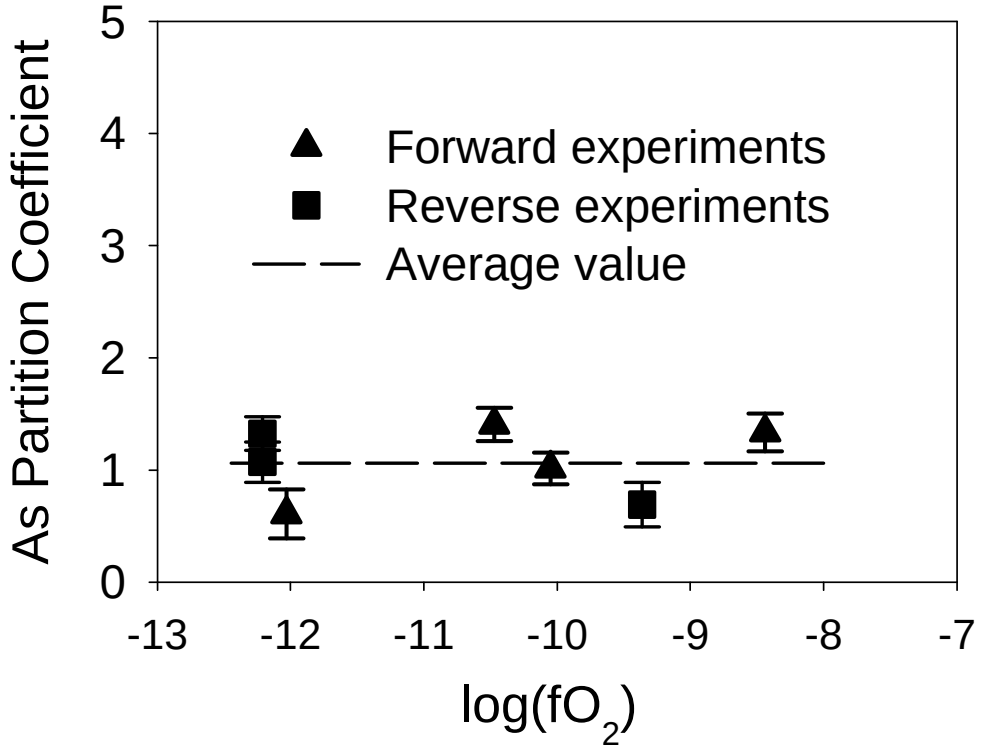

Figure 2.4 Oxygen fugacity (f_{O_2}) has no effect on As partitioning between granitic melt and fluid at 800 °C and 200 MPa. The triangles are forward experiments and the squares are reverse experiments. The average value (± 1σ) of As partition coefficients is 1.1 ± 0.3, shown as the dashed line.

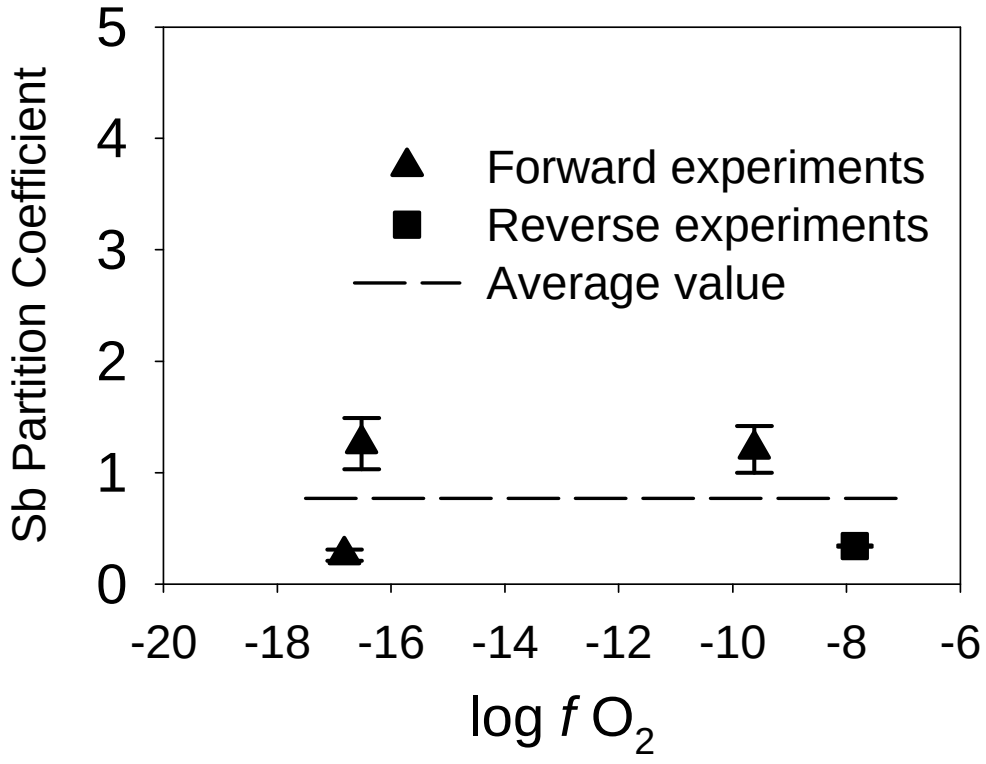

Figure 2.5. Oxygen fugacity (f_{O_2}) has no effect on Sb partitioning between granitic melt and fluid at 800 °C and 200 MPa, with ASI ranging from 0.99 to 1.04. The triangles are forward experiments and the square is a reverse experiment. The average value (± 1σ) of Sb partition coefficients is 0.8 ± 0.5, shown as the dashed line.

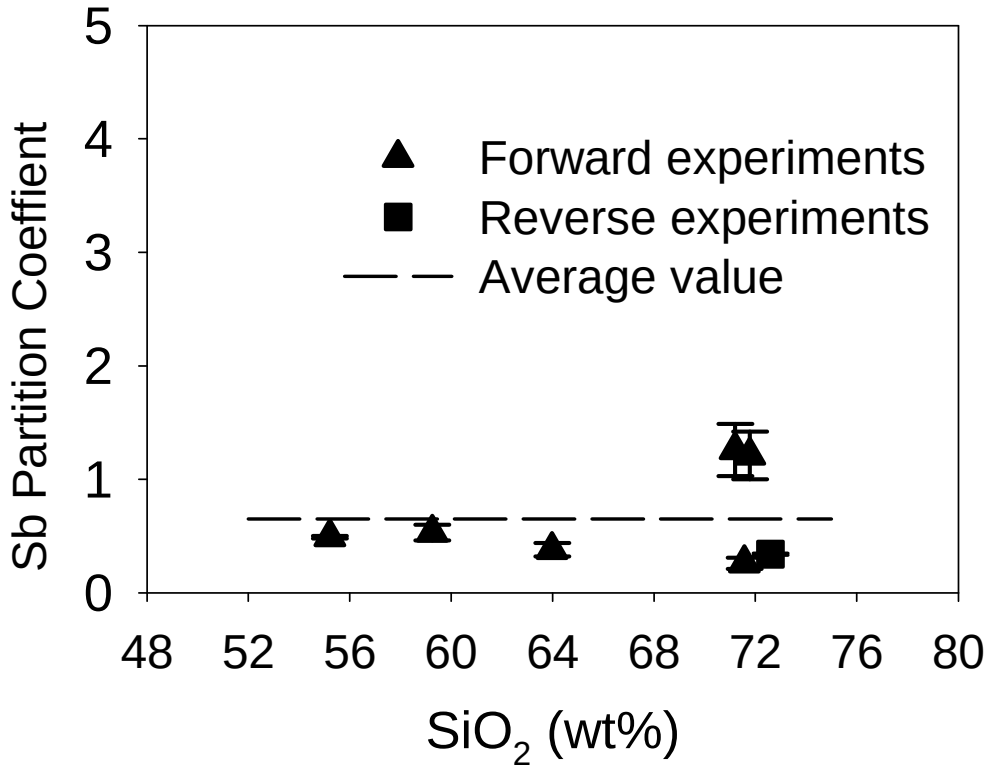

Figure 2.6 SiO_2 content of the melt has no effect on Sb partitioning between melt and fluid at 800 °C and 200 MPa, with ASI ranging from 0.99 to 1.06. The triangles are forward experiments and the square is a reverse experiment. The average value ($\pm 1\sigma$) of Sb partition coefficients is 0.7 ± 0.4, shown as the dashed line.

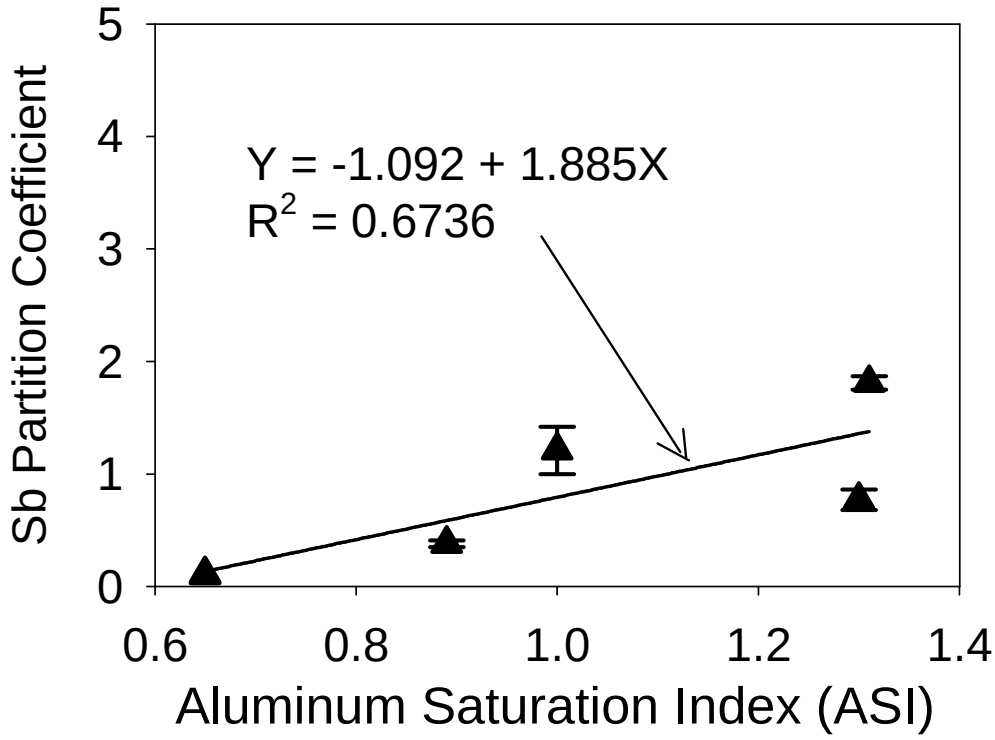

Figure 2.7 The data show a clear trend that Sb partition coefficient increases with increasing ASI of melt at 800 °C and 200 MPa, with SiO_2 content ranging from 70.84 to 71.80 wt%. All data points are from the forward experiments.

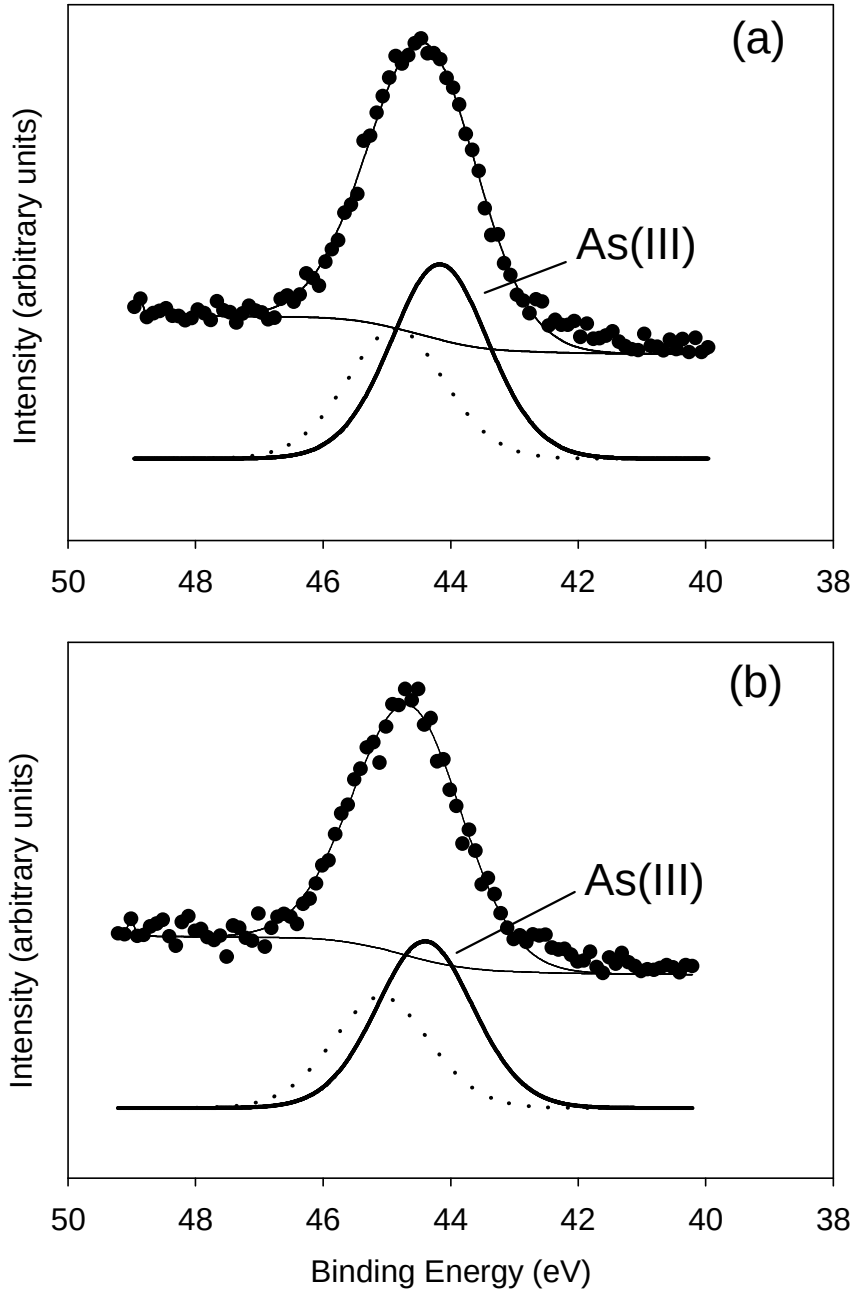

Figure 2.8. High resolution scan of As(3d) XPS spectra. The thin solid line is the fit curve which only has As(III) components. The spectra show that As(III) is the only species in the two run product glasses. The As $3d_{5/2}$ spectra of As(V) oxide species is at 45.3 eV (Nesbitt et al., 1995). (a) As-2; (b) As-6. Fit curves include As $3d_{5/2}$ (solid line) and As $3d_{3/2}$ (dotted line).

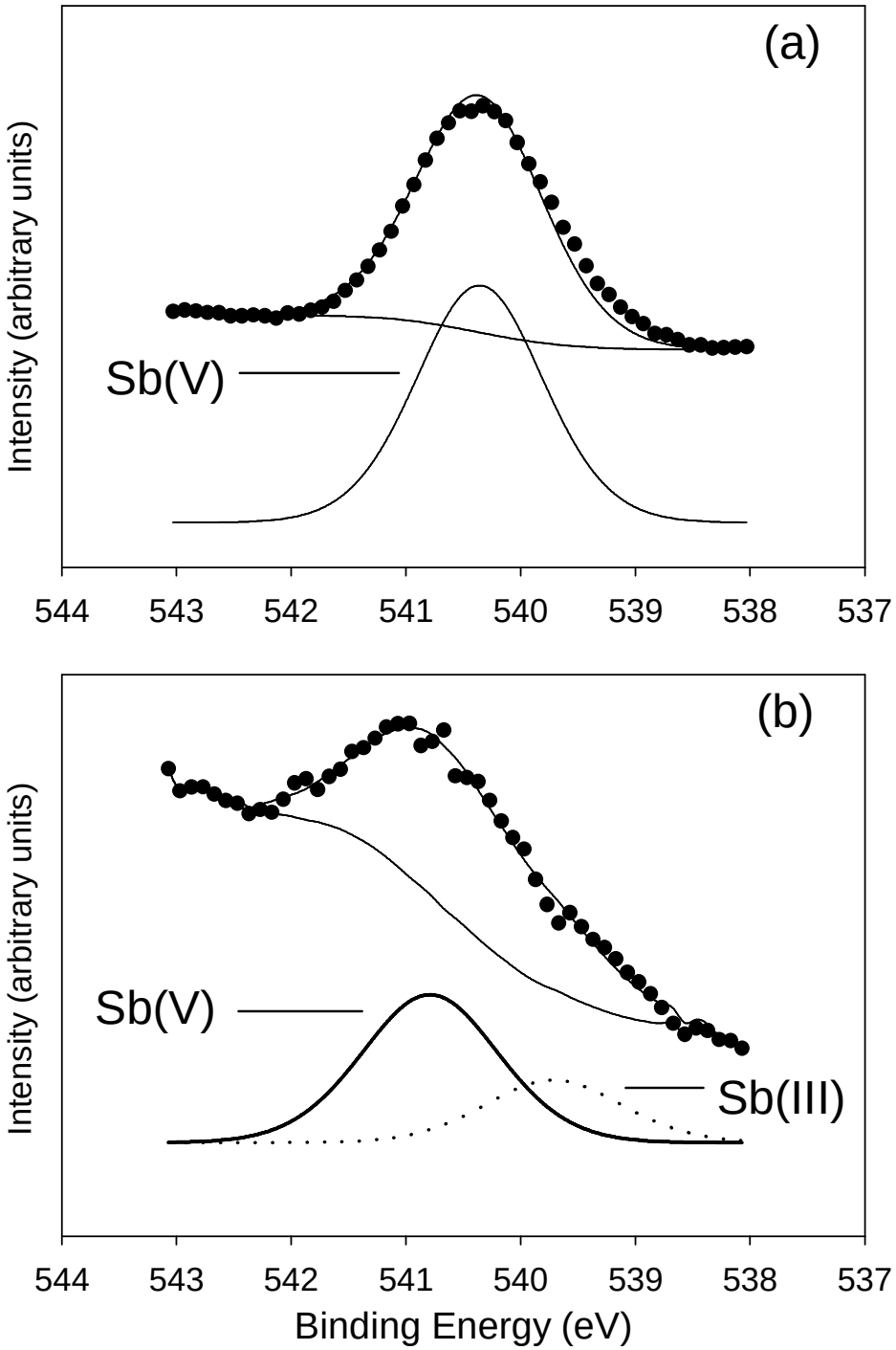

Figure 2.9. High resolution scan of Sb($3d_{3/2}$) XPS spectra. The thin solid line is the fit curve. The spectra show that Sb(V) is the only species in the glass sample of (a) Sb-10 and the dominant species in that of (b) Sb-1.

Chapter 3

Biogeochemistry of Two Types of Permeable Reactive Barriers, Organic Carbon and Iron-Bearing Organic Carbon: Column Experiments

3.1 Abstract

Permeable reactive barriers (PRBs) are an alternative technology to treat mine drainage containing sulfate and heavy metals. Two column experiments were conducted to assess the suitability of an organic carbon (OC) based reactive mixture and an Fe^0-bearing organic carbon (FeOC) based reactive mixture, under controlled groundwater flow conditions. The organic carbon mixture contains about 30% (volume) organic carbon and 70% (volume) sand and gravel. The Fe^0-bearing organic carbon mixture contains 10% (volume) zero-valent iron, 20% (volume) organic carbon, 10% (volume) limestone, and 60% (volume) sand and gravel. Simulated groundwater containing 380 ppm sulfate, 5 ppm As, and 0.5 ppm Sb was passed through the columns at flow rates of 64 (OC) and 62 (FeOC) mL d^{-1}, which are equivalent to 0.8 (OC) and 0.8 (FeOC) pore volume (PV) per week. The OC column showed an initial sulfate reduction rate of 0.4 μmol $g(oc)^{-1}$ d^{-1} and exhausted its capacity to promote sulfate reduction after 30 PV, or 9 months of flow. The FeOC column sustained a relative constant sulfate reduction rate of 0.9 μmol $g(oc)^{-1}$ d^{-1} for at least 65 PVs (17 months). In FeOC, the $\delta^{34}S$ values increase with the decreasing sulfate concentration. The sulfur isotope fractionation follows a Rayleigh fractionation

model with an enrichment factor of 21.6‰. The performance decline of OC column was caused by the depletion of substrate or electron donor. The cathodic production of H_2 by anaerobic corrosion of Fe probably sustained a higher level of SRB activity in FeOC column. These results suggest that zero-valent iron can also be used to provide an electron donor in sulfate reducing PRBs. A sharp increase in the $\delta^{13}C$ value of the dissolved inorganic carbon and a decrease in the concentration of HCO_3^- indicate hydrogenotrophic methanogenesis is occurring in the first 15 cm of the FeOC column. In the OC column a mildly increased $\delta^{13}C$ ratio for the dissolved inorganic carbon and an increase in HCO_3^- are attributed to acetotrophic methanogenesis.

3.2 Introduction

Permeable reactive barriers (PRBs) are a promising alternative technology for the in situ remediation of both organic and inorganic contaminants in groundwater, compared to the traditional pump and treat method (Scherer et al.,2000; Jambor et al., 2005). Zero-valent iron is a component of the reactive medium in many PRBs, about three-quarters of the current full-scale PRBs use iron metal as the reactant medium (Jambor et al., 2005). PRBs containing zero-valent iron can effectively remediate a variety of contaminants in groundwater including chlorinated solvents, inorganic contaminants, such as Cr, Se, U, As, and nitrate. Organic carbon (wood chips, paper mill pulp, municipal compost, etc.) has been used to treat acidic drainage at mine sites and groundwater contamination at industrial sites which is rich in sulfate and heavy metals (Benner et al. 1997, 1999, 2000). Under favourable conditions, sulfate-reducing bacteria (SRB) catalyze the oxidation of organic carbon coupled with the reduction of sulfate to sulfide through the following reaction:

$$SO_4^{2-} + 2CH_2O \rightarrow H_2S + 2HCO_3^- \quad (1)$$

where CH_2O represents simple organic compounds. Increased H_2S concentrations enhance the precipitation of metals as metal sulfides:

$$M^{2+} + S^{2-} \rightarrow MS \quad (2)$$

where M^{2+} denotes a divalent metal such as Fe, Cd, Ni, Cu, Co, and Zn. Rates of sulfate reduction, and metal removal capacity in organic carbon reactive barriers have been studied previously, as have changes in groundwater and solid phase geochemistry, and microbial communities in these systems (Benner et al. 1997, 2000; Herbert et al., 1998, 2000; Waybrant et al., 1998, 2002; Ludwig et al., 2002; Jambor et al., 2005; Logan et al., 2005).

A previous study combined zero-valent iron and organic carbon together to treat groundwater contaminated with sulfate and heavy metals at an industrial site near Vancouver, British Columbia. The lab tests prior to the installation of the full scale barrier showed that a mixture containing organic carbon and iron filings increased both the extent and the rate of sulfate reduction and metal removal, compared to the organic material alone (Mountjoy and Blowes, 2002). However, biogeochemical and isotopic changes coupled with microbial activity are not well understood.

The objectives of this study are: 1) to examine the microbiology and isotope geochemistry of organic carbon reactive mixture, 2) to examine the sulfate reduction rate, geochemistry, isotope geochemistry and microbiology of Fe^0-bearing organic carbon mixture, and 3) to compare the biogeochemical characteristics of the two reactive mixtures.

3.3 Experimental and Analytical Methods

3.3.1 Column Design and Experimental Setup

The experimental setup and procedures were similar to those used by Waybrant et al. (2000). Two acrylic columns (7.6 cm inner diameter, 41 cm long) were packed with silica sand, gravel, and reactive material (Table 3.1). The OC column contains 30% (volume) organic carbon and FeOC contains 10% (volume) zero-valent iron and 20% (volume) organic carbon. The organic carbon is composted leaf mulch obtained from a municipal recycling program. The zero-valent iron is from Connelly GPM Inc., Chicago, Il. Ottawa sand is coarse pure silica sand. The silica sand was added as an inert material, intended to maintain the permeability of the reactive mixture, and to retain the reactive material within the column. A thin layer (2 cm thick) of sediment, obtained from a stream flowing

through the University of Waterloo campus was added. This sediment, which was obtained from an area where sulfate reducing conditions were indicated by a strong odour of H_2S was added to provide a source of sulfate reducing bacteria to the column mixture.

Carbon dioxide gas was bubbled through the columns for twelve hours in order to displace the less soluble air from the pore spaces, and thereby increase the level of saturation of the column materials. The reactive mixtures were saturated with a solution containing 1000 mg/L SO_4 as $CaSO_4$ and 5% sodium lactate to help promote sulfate-reducing bacteria activity. The columns were transferred into an anaerobic glovebox. The anaerobicity of the glovebox was monitored regularly using methylene blue anaerobic strip indicators (GasPak).

The same simulated groundwater as the input solution was used for both columns. The chemical composition (Table 3.2) of the simulated groundwater was based on the water chemistry analysis of groundwater collected in January 1997 from monitoring well MMW5 at Getchell gold mine, Nevada (Tempel et al., 2000).

The pore volumes were 568 ml for OC and 556 ml for FeOC. A variable speed, multichannel pump (ISMATEC) was used to pump the influent through each of the columns. The column effluent solutions were collected in flow-though sample cells within the glovebox, and overflow was directed to waste jugs outside of the glovebox. Flow rates were determined by measuring the overflow. The average flow rate of OC was 64 ml day^{-1} or 17 m a^{-1} and that of FeOC was 62 ml day^{-1} or 17 m a^{-1}, which are equivalent to 0.8 (OC) and 0.8 (FeOC) pore volumes (PV) per week.

3.3.2 Geochemical Analysis

Each column has 15 sampling ports. Port 1 and 15 are 3 cm from the bottom and the top, respectively, and every two ports are separated by 2 cm. Samples from influent, effluent and various ports were collected within the glovebox for Eh, pH, anion, cation, and isotope analyses. Measurements of pH, Eh and alkalinity were determined immediately after sampling. The pH and Eh were measured on unfiltered samples in sealed cells outside of glovebox to minimize O_2 exposure. Some measurements were made inside the glovebox, but no difference was found between measurements inside and outside the glovebox. Electrode calibration and performance were checked before and after each sample measurement. The pH electrode (Orion pH 9107BN) was calibrated using standard 7.0 and 10.0 buffers (J.T. Baker), and the Eh electrode (Orion 9678BN) was checked using Zobell's solution.

Samples were filtered through a 0.45-μm cellulose acetate filter, and both acidified and nonacidified samples were collected and stored at 5ºC until analysed. Alkalinity was determined on the filtered samples using standardized H_2SO_4 and a Hach digital titrator. Concentrations of cations (Ca, Fe, K, Mg, Na, and Mn) and total S were determined using inductively coupled plasma atomic emission spectroscopy (ICP-AES), SO_4 analyses were conducted using ion chromatography (IC). Analyses were completed within 60 days unless otherwise specified. Dissolved S^{2-} was measured using a spectrophotometer (HACH DR/2010). Selected samples were also analyzed for $\delta^{34}S\text{-}SO_4$, $\delta^{18}O\text{-}SO_4$ and $\delta^{13}C\text{-}CO_3$ in the Environmental Isotope Laboratory at the University of Waterloo.

3.3.3 Solid Phase Analysis

At about PV 71, the experiment was terminated and solid samples were taken from both columns and dried in a vacuum desiccator inside the glovebox for x-ray

photoelectron spectroscopy (XPS) and x-ray absorption near edge spectroscopy (XANES) analyses. The XPS analysis was conducted using a Kratos Axis Ultra X-ray photoelectron spectrometer. XPS analyzes a surface area of 300 x 700 microns and probes the surface of the sample to a depth of 7-10 nanometers. All high-resolution spectra were charge-corrected to the main peak of the carbon 1s spectrum set to 285.0 eV. The XANES analysis was carried out at beamline X15B, National Synchrotron Light Source (NSLS) at Brookhaven National Laboratory (Upton, NY). Elemental sulfur (99.998%, Sigma-Aldrich,USA) was used as reference and the energy was calibrated at 2472 eV with this compound. Analysis conditions were similar to those of Einsiedl et al., (2007).

3.3.4 Microbiological Analysis

Microbial enumerations were conducted to assess the populations of sulfate-reducing bacteria (SRB), iron-reducing bacteria (IRB), and fermentative acid-producing bacteria (APB). The most probable number (MPN) technique (Cochran, 1950) was used to determine the number of bacteria. The procedures for enumerating SRB, IRB, and APB have been described in detail in Benner et al. (2000), Gould et al. (2003), and Hulshof et al. (2003), respectively. Spectrophotometric determination of the hydrolysis of fluorescein diacetate (FDA) (Schnurer et al., 1982) was also used to measure the general microbial activity in columns. Enumerations were conducted on samples of the column material immediately following the termination of the column experiments. For each column, 7 samples (Port 2, 4, 6, 8, 10, 12 and 14) were extracted.

3.3.5 Geochemical Modeling

The geochemical-speciation mass-transfer model MINTEQA2 (Allison et al., 1990) was used to assist in the interpretation of the water chemistry data and to indicate chemical equilibrium reactions potentially controlling the concentrations of dissolved constituents in column water. The MINTEQA2 thermodynamic database was modified to be consistent with the WATEQ4F database (Ball and Nordstrom, 1991).

3.4 Results and Discussion

3.4.1 Sulfate Reduction and ^{34}S

Sulfate concentration changes are quite different in the two columns. In the OC column, about 10% to 50% sulfate was removed in the first 20 PVs, after 30 PVs no removal was observed (Fig. 3.1). Sulfate concentration in the FeOC column decreased by about 50% consistently. The sulfate removal rate did not diminish after 65 PVs (Fig. 3.1). The sulfate profile of OC at PV 25-29 shows no removal from the bottom to the top of the column, while on the profile of FeOC over the same period of time sulfate concentration continuously decreases from influent to effluent (Fig. 3.2). The sulfate removal capacity of the OC column is 42 μmol g^{-1} (dry weight of organic carbon). The sulfate removal rate of FeOC column is 0.9 μmol $g(oc)^{-1}$ d^{-1}. Since the removal rate is relatively stable from the start to PV 65, the actual removal capacity of FeOC was not attained. However, the total sulfate removed from influent to Port 2 was used to calculate the minimum estimate of the removal capacity. The minimum sulfate removal capacity of the FeOC column is 816 μmol g^{-1} (dry weight of organic carbon), almost 20 times of the removal capacity of the OC column material.

The possible sulfate sinks are precipitation, adsorption and reduction. Geochemical calculation with MINTEQA2 shows undersaturation with respect to all of the sulfate minerals in the database, indicating that there is no tendency for sulfate minerals to precipitate (Fig. 3.10). The only material in the mixtures that can adsorb sulfate significantly is goethite, but sulfate adsorption capacity of goethite is relatively low at pH > 7 (Liu et al., 1999). Many indicators suggest that sulfate is reduced to sulfide. Dissolved hydrogen sulfide was found in both columns. Black Fe sulfides were visible in both columns. XANES and XPS analysis also found reduced sulfur species in solid samples (Fig 3.6 and 3.7).

Isotopic measurements indicate that the sulfate reduction was mediated by sulfate-reducing bacteria (SRB) (Fig. 3.2). Stable isotope composition of sulfur is reported as $\delta^{34}S$, ratio of $^{34}S/^{32}S$ in per mil relative to the standard Canyon Diablo Troilite (CDT).

$$\delta^{34}S(\text{in } ‰) = (^{34}S/^{32}S_{sample} / {}^{34}S/^{32}S_{standard} - 1) \times 1000 \quad (3)$$

Sulfate-reducing bacteria preferentially remove the light isotopes ^{32}S and ^{16}O from the sulfate in the solution and cause isotopic enrichments of both ^{34}S and ^{18}O in the residual sulfate and the accumulation of light isotopes ^{32}S in the sulfides (Strebel et al., 1990). The $\delta^{34}S$ and $\delta^{18}O$ values of the residual sulfate increase with decreasing sulfate concentrations in a manner that is consistent with bacterial reduction of the aqueous sulfate. From the influent to the effluent in FeOC column, $\delta^{34}S$ increases from 4.37‰ to 20.33‰ and then decreases to 14.81‰, and $\delta^{18}O$ goes from 9.27‰ to 12.34‰. The OC column has much smaller increase in $\delta^{34}S$ (from 4.37‰ to 5.73‰), which is consistent with the observation that the OC column lost most of its sulfate removal capacity after 25 PVs. Both sulfur and oxygen isotope data suggest that sulfate reduction is bacteria-mediated.

The profiles of SO_4 and $\delta^{34}S$ show a close relationship between sulfate removal and sulfur isotope composition (Fig. 3.2): the $\delta^{34}S$ increases as the sulfate concentration decreases. The Rayleigh equation can be used to describe this fractionation:

$$\delta^{34}S = [(\delta^{34}S_0 + 10^3)\, f^{(\alpha-1)}] - 10^3 \quad (4)$$

where $\delta^{34}S_0$ and $\delta^{34}S$ refer to the $\delta^{34}S$ value of the aqueous sulfate of the influent and the samples at different sampling ports, respectively, and f is the fraction of the remaining sulfate, and α is the instantaneous isotope fractionation factor. α is defined by

$$\alpha = R_{prod} / R_{react} \quad (5)$$

where R_{prod} and R_{react} are the $^{34}S/^{32}S$ ratios of the sulfide and sulfate at an instant during sulfate reduction. The extent of the fractionation or the ^{34}S enrichment in the residual sulfate also can be indicated by the enrichment factor ε, which is defined by

$$\varepsilon = (\alpha\text{-}1) \times 1000 \quad (6)$$

Only if the fractionation factor α is found constant throughout the column, then $\delta^{34}S$ can be used to indicate how much sulfate is reduced.

α and ε values were calculated using best-fit curves of the data from FeOC column of this study and from Column 1 and 2 of Waybrant et al. (2002) (Fig. 3.3 and Table 3.3). In all cases, the data fit the Rayleigh fractionation model within the uncertainties of the measurements. The two columns of Waybrant et al. (2002) have similar enrichment factors (38.4‰ and 40.7‰), but FeOC column has a smaller fractionation (21.6‰). The results suggest that within a PRB $\delta^{34}S$ can be used to determine the extent of sulfate reduction, but $\delta^{34}S$ fractionation is not consistent between reactive materials.

3.4.2 SRB and H_2

Microbial enumerations show that both FeOC and OC have from 5.2 x 10^3 to 3.2 x 10^5 MPN/g SRB throughout column, except there are two large peaks (10^7 MPN/g) of SRB at Port 2 and Port 10 of FeOC (Fig. 3.4). Because of the two peaks, the average SRB population of FeOC (1.4 x 10^7 MPN/g) is two orders of magnitude higher than the average SRB population of OC (1.4 x 10^5 MPN/g). Because the rate of sulfate reduction had declined in the OC column prior to the sampling for the enumerations, it is possible that the SRB population of the OC column was inactive. The SRB population of FeOC still actively participated in sulfate reduction. Population size is not a good indicator of activity. A large population of SRB does not necessarily indicate significant sulfate reducing activity. For example, Hines et al. (1999) observed that the relative abundance SRB in a salt marsh did not vary much throughout the year, despite the large temporal change of sulfate reduction rate.

PRB systems usually perform very well in the first months after bacterial activity is established (Waybrant et al., 1998; Hulshof et al., 2003), but longer-term performance in both field and laboratory-scale systems consistently declines well before the theoretical capacities of the barriers have been reached (Blowes et al., 2000). Sulfate reduction of OC column stopped after 9 months, while FeOC column was showing a much longer and better performance (Fig. 3.1). Potential causes of the decline in performance include depletion of a reactive component of a mixture, a decline of surface area resulting from precipitation of secondary minerals on reactive surfaces, clogging and preferential flow (Blowes et al., 2000). The decline of surface area is not likely the cause of the performance decline of OC column, because microscopic analysis of the solid samples shows that FeOC has much more carbonate and sulfide precipitation than OC. Reactive components in PRB usually include a variety of cellulosic organic substrates which act as

the source of carbon and nutrients, such as N, P, etc. (Logan et al., 2005). Both columns had the same organic material as the carbon source and nutrients sources, and the OC column maintained a stable neutral pH. Nutrients, sulfate and pH were similar and so are not consider to be the main contributors of the performance differences between the two columns.

SRB utilize simple compounds such as H_2, ethanol, acetate, and lactate, and require upstream cellulolytic microbes and fermenters to break down complex polymers such as cellulose and lignin to simple compounds. Decomposition and fermentation can limit microbial activity in anaerobic ecosystem (Megonigal et al., 2003). Cellulolysis is considered the limiting factor in PRB performance (Logan et al., 2005). So the depletion of substrate or energy source could be the cause of the performance decline observed in the OC column.

In PRB systems, only a small fraction of the organic matter originally in the reactive mixture is immediately available to SRB (Benner et al., 1999), after it is consumed SRB depend on cellulolytic and fermentative organisms to provide the substrate. Cellulolytic and fermentative bacteria can greatly outnumber SRB in environments where the SRB are totally dependent on the fermentative products. For example, in sulfate reducing sediments, SRB typically account for ~5% of the all bacteria present, while most bacteria are involved in polymer hydrolysis and fermentation (Devereux et al., 1996). The microbial enumeration results show that the populations of ACP are about 4 orders of magnitude less than those of SRB in the OC columns (Fig 3.4). The small population of fermenters may not provide sufficient substrate to sustain the much larger population of SRB, resulting in the observed decline in the rate of sulfate reduction.

In FeOC column, another substrate is available, H_2, produced by anaerobic Fe corrosion:

$$Fe + 2H_2O \rightarrow Fe^{2+} + H_2 + 2OH^- \quad (7)$$

H_2 is the most common electron donor in terminal anaerobic metabolism (Megonigal et al., 2003). Methanogens, SRB, iron reducer and other hydrogen-oxidizing bacteria consume cathodic hydrogen and accelerate anaerobic iron corrosion. SRB are regarded as the chief agent of biocorrosion in anaerobic environments (Rajagopal and LeGall, 1989). Hydrogen generated by Fe corrosion also stimulated the growth of microbial populations and increased sulfate reduction in zero-valent iron packed columns (Gu et al., 1999). Although the APB population (~20 MPN/g) is also much less than that of SRB (1.4×10^7 MPN/g) in FeOC column, cathodic H_2 is able to sustain a high sulfate reduction rate and high SRB population. A similar situation is also found in temperate salt marches, where sulfate reduction rate is high and SRB populations on roots can account for over 30% of the total microbial community, because SRB can use acids and alcohols released directly by plant roots and do not depend on fermentation (Rooney-Varga et al., 1997; Hines et al., 1999).

Hydrogen might also play a role in sulfur isotope fractionation. Electron donor effect on sulfur isotope fractionation of *Desulfovibrio desulfuricans* was studied and the fractionation was significantly lower when H_2 was the electron donor than when other donors such as lactate, acetate, and ethanol were consumed (Kaplan and Riggenberg, 1964). This difference might explain why the two columns of Waybrant et al. (2002), where the substrate is likely lactate and acetate, have larger fractionation (ε = -38.4‰ and -40.7‰) than FeOC column (ε = -21.6‰) (Table 3.3 and Fig. 3.3).

Populations of IRB were also enumerated. IRB of OC column (average 1.1 x 10^5 MPN/g) is slightly larger than that of FeOC column (average 3.6 x 10^4 MPN/g) (Fig 3.4). Hydrolysis of fluorescein diacetate (FDA) indicates the general microbial activity. FDA measurements of the OC column (4.3 x 10^{-3} nmol/h/g) is greater than that of the FeOC column (1.8 x 10^{-3} nmol/h/g) (Fig 3.4). This difference may indicate the lower activities of upstream cellulolytic and fermentative bacteria in the FeOC column than in the OC column.

3.4.3 Methanogenesis and ^{13}C

Carbon isotopic data indicates methanogenesis in the first 15 cm (from the influent to Port 6) of both columns. The very negative $\delta^{13}C$ value -33.2‰ of the influent (Table 3.4 and Fig. 3.5) is probably derived from the CO_2 gas ($\delta^{13}C$ value around -30‰ to -35‰), which is used to dissolve $CaCO_3$ and $CaSO_4$ when the simulated groundwater is prepared. From influent to Port 2, $\delta^{13}C$ values increases dramatically from -33.2‰ to -7.1‰ in FeOC column and mildly from -33.2‰ to -22.3‰ in OC column and continue to increase until Port 6. In natural waters, very positive values of $\delta^{13}C$ of dissolved inorganic carbon (DIC) are a useful indicator of methanogenesis (Kendall and Doctor, 2003). Carbonate dissolution has a much smaller fractionation factor. In FeOC column, the increase in $\delta^{13}C$ is also accompanied by loss of DIC. The isotopic mass balance calculation shows that the lost DIC has a $\delta^{13}C$ value of –67.4‰ (Table 3.4), which is within the typical $\delta^{13}C$ range –52‰ to –80‰ of the methane produced by fermentation of organic matter and subsequent methanogenesis (Kendall and Doctor, 2003). So it is likely, therefore, that methanogenesis causes the increase in the $\delta^{13}C$ of the DIC.

The differences between the changes in $\delta^{13}C$ and alkalinity from influent to Port 6 between the two columns could be due to the different methanogenic pathways. Methanogenic bacteria use a more limited variety of simple energy sources compared to SRB, iron reducers and nitrate reducers. The most important energy sources for methanogens are H_2 and acetate (Megonigal et al., 2003). The OC column contains only organic carbon, and no Fe^0, so the methanogenesis is most likely acetotrophic. In this case, acetate is both the electron donor and acceptor, and the energy source.

$$CH_3COO^- \rightarrow HCO_3^- + CH_4 \quad (8)$$

If we assume the $\delta^{13}C$ value of CH_3COOH equal that of the organic carbon (-28‰), that of CH_4 is -67‰, then the $\delta^{13}C$ of methanogenic DIC would be 11‰. This pathway produces DIC, which is consistent with the alkalinity increase of OC column (Fig. 3.5). This DIC, plus the DIC produced by other fermentation processes ($\delta^{13}C$ values -28‰) increase the DIC pool. The positive $\delta^{13}C$ of methanogenic DIC mixed in a larger DIC pool causes relatively mild increase in $\delta^{13}C$ from -33.2‰ to -22.3‰. In FeOC column, cathodic H_2 is more abundant than labile organic carbon and its methanogenesis should be hydrogenotrophic, in which H_2 is the source of electrons and DIC is both an electron acceptor and the source of cellular carbon (Megonigal, et al., 2003):

$$4H_2 + HCO_3^- \rightarrow CH_4 + 2H_2O + OH^- \quad (9)$$

This pathway consumes DIC, which is consistent with the alkalinity decrease of FeOC column (Table 3.4 and Fig. 3.5). The very negative $\delta^{13}C$ of CH_4 causes dramatic increase in $\delta^{13}C$ of the smaller residual DIC pool from -33.2‰ to –7.1‰. From Port 6 to effluent, $\delta^{13}C$ gradually decreased (Fig. 3.5) in both columns, accompanied with a small alkalinity decrease in OC column and a small alkalinity increase in FeOC. This is the exactly opposite effects of the two methanogenesis reactions discussed above and can be

explained by a decline in the rate of methanogenesis. Hydrogen concentrations were not measured during the experiments.

3.4.4 Sulfur Speciation on Solid Surface

Both sulfate and sulfide phases were found in XANES and XPS results (Fig. 3.6 and 3.7). Sulfate was not one of the original solid phases. To protect surface properties, samples were not rinsed with deionised water prior to drying. Dissolved sulfate in porewater probably precipitated during drying. Geochemical modelling shows no sulfate minerals reach saturation in either column (Fig. 3.10). XANES spectra show that Sample FeOC Port 1 has sulfur species similar to orpiment, and Samples FeOC Port 2 and OC Port2 have sulfur species close to troilite and pyrite. (Fig 3.6). S(2p) XPS spectra collected from OC Port 2 and FeOC Port 2 samples are similar. Both have a high-energy and a low-energy broad peaks. The high-energy peak is attribute to sulfate with a binding energy of 168.5 eV and the low-energy peak is best fit with monosulfide (161.7~161.8 eV) and polysulfide (163.4~163.8 eV) (Fig 3.7, Table 3.5 and 3.6). It is generally proposed that formation of pyrite proceeds via the following pathway: amorphous FeS or disordered mackinawite -> mackinawite (FeS) -> greigite ($Fe^{2+}Fe^{3+}{}_2S_4$) -> pyrite (FeS_2) (Wilkin and Barnes, 1997; Jambor et al., 2005). The polysulfide species in XPS spectra suggests that mackinawite is being oxidized to form greigite. The species close to troilite and pyrite in XANES spectra are also consistent with the early stages of this sequence.

3.4.5 pH, Eh, Alkalinity, Ca, and Fe

Because CO_2 gas was used to dissolve $CaCO_3$ and $CaSO_4$ when the simulated groundwater was prepared, the pH at the beginning of each batch of input solution was

~6. Then it gradually rose to 8.3 as the CO_2 degassing proceeded. But both columns have strong pH buffer capacity and the pH values in both columns (except that of Port 2, OC column) generally are not affected by the oscillating pH value of the input solution (Fig. 3.8 and 3.9). pH values in OC column are relatively stable between 7.0 and 7.4, which is similar to other organic carbon PRBs (Waybrant et al., 1998, 2002). The pH value increases rapidly from ~7.5 at Port 2 up to ~9.5 at Port 4 and stays ~9 in the rest of the FeOC column, which is lower than the typical pH values associated with iron-bearing PRBs (Gu et al., 1999). This increase in pH is caused by anaerobic corrosion of Fe (Eqn. 7).

Generally Eh values decrease from 400 mV in the input solution to <200 mV in both columns, which reflects the change from aerobic to anaerobic environments (Fig. 3.8 and 3.9). But the Eh measurements are unstable and inconsistent. This level of variability probably results from the sampling procedures.

Alkalinity shows quite different trends between the two columns (Fig. 3.5 and 3.10). The alkalinity increased in the OC column, although the extent of the increase diminished from PV 1 to PV 40. On the contrary, in the FeOC column alkalinity decreased and the extent of the decrease is greater during the same period of time. Both changes are most dramatic in the first 15 cm of the columns (from influent to Port 6). The causes for these changes were discussed above.

Calcium concentrations were relatively uniform in the OC column after 15 PVs, there was not much change in concentration between influent and effluent (Fig. 3.8 and 3.10). This observation is consistent with the microscopic observation that no secondary calcium-bearing minerals were detected in solid samples. In FeOC column 60% to 70% Ca was constantly removed from the solution and after 25 PVs much of the removal

happened before Port 2 (the first 5.5 cm). Geochemical modelling shows that calcite was precipitated (Fig. 3.11) and mineralogical observations confirmed the presence of significant carbonate minerals in solid samples.

Iron concentrations were very low in both columns (Fig. 3.8 and 3.10). Because there is no Fe in the input solution, the dissolved Fe is attributed to the reductive dissolution of Fe oxides in solid material (iron oxide coating of sand and gravel in OC column and on the zero-valent iron in FeOC column) and from anaerobic corrosion of Fe. Fe concentrations are controlled by precipitation of Fe monosulfides. Poorly crystalline Fe monosulfides or disordered mackinawite are the primary sink for Fe and S in a PRB at Nickel Rim mine site (Herbert et al., 2000) and black Fe sulfides were visible in FeOC column.

3.4.6 Geochemical Modeling

Saturation indices (SI) of various minerals were calculated for the effluent samples of both columns (Fig. 3.11). Both columns were oversaturated with respect to FeS precipitation, which is consistent with the results of the solid-phase analysis (Fig. 3.6 and 3.7). The effluent water from both columns was undersaturated with respect to gypsum and other sulfate minerals (not shown here), suggesting that it is unlikely that secondary sulfate minerals precipitated in the columns. This is most obvious in the OC column because Ca and sulfate did not change from influent to effluent after 25 PVs. In the FeOC column Ca decreased with decreasing alkalinity, which suggests calcite precipitation rather than gypsum precipitation. The SI values for siderite indicated supersaturation in the OC column and for the FeOC column at early time (< 17 PVs). Because the alkalinity and Fe concentration in the FeOC column decreased after 17 PVs, siderite became

undersaturated. Siderite was proposed as a minor Fe sink in areas of high Fe flux in a PRB system (Herbert et al., 2000). Fe concentrations in both columns were very low, so siderite was not expected to control either Fe or alkalinity.

3.5 Implications

Fe^0-bearing organic carbon reactive mixture has the potential to provide a comprehensive method to remove many inorganic contaminants (such as Cr, U, Cu, Zn, As, Sb, Se, SO_4^{2-}, NO_3^- etc.) in acid mine drainage and groundwater. 1) Fe can immobilize metals by reduction, such as $Cr^{6+} \rightarrow Cr^{3+}$ (Blowes, et al., 1997) and $U^{6+} \rightarrow U^{4+}$ (Gu, et al., 1998). 2) Hydrous Fe oxides produced by Fe corrosion is a strong absorbent to remove As (McRae et al., 1999; Bain et al., 2003). 3) Cathodic H_2 produced by anaerobic Fe corrosion is an electron donor for SRB and can sustain a high sulfate reduction rate. 4) Cathodic H_2 can also be used by denitrifying bacteria (Megonigal et al., 2003) and has a potential to enhance denitrification. 5) Anaerobic Fe corrosion also produces OH^- and helps to neutralize the acid in mine drainage.

Several processes can affect the concentration of sulfate in mine drainage or groundwater, such as dilution, sulfate mineral dissolution and precipitation, and sulfate reduction. So sulfate concentration alone can not truly show how much sulfate has been reduced. Bacterial reduction of sulfate is the primary source of the variability of sulfate isotopic compositions in natural aquatic systems (Kendall and Doctor, 2003). Dissolution of sulfate minerals does not significantly fractionate sulfate isotopic compositions and precipitation of sulfate minerals is accompanied by only slight isotopic fractionation

(fractionation factor < 2‰, Holser and Kaplan, 1966). The $\delta^{34}S$ measurements from this study and from Waybrant et al. (2002) confirm that $\delta^{34}S$ provides a good indicator of the extent of sulfate reduction. Thus $\delta^{34}S$ measurements provide a useful tool for evaluating the performance of remediation methods based on bacterial sulfate reduction, such as organic carbon PRB.

3.7 Conclusions

The results of this study demonstrate:

- The Fe^0-bearing organic carbon reactive mixture sustained a higher sulfate reduction rate for a longer period of time than the organic carbon reactive mixture.
- The microbial enumerations and isotopic measurements indicate that the sulfate reduction was mediated by SRB.
- The cathodic production of H_2 by anaerobic corrosion of Fe probably is the cause of the difference in sulfate reduction rates between the two reactive mixtures.
- Zero-valent iron can be used to provide an electron donor in sulfate reducing PRBs and Fe^0-bearing organic carbon reactive mixture has a potential to improve the performance of organic carbon PRBs.
- The $\delta^{34}S$ values can be used to determine the extent of sulfate reduction, but $\delta^{34}S$ fractionation is not consistent between reactive materials.

- The $\delta^{13}C$ values indicate that methanogenesis is occurring in the front part of the both columns.

3.8 Acknowledgements

We thank Laura Groza, Jeff Bain, and Matt Lindsay for their assistance with lab work and helpful comments. Mark Biesinger's help in XPS analysis and interpretation and Paul Northrup's assistance in x-ray adsorption near edge spectroscopy analysis are greatly appreciated. Funding for this research was provided by the Natural Sciences and Engineering Research Council of Canada, through a grant provided to D.W. Blowes.

3.9 References

Allison, J.D., Brown, D.S., Novo-Gradac, K.J., 1990. A geochemical assessment model for environmental systems: version 3.0 user's manual, Environmental Research Laboratory, U.S. Environmental Protection Agency, Athens, GA, 106 p.

Bain, J., Spink, L., Blowes, D.W., Smyth, D., 2003. The removal of arsenic from groundwater using permeable reactive materials, In: Sudbury '03 – Mining and the Environment III, Sudbury, Ontario.

Ball, J.W., Nordstrom, D.K., 1991, User's Manual for WATEQ4F, with Revised Thermodynamic Data Base and Test Cases for Calculating Speciation of Major, Trace, and Redox Elements in Natural Waters, US Geological Survey, Open-File Report 91-183, 192p, 2 tab, 103 ref, 6 append.

Benner, S.G., Blowes, D.W., Ptacek, C.J., 1997. A full-scale porous reactive wall for prevention of acid mine drainage, Ground Water Monitoring and Remediation 17 (4), 99-107.

Benner, S.G., Blowes, D.W., Gould, W.D., Herbert, R.B.Jr., C.J. Ptacek, 1999. Geochemistry of a permeable reactive barrier for metals and acid mine drainage, Environmental Science Technology 33, 2793-2799.

Benner, S.G., Gould, W.D., Blowes, D.W., 2000. Microbial populations associated with the generation and treatment of acid mine drainage, Chemical Geology 169, 435-448.

Blowes, D.W., Ptacek, C.J., Benner, S.G., McRae, C.W.T., Bennett, T.A., Puls, R.W., 2000. Treatment of inorganic contaminants using permeable reactive barriers, Journal of Contaminant Hydrology 45, 123-137.

Blowes, D.W., Ptacek, C.J., Jambor, J.L., 1997. In-situ remediation of Cr(VI)-Contaminated Groundwater using permeable reactive walls: laboratory studies, Environmental Science and Technology 31, 3348-3357.

Boursiquot, S., Mullet, M., Abdelmoula, M., Genin, J.M., Ehrhardt J.J., 2001. The dry oxidation of tetragonal FeS_{1-x} mackinawite, Physics and Chemistry of Minerals 28, 600-611.

Buchardt, B., Fritz, P., 1980. Environmental isotopes as environmental and climatological indicators, In Handbook of Environmental Isotope Geochemistry (eds. Fritz, P. and Fontes, J.Ch.), 473-504.

Cochran, W.G., 1950. Estimation of bacterial densities by means of the "Most Probable Number", Biometrics 6, 105-116.

Devereux, R., Hines, M.E., Stahl, D.A., 1996. S cycling: characterization of natural communities of sulfate-reducing bacteria by 16S rRNA sequence comparisons, Microbial Ecology 32, 283-292.

Einsiedl, F., Schafer, T., Northrup, P., 2007, Combined Sulfur K-edge XANES Spectroscopy and Stable Isotope Analysis of Fulvic Acids and Groundwater Sulfate Identify Sulfur Cycling in a Karstic Catchment Area, Chemical Geology 238, 268-276.

Gould, W. D., M. Stichbury, M. Francis, L. Lortie, D.W. Blowes., 2003. An MPN method for the enumeration of iron-reducing bacteria, Mining and Environment conference III, Sudbury, Ontario.

Gu, B., Liang, L., Dickey, M.J., Yin, X, Dai, S., 1998. Reductive precipitation of uranium (VI) by zero-valent iron, Environmental Science and Technology 32, 3366-3373.

Gu, B., Phelps, T.J., Liang, L., Dickey, M.J., Roh, Y., Kinsall, B.L., Palumbo, A.V., Jacobs, G.K., 1999. Biogeochemical dynamics in zero-valent iron columns: implications for permeable reactive barriers, Environmental Science and Technology 33, 2170-2177.

Herbert Jr. R.B., Benner, S.G., Pratt, A.R., Blowes, D.W., 1998. Surface chemistry and morphology of poorly crystalline iron sulfides precipitated in media containing sulfate-reducing bacteria, Chemical Geology 144, 87-97.

Herbert Jr. R.B., Benner, S.G., Blowes, D.W., 2000. Solid phase iron-sulfur geochemistry of a reactive barrier for treatment of mine drainage, Applied Geochemistry 15, 1331-1343.

Hines, M.E., Evans, R.S., Genthner, B.R.S., Willis, S.G., Friedman, F., Rooney-Varga, J.N., Devereux, R., 1999. Molecular phylogenetic and biogeochemical studies of sulfate-reducing bacteria in the rhizosphere of spartina alterniflora, Applied and Environmental Microbiology 65 (5), 2209-2216.

Holser, W.T., Kaplan, I.R., 1966. Isotope geochemistry of sedimentary sulfates, Chemical Geology 1, 93-135.

Hulshof, A.H., Blowes, D.W., Ptacek, C.J., Gould, W.D., 2003. Microbial and nutrient investigations into the use of in situ layers for treatment of tailings effluent, Environmental Science and Technology 37, 5027-5033.

Jambor, J.L., Raudsepp, M., Mountjoy, K., 2005. Mineralogy of permeable reactive barriers for the attenuation of subsurface contaminants, Canadian Mineralogist 43, 2117-2140.

Jones, C.F., LeCount, S., Smart, R.C., 1992. Compositional and structural alteration of pyrrhotite surfaces in solution: XPS and XRD studies, Applied Surface Science 55, 65-85.

Kaplan, I.R., Riggenberg, S.C., 1964. Microbiological fractionation of sulfur isotopes, Journal of General Microbiology 34, 195-212.

Kendall, C., Doctor, D.H., 2003. Stable isotope applications in hydrologic studies, In Treaties on Geochemistry 5, Elsevier, 319-364.

Liu, F., He, J., Colombo, C., Violante, A., 1999. Competitive adsorption of sulfate and oxalate on goethite in the absence of presence of phosphate, Soil Science 164 (3), 180-189.

Logan, M.V., Reardon, K.F., Figueroa, L.A., McLain, J.E.T., Ahmann, D.M., 2005. Microbial community activities during establishment, performance, and decline of bench-scale passive treatment systems for mine drainage, Water Research 39, 4537-4551.

Ludwig, R.D., McGregor, R.G., Blowes, D.W., Benner, S.G., Mountjoy, K., 2002. A permeable reactive barrier for the treatment of dissolved metals, Ground Water 40(1), 59-66.

McRae, C.W.T., Blowes, D.W., Ptacek, C.J., 1999. In situ removal of arsenic from groundwater using permeable reactive barriers: a laboratory study. Sudbury ’99 - Mining and the Environment II Conference, September 13-17, Sudbury, Ontario, 601-609.

Megonigal, J.P., Hines, M.E., Visscher, P.T., 2003. Anaerobic metabolism: linkages to trace gases and aerobic processes, In Treaties on Geochemistry 8, Elsevier , 317-424.

Mountjoy, K.J., Blowes, D.W., 2002. Installation of a full scale permeable reactive barrier for the treatment of metal contaminated groundwater. In Proceedings of the Third International Conference on Remediation of Chlorinated and Recalcitrant Compounds 2. Battlle Press, Columbus, Ohio, 281-289.

Pratt, A.R., Muir, I.J., Nesbitt, H.W., 1994a. X-ray photoelectron and Auger electron spectroscopic studies pyrrhotite and mechanism of air oxidation, Geochimica et Cosmochimica Acta 58, 327-841.

Pratt, A.R., Nesbitt, H.W., Mycroft, J.R., 1994b. The increased reactivity of pyrrhotite and magnetite phases in sulfide mine tailings, Journal of Geochemical Exploration 56, 1-11.

Rajagopal, B.S., LeGall, J., 1989. Utilization of cathodic hydrogen by hydrogen-oxidizing bacteria, Applied Microbiology and Biotechnology 31, 406-412.

Rooney-Varga, J.N., Devereux, R., Evans, R.S., Hines, M.E., 1997. Seasonal changes in the relative abundance of uncultivated sulfate-reducing bacteria in a salt marsh sediment and in the rhizosphere of spartina alternifluora, Applied and Environmental Microbiology 63, 3895-3901.

Scherer, M.M., Richter, S., Valentine, R.L., Alvarez, P.J.J., 2000. Chemistry and microbiology of permeable reactive barriers for in situ groundwater clean up, Critical Reviews in Microbiology 26 (4), 221-264.

Schnurer, J. and Rosswall, T., 1982. Fluorescein Diacetate Hydrolysis as a Measure of Total Microbial Activity in Soil and Litter, Applied and Environmental Microbiology 43, 1256-1261.

Strebel, O., Bottcher, J., Fritz, P., 1990. Use of isotope fractionation of sulfate-sulfur and sulfate-oxygen to assess bacterial desulfurication in a sandy aquifer, Journal of Hydrology 121, 155-172.

Tempel, R.N., Shevenell, L.A., Lechler, P., Price, J., 2000, Geochemical modeling approach to predicting arsenic concentrations in a mine pit lake, Applied Geochemistry 15, 475-492.

Thomas, J.E., Jones, C.F., Skinner, W.M., Smart R.C., 1998. The role of surface sulfur species in the inhibition of pyrrhotite dissolution in acid conditions, Geochimica et Cosmochimica Acta 62, 1555-1565.

Vairavamurthy A. (1998), Using x-ray absorption to probe suklfur oxidation states in complex molecules, Spectrochimica Acta Part A 54, 2009-2017.

Waybrant, K.R., Blowes, D.W., Ptacek, C.J., 1998. Selection of reactive mixtures for use in permeable reactive walls for treatment of mine drainage, Environmental Science and Technology 32,1972-1979.

Waybrant, K.R., Ptacek, C.J., Blowes, D.W., 2002. Treatment of mine drainage using permeable reactive barriers: column experiments, Environmental Science and Technology 36, 1346-1356.

Wilkin, R.T., Barnes, H.L., 1997. Formation processes of framboidal pyrite, Geochimica et Cosmochimica Acta 61, 323-339.

Table 3.1 Composition of Reactive Mixture in Columns

Composition	OC column dry wt%	FeOC column dry wt%
Top layer (4 cm)		
Ottawa sand	100	100
Middle layer (33 cm)		
Composted leaf mulch	14	8
Cornnelly zero-valent iron	0	17
limestone	0	3
Ottawa sand	33	30
Pea gravel	53	42
River sediments layer (2 cm)		
Fresh river sediments	7	4
Composted leaf mulch	7	4
Cornnelly zero-valent iron	0	17
limestone	0	3
Ottawa sand	33	30
Pea gravel	53	42
Bottom layer (2 cm)		
Silica sand	100	100

Table 3.2 Chemical Composition of Simulated Groundwater (10^{-3} mol/L)

Na	K	Mg	Ca
1.00	0.051	0.49	4.77
HCO3	SO4	Sb	As
3.20	3.96	0.0041	0.067

Table 3.3 Sulfur isotopic fractionation of reactive materials.

Reactive material	α [b]	ε [c] (‰)
FeOC	0.9784	-21.6
Column 1[a]	0.9616	-38.4
Column 2[a]	0.9593	-40.7

[a] from Waybrant et al. (2002)

[b] calculated from best-fit curves (see Fig 3.) using δ34S and *f* data of this study and of Waybrant et al. (2002).

[c] calculated using Equation (3) instead of $\varepsilon = (\delta s - \delta m) / \ln f$ used in Waybrant (2002), which is not accurate when $|\delta| > 10$.

Table 3.4 Carbon isotopic composition of FeOC influent and Port 2 water

	Concentration 10^{-3} mol/L	$\delta^{13}C$ ‰
Influent DIC	4.99[a]	-33.2
Influent Ca	5.88	
Port 2 DIC	1.36 [a]	-7.1
Port 2 Ca	3.43	
$CaCO_3$ ppt	2.45[b]	-31.2[c]
lost DIC	1.18[d]	-67.4[e]

[a] Calculated from pH and alkalinity using MINTEQA2 (Allison et al., 1990).

[b] CaCO3 precipitation = Influent Ca – Port 2 Ca

[c] $\delta^{13}C_{CaCO3\ ppt} = \delta^{13}C_{HCO3-} + 2$ (Buchardt and Fritz, 1980)

[d] lost DIC = Influent DIC – Port 2 DIC – $CaCO_3$ ppt

[e] $\delta^{13}C_{lost\ DIC}$ = (Influent DIC $\times$ $\delta^{13}C_{Influent\ DIC}$ − Port 2 DIC $\times$ $\delta^{13}C_{Port\ 2\ DIC}$ − $CaCO_3$ ppt $\times$ $\delta^{13}C_{CaCO3\ ppt}$) / lost DIC

Table 3.5 Binding energies for S(2p) in various references.

Species	BE (eV)	References
monosulfide S^{2-}	160.9	Herbert et al. (1998)
	161.3	Pratt et al. (1994a)
	161.6	Boursiquot et al. (2001)
bisulfide S_2^{2-}	162.2	Herbert et al. (1998)
	162.4	Thomas et al. (1998)
polysulfide S_n^{2-}	163.3	Pratt et al., (1994b)
	163.4	Thomas et al. (1998)
sulfate SO_4^{2-}	168.5	Jones, et al. (1992)
	169.1	Pratt et al. (1994b)

Table 3.6 Binding energies, peak full width at half maximum (FWHM), and peak areas for S(2p) XPS spectra

BE (eV)[a]	FWHM (eV)	Area(%)[b]	Species
Wood chips of OC column Port 2			
161.72	1.47	54.8	monosulfide
163.81	1.47	45.2	polysulfide
168.53	2.00	0 [c]	sulfate
Wood chips of FeOC column Port 2			
161.81	1.56	32.0	monosulfide
163.77	1.56	68.0	polysulfide
168.49	2.11	0c	sulfate
Iron chips of FeOC column Port 2			
163.42	1.38	100.0	polysulfide
168.27	2.07	0c	sulfate

[a] All binding energy peak locations were charge corrected to the main peak of the carbon 1s spectrum set to 285.0 eV.

[b] Area includes $2p_{1/2}$ and $2p_{3/2}$ contributions

[c] Sulfate is not included in area calculation, see text.

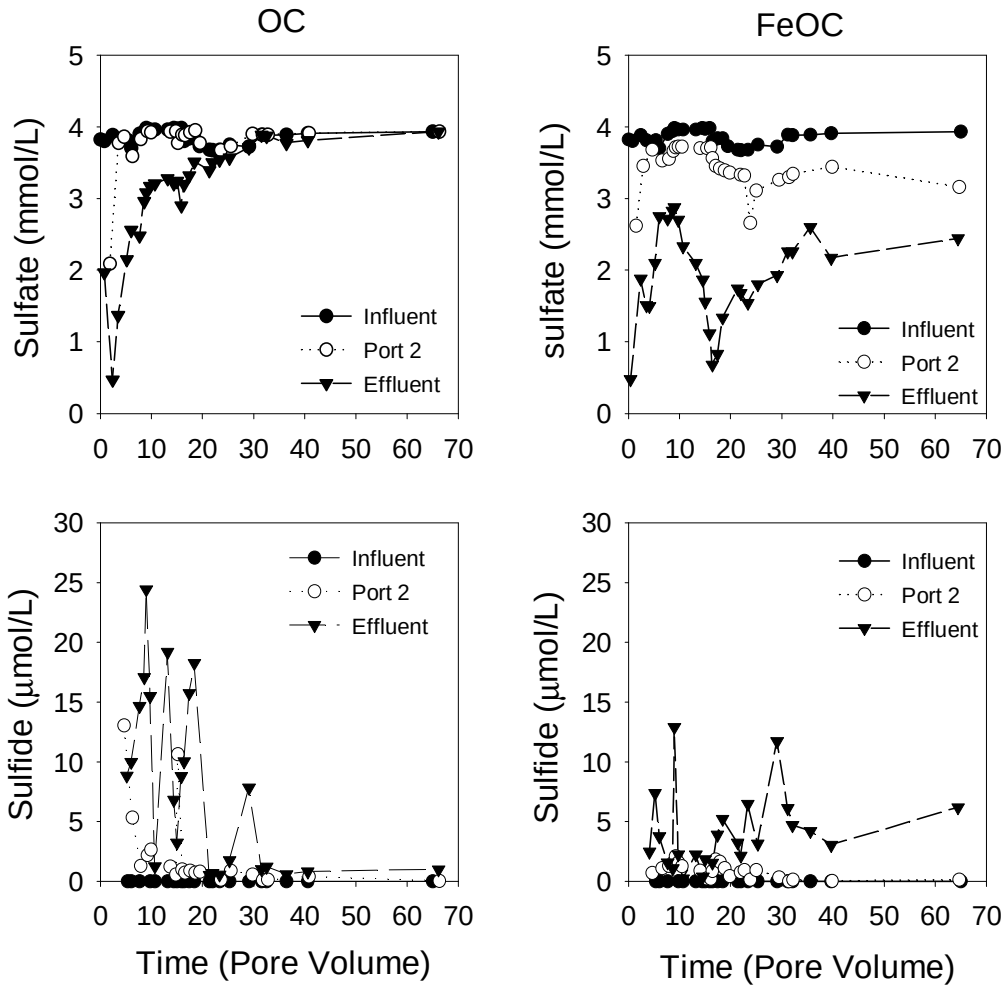

Figure 3.1 Temporal changes in sulfate and sulfide of the OC and FeOC columns. Port 2 is at 5 cm from the bottom of column. The FeOC column removed more sulfate than the OC column.

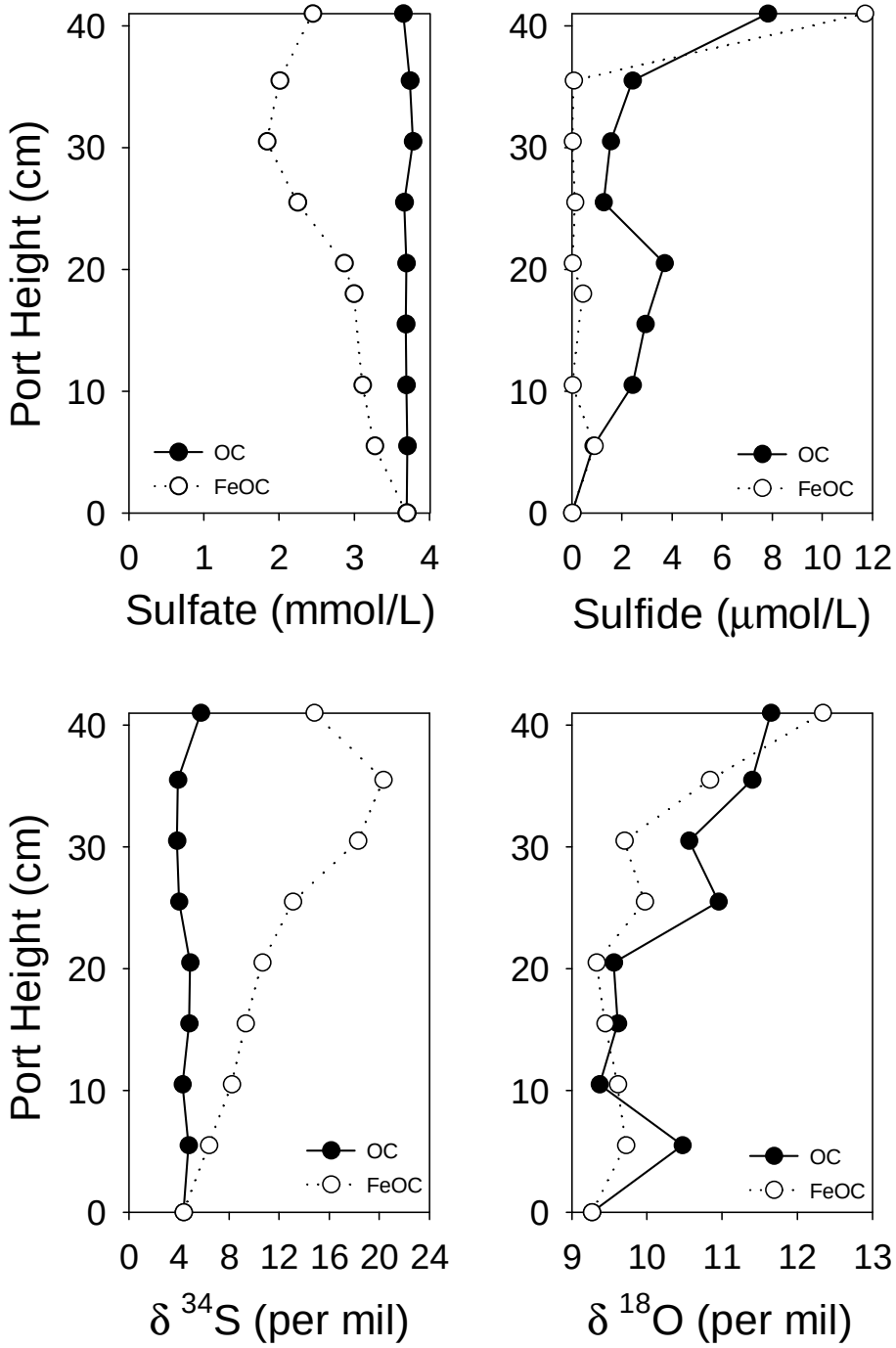

Figure 3.2 Profiles of sulfate, sulfide, $\delta^{34}S$, and $\delta^{18}O$. The FeOC column removed more sulfate than the OC column through out the column. $\delta^{34}S$ values in the FeOC column increased from bottom to top, but those in the OC column were constant.

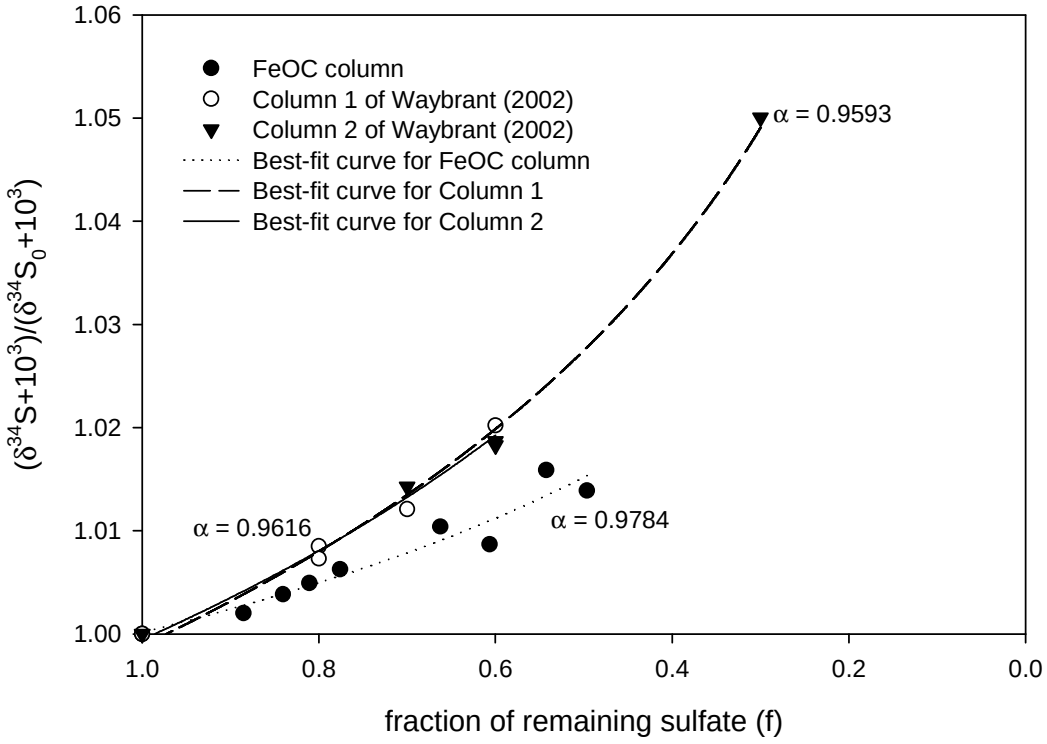

Figure 3.3 $(\delta^{34}S+10^3)/(\delta^{34}S_0+10^3)$ vs. fraction of remaining SO_4. $\delta^{34}S_0$ and $\delta^{34}S$ are the $\delta^{34}S$ values of the aqueous sulfate of the influent and the samples at different sampling ports, respectively. Instantaneous fractionation factor α was calculated using best-fit curves.

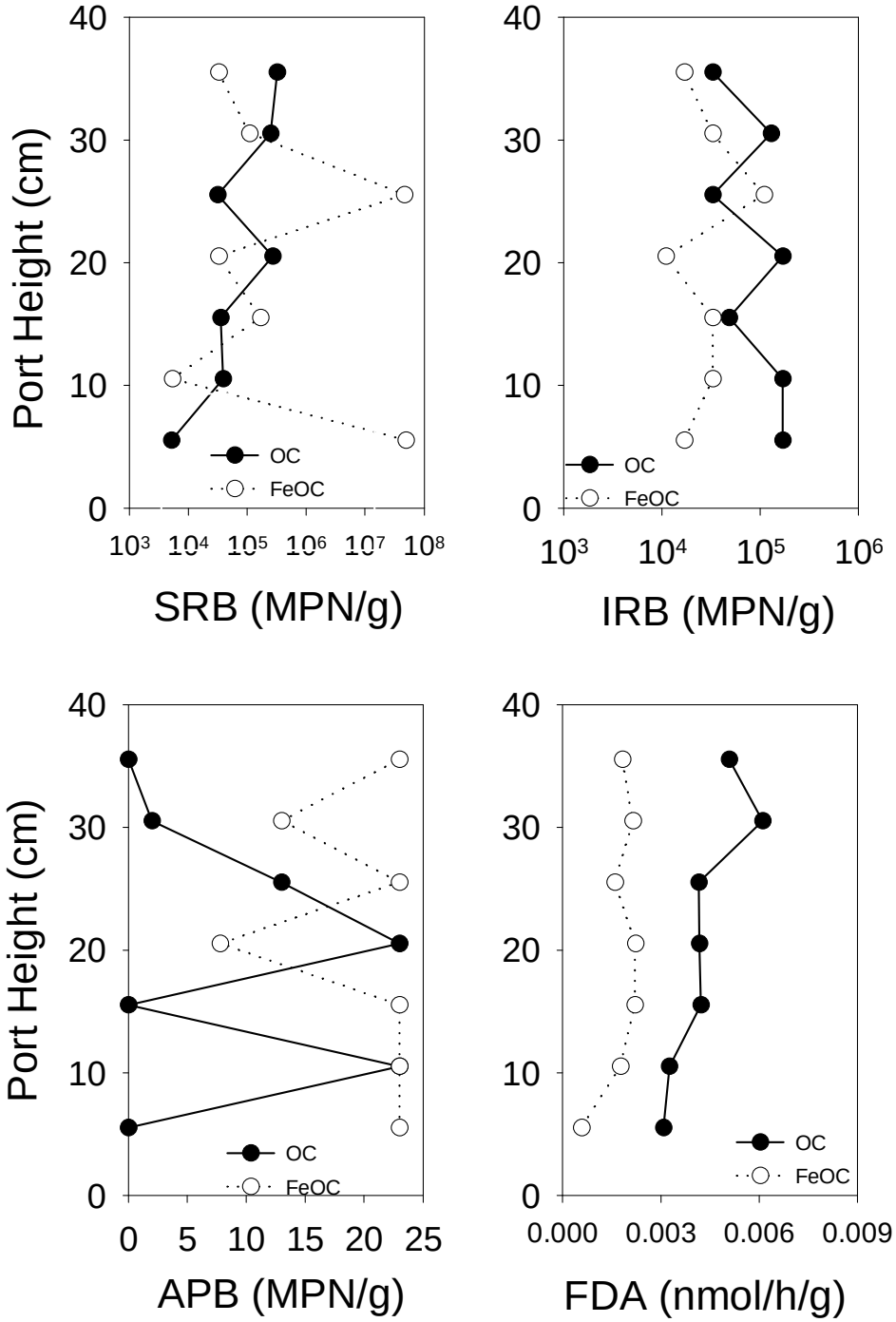

Figure 3.4 Profiles of SRB, IRB, APB, and FDA. SRB population of the FeOC column is greater than that of the OC column. IRB population and FDA concentration of the OC column are slightly larger than those of the FeOC column. APB populations in both columns are much smaller than SRB and IRB populations.

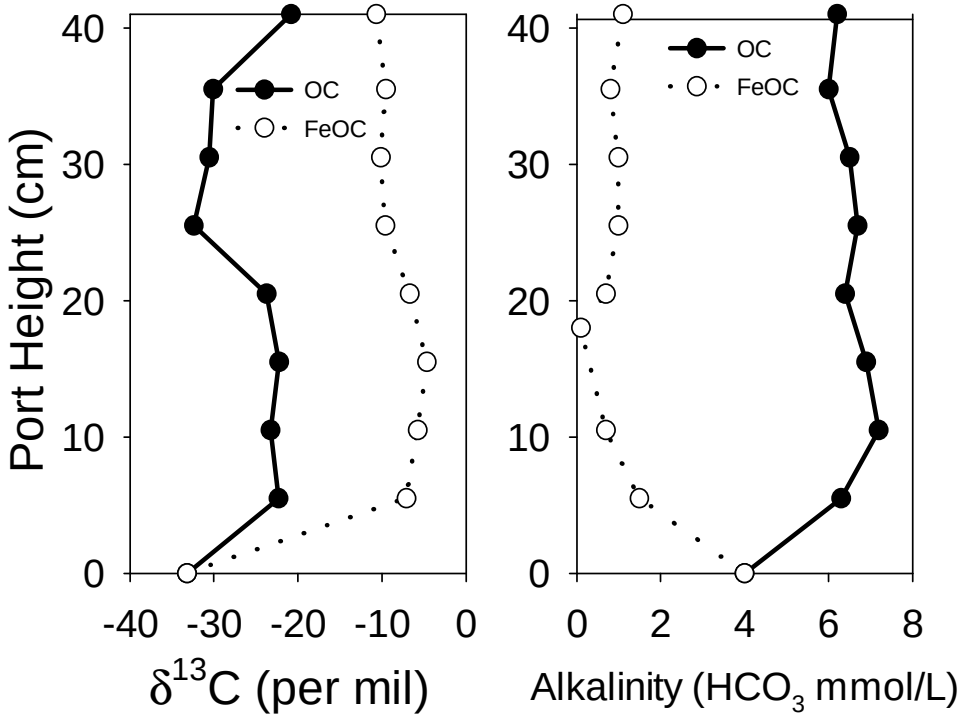

Figure 3.5 Profiles of $\delta^{13}C$ and alkalinity. From influent to Port 2 (5.5 cm), $\delta^{13}C$ values increases dramatically from -33.2‰ to -7.1‰ in the FeOC column and mildly from -33.2‰ to -22.3‰ in the OC column and continue to increase until Port 6 (15 cm), and DIC decreases in the FeOC column and increases in the OC column.

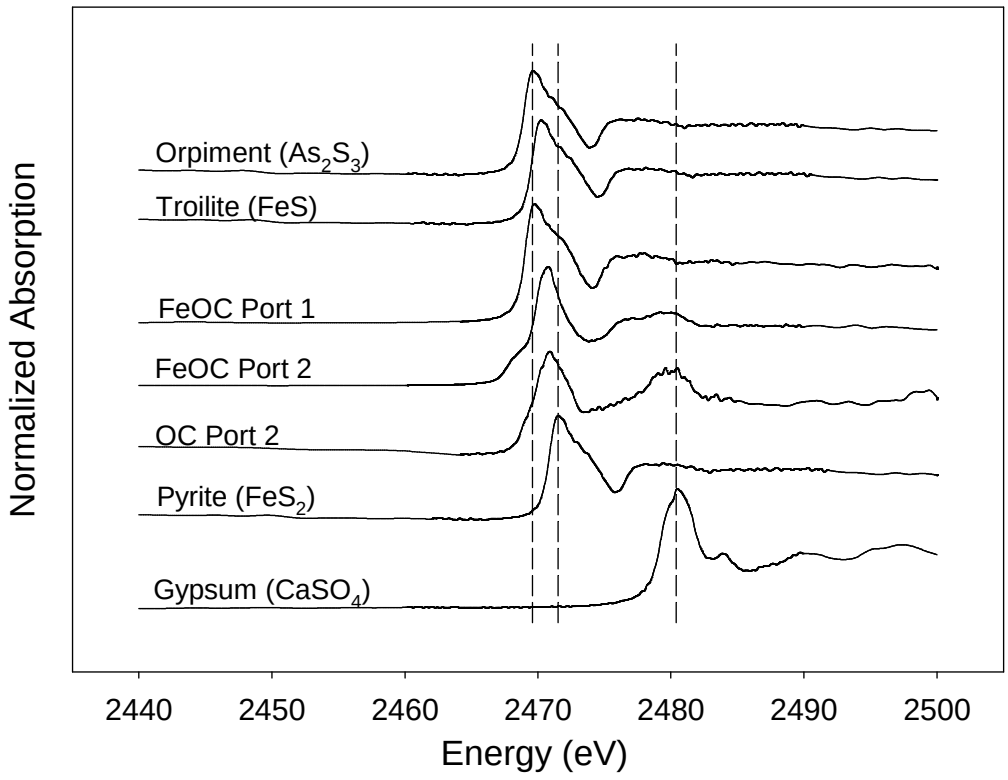

Figure 3.6 Sulfur K-edge XANES spectra. Orpiment, troilite, pyrite, gypsum are reference material. Orpiment and gypsum were analyzed under the same conditions as with the three samples. The spectra of troilite and pyrite are the approximation using the data (corrected to the peak of element sulfur set to 2472.0) from Vairamurthy (1998). Sample FeOC Port 1 has sulfur species similar to orpiment. Samples FeOC Port 2 and OC Port2 have sulfur species close to troilite and pyrite.

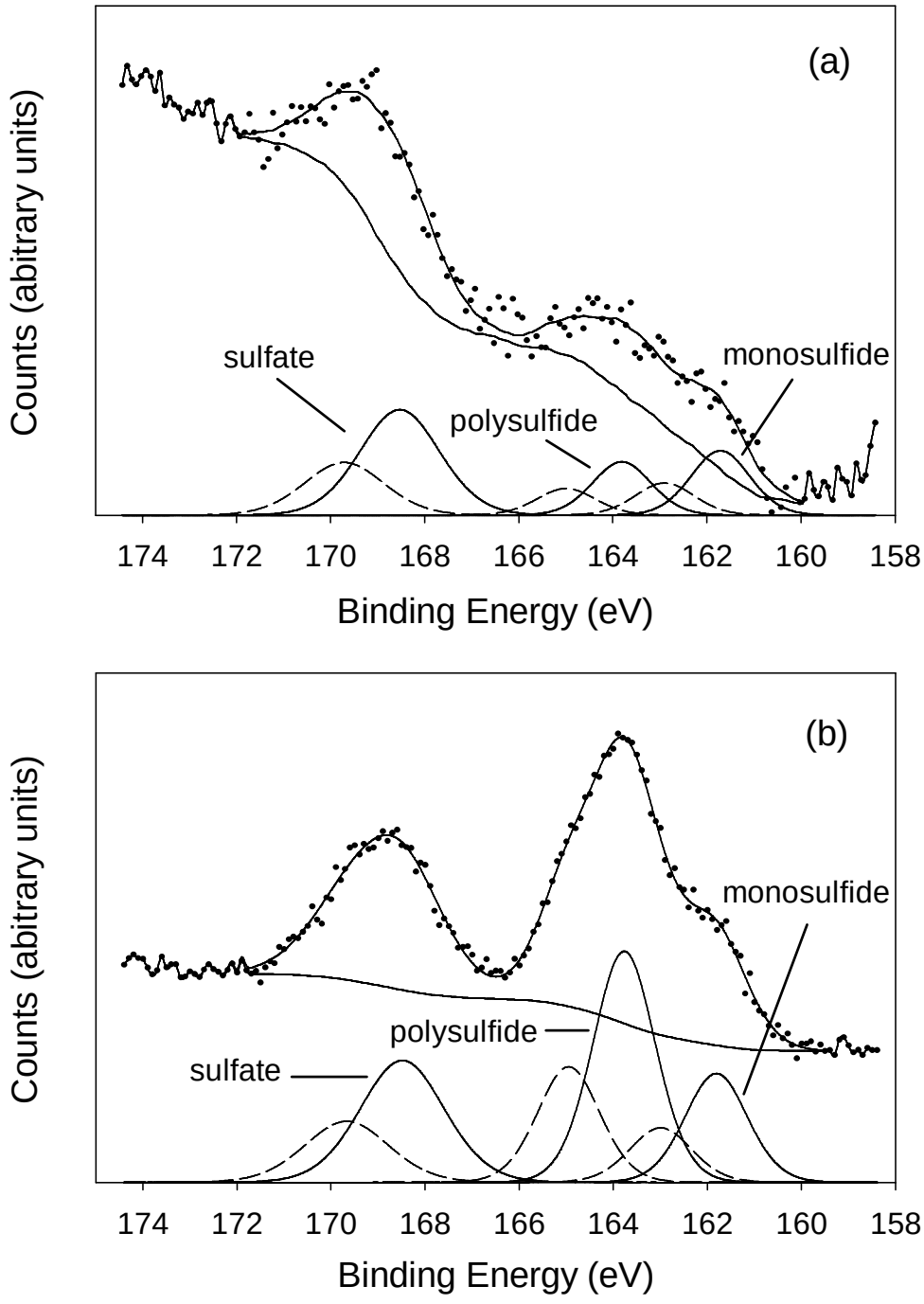

Figure 3.7 High resolution scan of S(2p) XPS spectra. (a) OC column Port 2; (b) FeOC column Port 2. Fit curves include $2p_{3/2}$ (solid line) and $2p_{1/2}$ (dashed line) components.

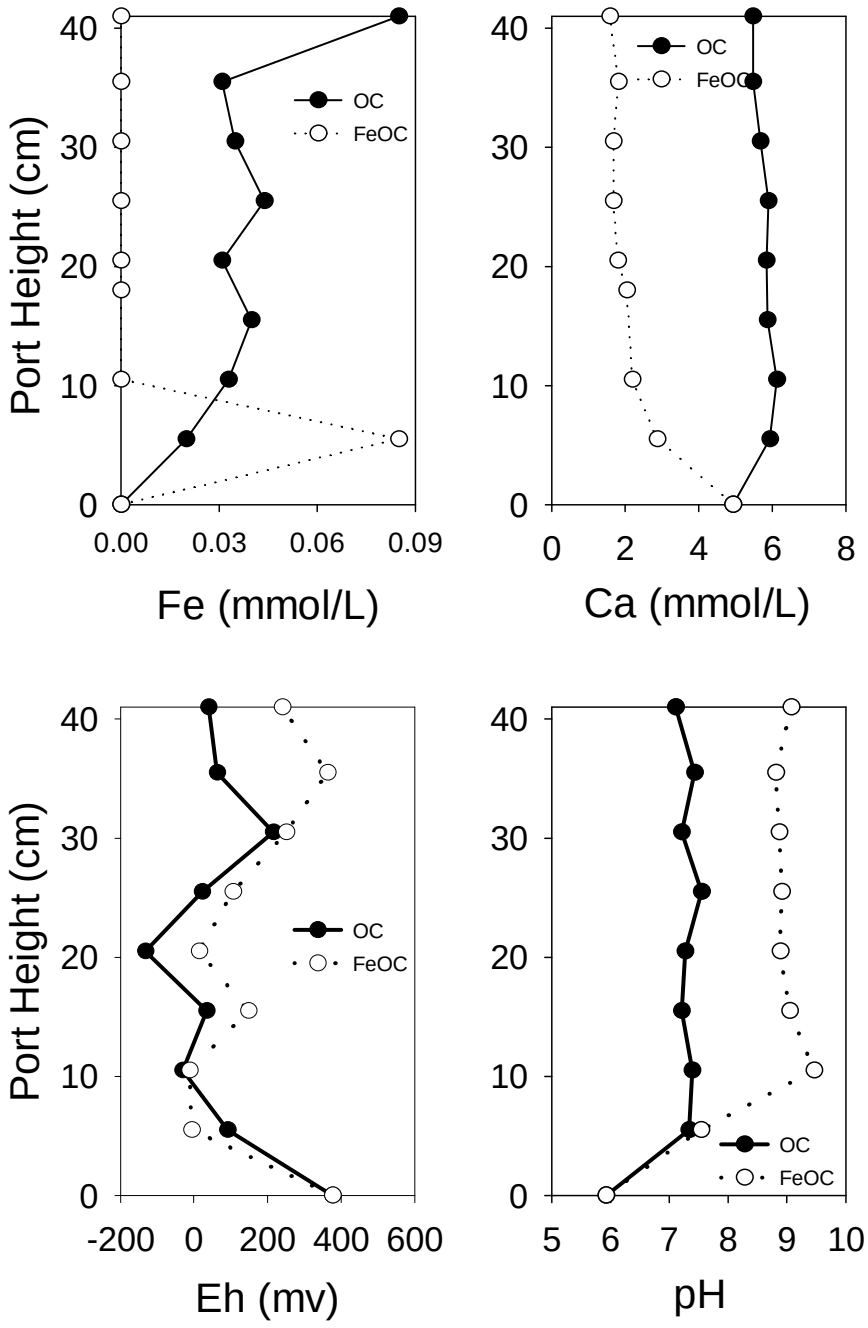

Figure 3.8 Profiles of Fe, Ca, Eh, and pH. Fe concentrations in the OC column were greater than the FeOC column. Ca concentrations decreased in the first 15 cm of the FeOC column, but increased mildly in the same section of the OC column. From 10 cm to the top, pH in the FeOC column is greater than that in the OC column.

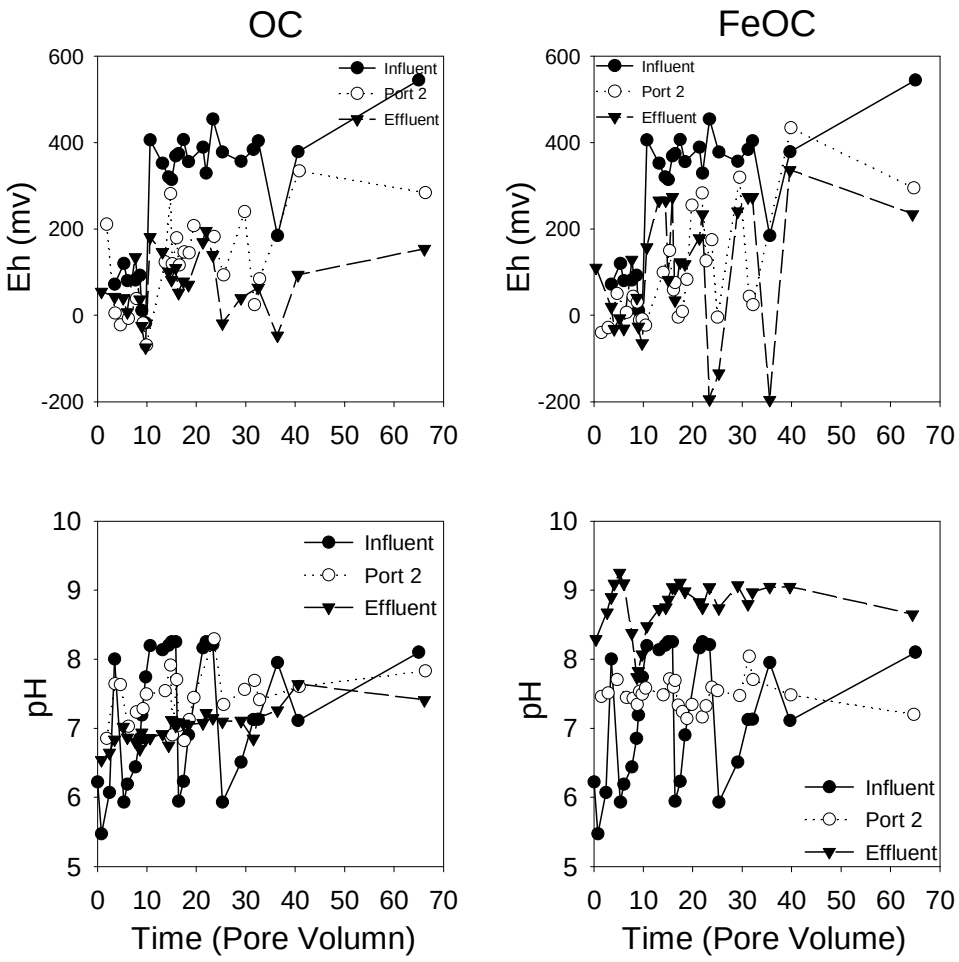

Figure 3.9 Temporal changes of Eh and pH. pH values of the OC column is smaller than those of the FeOC column, which is caused by anaerobic corrosion of Fe. Eh values decrease from 400 mV in the influent to <200 mV in both columns, which reflects the change from aerobic to anaerobic environments.

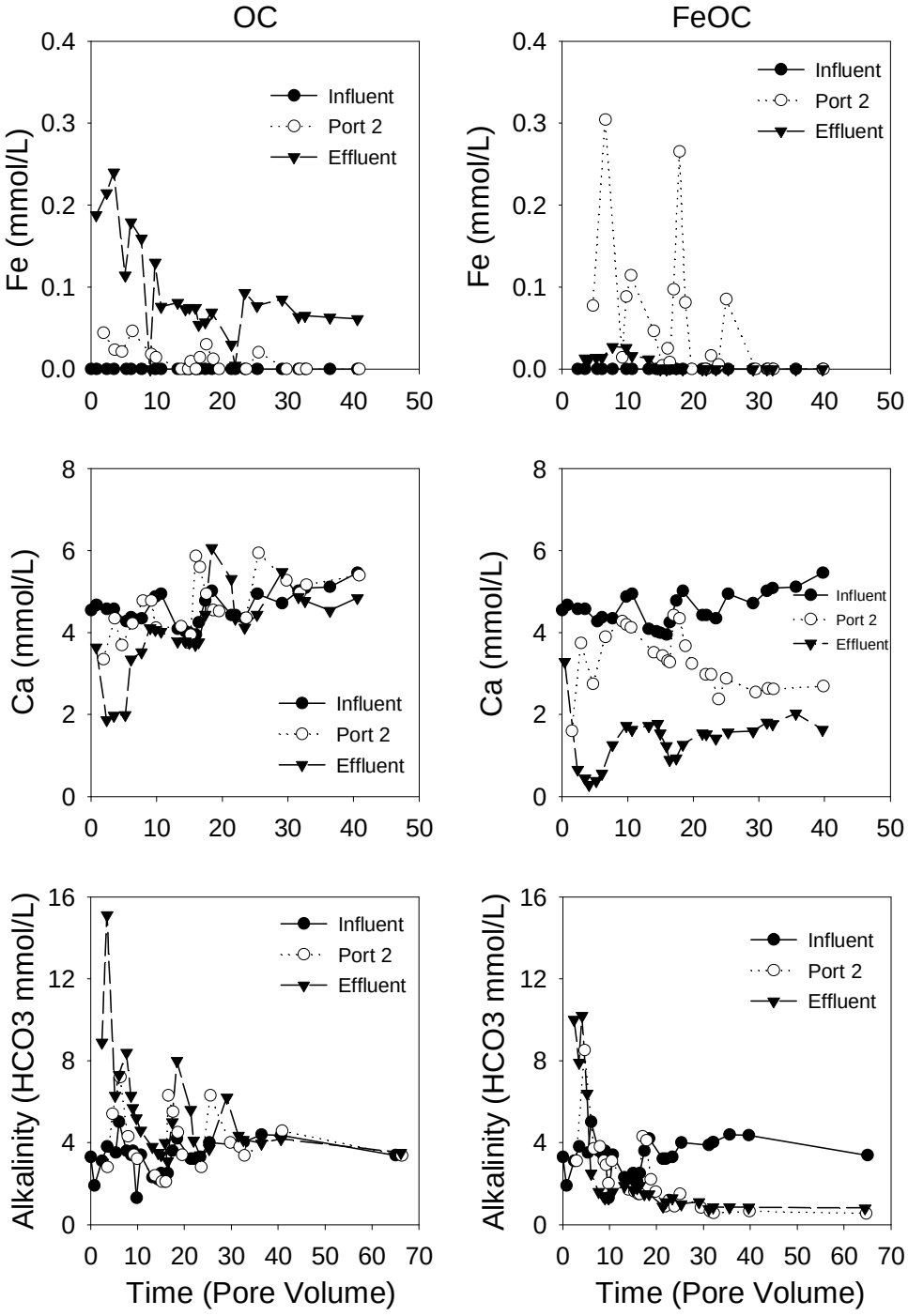

Figure 3.10 Temporal changes of Fe, Ca, and alkalinity. From the influent to Port 2, the alkalinity and Ca concentrations decrease in the FeOC column. In the OC column, alkalinity increases from the influent to Port 2 and Ca concentrations does not change much after 15 PVs. Fe concentrations are low in both columns.

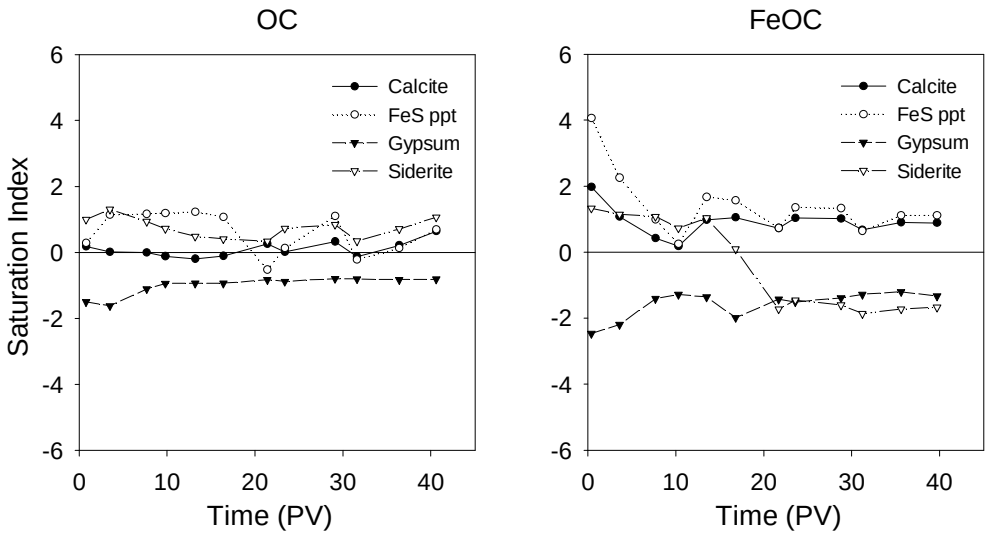

Figure 3.11 Saturation indices (SI) for selected mineral phases for effluent samples from OC and FeOC columns. Both columns are oversaturated with respect to FeS, but undersaturated with respect to gypsum. The SI values for siderite indicate supersaturation in the OC column and in the FeOC column at early time (<17 PVs).

Chapter 4

Remediation of Arsenic and Antimony Using Two Types of Permeable Reactive Barriers, Organic Carbon and Iron-Bearing Organic Carbon: Column Experiments

4.1 Abstract

Arsenic and antimony in groundwater are great threats to human health. The permeable reactive barrier (PRB) technology potentially is an efficient and cost-effective approach to remediate organic and inorganic contamination in groundwater. Two column experiments were conducted to assess the rates and capacities of organic carbon (OC) PRB and Fe-bearing organic carbon (FeOC) PRB to remove As and Sb under controlled groundwater flow conditions. The simulated groundwater contains 5 mg l^{-1} As and 0.5 mg l^{-1} Sb. Arsenic concentration in the effluent of the OC column was greater than 10 μg l^{-1} (EPA drinking water limit) from the beginning and reached 1000 ppb in 25 pore volumes. The As front (C = 10 μg l^{-1}) was within 5.5 cm into FeOC at PV 65 and the effluent concentration was close to 1 ppb for at least 65 PVs. The average As removal rate for the OC column was 13 nmole day^{-1} g^{-1} (dry weight of organic carbon) and its removal capacity was 11 μmole g^{-1} (dry weight of organic carbon). The remove rate of the FeOC material was 165 nmole day^{-1} g^{-1} (dry weight of organic carbon) or 53 nmole day^{-1} g^{-1} (dry weight of organic carbon and zero-valent iron) and its minimum removal capacity was 105 μmole g^{-1} (dry weight of organic carbon) or 34 μmole g^{-1} (dry weight of organic carbon and zero-valent iron). Both reactive mixtures remove Sb completely,

however the Sb front advanced more rapidly in the OC column than in the FeOC column. Antimony removal rate of the OC material decreases from 8.2 to 1.4 nmole day^{-1} g^{-1} (dry weight of organic carbon) and its removal capacity is 2.4 μmole g^{-1} (dry weight of organic carbon). The minimum removal rate of FeOC material is 13 (dry weight of organic carbon) or 4.3 nmole day^{-1} g^{-1} (dry weight of organic carbon and zero-valent iron) and its minimum removal capacity is 8.4 (dry weight of organic carbon) or 2.7 μmole g^{-1} (dry weight of organic carbon and zero-valent iron).

The As(III) : [As(III)+As(V)] ratio increased from 0.01 in the influent to 0.5 at port 2 (5.5 cm from the influent end of the column) and to 0.8 at port 6 (15.5 cm from the influent end of the column) in the OC column. X-ray absorption near edge spectroscopy (XANES) shows As(III)-sulfide species on solid samples. These results suggest that the dissolved As(V) species in pore water is reduced and precipitate as As(III) sulfides or coprecipitated with iron sulfides. The arsenic reduction rate suggests that As(V) reduction is mediated by bacterial activity in both columns.

4.2 Introduction

Arsenic and antimony are ubiquitous elements in the Earth's crust, mainly found in sulfide-bearing ore bodies, coal, oil shales and sediments. Under most groundwater conditions, they occur in two oxidation states As(III)/Sb(III) and As(V)/Sb(V). Arsenic and Sb can be released into groundwater through natural processes such as weathering reactions, biological activity and volcanic emissions, as well as through anthropogenic activities such as mining, combustion of fossil fuels, and the use of arsenical pesticides and wood preservatives, antimonial flame retardants, Pb-Sb alloy in batteries (Smedley and Kinniburgh, 2002; Filella, et al., 2002). In the environment, especially in drinking water, As is a great threat to human health. Arsenic is a teratogen, carcinogen and is chronically toxic at relatively low concentrations (<100ppb) (Manning et al. 2002). The WHO guideline value for As in drinking water was provisionally reduced in 1993 from 50 to 10 $\mu g\ l^{-1}$ (WHO, 1993). The US EPA drinking water limit for As was lowered from 50 $\mu g\ l^{-1}$ to 10 $\mu g\ l^{-1}$ in 2001. Canadian provisional drinking water limit is 25 ppb.

Antimony and its compounds are also considered as pollutants of priority interest by the EPA (USEPA, 1979) and the European Union (Council of European Communities, 1976). The EPA drinking water limit for Sb is 6 $\mu g\ l^{-1}$ (USEPA, 1999). Most environmental research on Sb is limited to studies on concentrations and speciation of Sb in environmental, biological, and geochemical samples (Filella et al, 2002). There are a few studies of the interactions between dissolved Sb and solid phases. Pilarski et al. (1995) found adsorption of Sb(III) by humic acids followed Langmiur-type isotherms with a saturation capacity of 23 μmol/g. Thanabalasingam and Pickering (1990) reported that

the hydrous oxides of Mn, Fe and Al sorbed antimony from dilute $Sb(OH)_3$ solution and capacity values decreased gradually along the sequence $MnOOH > Al(OH)_3 > FeOOH$. Very few studies have been done to remediate antimony pollution in groundwater.

The permeable reactive barrier (PRB) technology is a promising alternative for the *in situ* remediation of both organic and inorganic contaminants in groundwater. Zero-valent iron PRBs remove dissolved both As(III) and As(V) from groundwater through precipitation of arsenic sulfides or through adsorption to or co-precipitation with Fe and Mn oxides (McRae et al., 1999; Farrell et al., 2001; Su and Puls, 2001, 2003; Manning et al., 2002; Melitas, et al., 2002; Bain et al., 2003). Antimony and As are in the same group (group VA) of the periodic table of the elements, have two same redox states (III and V) in the environment, are both strongly sorbed by Fe, Al and Mn oxides, and precipitate both as sparingly soluble sulfide minerals. Thus zero-valent iron PRB might also be able to remove Sb from groundwater. Organic carbon (wood chips, paper mill pulp, municipal compost, etc.) is another widely used reactive material in PRBs to treat acid mine drainage and heavy metals (Benner et al., 1997, 1999; Ludwig et al., 2002). PRBs with organic carbon remove dissolved sulfate, Fe^{2+} and other metals through enhanced biological sulfate reduction and metal sulfide precipitation (Waybrant et al., 1998, 2002). Under favourable conditions, sulfate reducing bacteria (SRB) catalyze the oxidation of organic carbon coupled with the reduction of sulfate to sulfide through the following reaction:

$$SO_4^{2-} + 2CH_2O \rightarrow H_2S + 2HCO_3^- \qquad (1)$$

where CH_2O represents a simple organic carbon. Increased H_2S concentrations enhance the precipitation of metals as metal sulfides:

$$Me^{2+} + S^{2-} \rightarrow MeS \quad (2)$$

where M^{2+} denotes a divalent metal such as Cd, Fe, Ni, Cu, Co, and Zn.

Many mine drainage waters contain high concentrations of As and Sb (Boyle and Jonasson, 1984; Smedley and Kinniburgh, 2002). Laboratory and field results show that organic carbon and zero-valent iron mixtures rapidly removed As from groundwater (Spink, 2001; Bain et al., 2003). The objectives of this study are: 1) to evaluate the rates and capacities of the mixtures of organic carbon PRB and zero-valent iron PRB to remove dissolved As and Sb from groundwater; 2) to study the speciation of As and Sb in water and in solid phase and to understand the mechanisms of immobilization of As and Sb.

4.3 Experimental and Analytical Methods

4.3.1 Column Design and Experimental Setup

The column design and experimental setup are described in Chapter 3 and in Guo and Blowes (submitted).

4.3.2 Geochemical Analysis

The analysis procedures of pH, Eh, alkalinity, major cations (such as Ca, Fe, K, Mg, Na, and Mn) and anions (such as sulfate and sulfide) are described in Chapter 3 and in Guo and Blowes (submitted). Total concentration of As and Sb were analyzed using Hydride

Generation Atomic Absorption Spectroscopy (HG-AAS). And As species (III and V) of selected samples were separated using the anion exchange method of Edwards et al. (1998) and then analyzed with HG-AA.

4.3.3 Solid Phase Analysis

The sample extraction procedures are described in Chapter 3 and in Guo and Blowes (submitted). The XANES samples (not ground) were transferred in a small anaerobic container inside the glove box and then transported to the analysis lab in the container. The samples were exposed to air for a few hours before and during the analysis.The XANES analysis was carried out at beamline X27, National Synchrotron Light Source (NSLS) at Brookhaven National Laboratory (Upton, NY). Small wood chip and iron chip samples were put into a 0.5 mm thick acrylic holder with Mylar film (2.5 μm thick, Chemplex Industries, New York) to reduce the self-absorption effects.

4.3.4 Geochemical Modeling

The geochemical modeling methods are described in Chapter 3 and in Guo and Blowes (submitted).

4.4 Results and Discussion

4.4.1 Arsenic and Antimony Removal

Arsenic was removed in both of the columns, but the removal rate and capacity in two columns were quite different (Fig. 4.1 and 4.2). The average As concentration in the influent to both columns was 5300 μg l^{-1}, ranging from 4500 to 6200 μg l^{-1}. Arsenic concentration in the effluent of the OC column was greater than 10 μg l^{-1} (US EPA drinking water limit) from the beginning of the experiment and reached 1000 ppb in 25 pore volumes. The As front (C = 10 μg l^{-1}) was within 5.5 cm into the FeOC column (3.5 cm into the reactive mixture) at PV 65 and the effluent concentration was close to 1 ppb for at least 65 PVs. The removal rate and the removal capacity of the reactive mixtures are defined as:

removal rate = As or Sb mass removed / mass of OC or OC+Fe / duration of time (3)

removal capacity = As or Sb mass removed / mass of OC or OC+Fe (4)

The As or Sb mass removed was calculated using the differences in As or Sb concentrations between influent and effluent (or port 2 for the FeOC column) and the volume of the water flowing through the column during a period of time. The average As removal rate for the OC column was 13 nmole day^{-1} g^{-1} (dry weight of organic carbon) and its removal capacity was 11 μmole g^{-1} (dry weight of organic carbon). Because the As front did not extend beyond port 2, the As concentration of port 2 instead of effluent, the mass of organic carbon and zero-valent iron of the first 5.5 cm instead of the entire FeOC column, were used to calculate the removal rate and capacity. The remove rate of the FeOC material was 165 nmole day^{-1} g^{-1} (dry weight of organic carbon) or 53 nmole

day^{-1} g^{-1} (dry weight of organic carbon and zero-valent iron). Because more than 99% As was continuously removed at port 2 after PV 65, the actual removal capacity was not attained. Instead the minimum removal capacity was estimated using the total As removed from influent to Port 2 and the mass of organic carbon and zero-valent iron in the first 5.5 cm of the FeOC column. The minimum As removal capacity of the FeOC column is 105 μmol g^{-1} (dry weight of organic carbon) or 34 μmol g^{-1} (dry weight of organic carbon and zero-valent iron).

Bain et al. (2003) did similar column experiment using 100% zero-valent iron to remove As from contaminated groundwater and found that As concentration decreased from 7 to 16 mg l^{-1} in the influent to less than 5 to 20 μg l^{-1} within the first 10 cm of the reactive material and the removal rate was 5.2 to 11.9 mg l^{-1} day^{-1}. Considering that both the As concentration in the influent of Bain et al. (2003) were several times higher than that of FeOC column, the removal rates of the two experiments were reasonably consistent. Thanabalasingam and Pickering (1986) studied arsenic adsorption by humic acids and found that the adsorption capacity could be 90 mmol kg^{-1} for As(III) and 110 mmol kg^{-1} for As(V). Humic substances (including humic acids) are the major components of compost, the reactive material in OC column and XPS analysis shows wood chips of OC contain about 0.2 wt% As. There was also small amount of hydrous iron oxides in OC as impurities and coating of the aggregates.

Both reactive mixtures remove Sb completely, and Sb concentrations in the effluent to both columns were close to detection limit (1μg l^{-1}). However, the Sb front advanced more rapidly in the OC column than in the FeOC column. The Sb front (C = 6 μg l^{-1}) in

the OC column passed port 2 at PV 7 and the Sb front in the FeOC column had not reached port 2 for 65 PVs. Antimony removal rate of the OC material decreased from 8.2 to 1.4 nmole day^{-1} g^{-1} (dry weight of organic carbon) and its removal capacity is 2.4 μmole g^{-1} (dry weight of organic carbon). Because the Sb concentration of port 2 was still close to detection limit (1 μg l^{-1}) after 65 PVs, the actual Sb removal rate and capacity were not attained. Instead the minimum removal rate and capacity were estimated using the total Sb removed from influent to Port 2 and the mass of organic carbon and zero-valent iron in the first 5.5 cm of the FeOC column. The minimum removal rate of FeOC material is 13 nmole day^{-1} g^{-1} (dry weight of organic carbon) or 4.3 nmole day^{-1} g^{-1} (dry weight of organic carbon and zero-valent iron) and its minimum removal capacity is 8.4 (dry weight of organic carbon) or 2.7 μmole g^{-1} (dry weight of organic carbon and zero-valent iron).

4.4.2 Arsenic Speciation

Aqueous speciation of As was determined for the OC column only, because As concentrations of FeOC samples were too low. The trend of As(III) / [As(III) + As(V)] ratio was similar to that of the Eh profile of the OC column (Fig. 4.3). Arsenic in the influent was prepared with $Na_2HAsO_4 \cdot 7H_2O$, so nearly all the As was +5. As(III) increased sharply from 1% of the influent to 84% of port 6 as Eh decreased from 400 mV to around 0 mV. Then As(III) and Eh both levelled off for the rest of the column at about 80% and 0 mV, respectively (Fig. 4.3 and Table 4.1). This observation is consistent with the measurements made in strongly reducing aquifers (characterized by Fe(III)- and SO_4-

reducing conditions) and in the sulfate-reducing zones of some mine tailing impoundments or metal-contaminated sediments. As(III)/As_T ratios of the reducing As-rich groundwaters from Bangladesh are typically around 0.5-0.6, and the ratios for reducing waters from Inner Mongolia 0.6-0.9 (Smedley and Kinniburgh, 2002). The As(III) / [As(III) + As(V)] ratios for the pore water in the sulfate-reducing zone of the current tailings impoundment at Campbell Mine in Balmertown, ON, Canada are 0.7-0.9 (McCreadie et al., 2000; Stichbury et al., 2000), and the ratios are 0.6-0.9 for the pore water of the contaminated sediments in Milltown Reservoir in western Montana (Moore et al., 1988).

Arsenic solid speciation was measured using x-ray absorption near edge spectroscopy (XANES). XANES spectra show that As(V) is the dominant species in the one sample from the OC column and in one of the two samples from the FeOC column and that no As(III) oxide species was found in any of the three samples (Fig. 4.4). Given that the reactive mixtures in the two columns are in sulfate-reducing environments, we believe that As was oxidized by high energy incident x-ray during XANES analysis (Foster et al., 1998). XANES spectra of the FeOC port 2 sample indicate the presence of As(III) sulfide species. The detection of As(III) sulfide is probably because of the greater resistance to oxidation by high energy x-rays of this form than As(III) oxides.

4.3 Arsenic Removal Mechanisms

As(III) species were found in both columns, indicating that As(V) was reduced in both columns. As(III) species were also found in both aqueous and solid samples (Fig. 4.3 and

4.4, Table 4.1). Zobrist et al. (2000) also observed that arsenate was reduced to arsenite when arsenate was in solution as well as being adsorbed onto the surface of ferrihydrite.

Arsenic can be used in microbial anaerobic respiration as a terminal electron acceptor and As respiring bacteria are widespread and metabolically active in nature (Stolz and Oremland, 1999). Some sulfate-reducing bacteria and iron-reducing bacteria can also grow using arsenate as a terminal electron acceptor (Newman et al., 1997). Zobrist et al. (2000) found that *Sulfurospirillum barnesii* were able to reduce arsenate to arsenite in solution and on the surface of ferrihydrite. The bacteria-mediated As(V) reduction is also supported by the reduction rates. The As(V) reduction rate in OC column was more rapid than the abiotic chemical reduction rates reported by Newman et al.(1997) and Rochette et al.(2000). The possible reductants in OC column are sulfide and Fe^{2+}. But Zobrist et al. (2000) observed that Fe^{2+} could not reduce As(V) in the presence of ferrihydrite under anoxic conditions. Arsenate reduction by sulfide is a second order rate reaction, being first order with respect to both arsenate and sulfide:

$$d[H_2AsO_4^-]/dt = k\,[H_2AsO_4^-]\,[H_2S] \qquad (3)$$

and at pH > 7 it is a kinetically slow reaction with a rate constant k of about 1 $M^{-1}\,h^{-1}$ (Newman et al., 1997; Rochette et al., 2000). In pore water of the OC column the calculated rate of abiotic chemical reduction is 7.0×10^{-11} M h^{-1}, much less than the actual reduction rate of 8.0×10^{-7} M h^{-1}. Newman et al. (1997) also measured the reduction rate of microbial experiments (about 5.0×10^{-5} M h^{-1}). It is likely, therefore, that biotic reduction rate is also a function of the arsenate concentration. Thus the difference in the reduction rate between Newman et al. (1997) and the OC column might

be caused by the difference in As(V) concentrations: 2.5×10^{-3} M for Newman et al. (1997) and 7.3×10^{-5} M for the OC column, and the rate constants might be more comparable than the reduction rates. It is likely, therefore that the reduction of As(V) in the OC column is mediated by bacterial activity. The SRB activity and sulfate reduction rate of the FeOC column are much higher than the OC column, thus As(V) reduction in the FeOC column also probably is bacterially mediated.

XANES measurements show that As(III) sulfides in the solid sample from FeOC port 2. There are high levels of bacterial sulfate reducing activity in the FeOC column. Combined, these observations suggest As(V) reduction was mediated by bacterial activity and that As was removed by precipitation as a sulfide or coprecipitation with iron sulfides in both columns. Geochemical modeling also showed that the pore water of the OC column was oversaturated with respect to orpiment (As_2S_3), as well as an amorphous FeS precipitate (Figure 4.5). SI values of FeS precipitate were close to 0, but those of orpiment were much higher than 0, indicating that As concentrations in pore water were controlled by coprecitpiatation with iron sulfide, not by orpiment. Arsenic sulfides or As-bearing iron sulfides are also believed to be the As sinks in similar geochemical environments. McCreadie et al. (2000) and Stichbury et al. (2000) suggested that the precipitation with sulfides or the coprecipitation with iron sulfides caused As concentration decreased sharply in sulfate reducing zone of the current tailings impoundment at Campbell Mine in Balmertown, ON, Canada. Field and laboratory studies show that As was immobilized as an iron-arsenic-sulfide solid phase by bacterial sulfate reduction in the reduced zone of the contaminated sediments in Milltown

Reservoir in western Montana (Moore et al., 1988; Rittle et al., 1995). Kirk et al. (2004) found that in a glacial aquifer in central Illinois, As levels are controlled by the rate of bacterial sulfate reduction: when SRB are active, As precipitates with sulfide or coprecipitate with iron sulfides, and therefore As concentrations are low; in the absence of sulfate reduction, methanogenesis is the dominant metabolism and As concentrations are high.

4.5 Conclusions

The results of this study demonstrate that Fe-bearing organic carbon reactive mixture sustained higher removal rates and capacities for As and Sb in groundwater than organic carbon reactive mixture. As(V) was reduced to As(III), which was mediated by bacterial activity. There were high levels of bacterial sulfate reduction in both reactive mixtures and As was immobilized through precipitation with sulfide or coprecipitation with iron sulfides.

4.6 Acknowledgements

We thank Laura Groza, Jeff Bain, and Matt Lindsay for their assistance with lab work and helpful comments. Mark Biesinger's help in XPS analysis and interpretation and Paul Northrup's assistance in x-ray adsorption near edge spectroscopy analysis are greatly appreciated. Funding for this research was provided by the Natural Sciences and Engineering Research Council of Canada, through a grant provided to D.W. Blowes.

4.7 References

Bain, J., Spink, L., Blowes, D.W., and Smyth, D. (2003), The removal of arsenic from groundwater using permeable reactive materials, In: Sudbury ’03 – Mining and the Environment III, Sudbury, Ontario, Canada

Benner, S.G., Blowes, D.W., and Ptacek, C.J. (1997), A full-scale porous reactive wall for prevention of acid mine drainage, Ground Water Monitoring and Remediation, Vol. 17 (4), pp. 99-107.

Benner, S.G., Blowes, D.W., Gould, W.D., Herbert, R.B.Jr., and C.J. Ptacek (1999), Geochemistry of a permeable reactive barrier for metals and acid mine drainage, Environmental Science and Technology, Vol. 33 pp. 2793-2799.

Boyle, R.W. and Johnson, I.R. (1984), The geochemistry of antimony and its use as an indicator element in geochemical prospecting, Journal of Geochemical Exploration, Vol., 20, pp. 223-302.

Council of European Communities (1976), Council Directive 76/464/EEC of 4 May 1976 on pollution caused by certain dangerous substances discharged into the aquatic environment of the Community. Official Journal L 129, 18/05/1976, pp. 13-29.

Edwards, M., McNeill, L., Patel, S., Chen, H.W., Frey, M., Eaton, A.D., Antweiler, R.C., and Taylor, H.E. (1998), Considerations in As analysis and speciation, Journal of the American Water Works Association, Vol. 90 (3), pp. 103-113.

Farrell, J., Wang, J., O’Day, P., and Conklin, M. (2001), Electrochemical and spectroscopic study of arsenate removal from water using zero-valent iron media, Environmental Science and Technology, Vol. 35, pp. 2026-2032.

Filella, M., Belzile, N., and Chen, Y. (2002), Antimony in the environment: a review focused on natural waters I. Occurrence, Earth-Science Reviews, Vol. 57, pp. 125-176.

Foster, A.L., and Brown, G.E., and Parks, G.A. (1998), X-ray absorption fine-structure spectroscopy studey of photocatalyzed, heterogeneous As(III) xidation on kaolin and antase, Environmental Science and Technology 32, 1444-1452.

Guo, Q., and Blowes, D.W. (submitted), Biogeochemistry of two types of permeable reactive barriers, organic carbon and Fe-bearing organic carbon: column experiments, submitted to Journal of Contaminant Hydrology.

Ludwig, R.D., McGregor, R.G., Blowes, D.W., Benner, S.G., Mountjoy, K. (2002), A permeable reactive barrier for the treatment of dissolved metals, Ground Water 40, 59-66.

Manning, B.A., Hunt, M.L., Amrhein, C., and Yarmoff, J.A. (2002), Arsenic(III) and arsenic(V) Reactions with Zero-valent Iron Corrosion Products, Environmental Science and Technology, Vol. 36, pp. 5455-5461.

McCreadie H., Blowes D.W., Ptacek C.J., and Jambor J.L. (2000), Influence of reduction reactions and solid-phase composition on porewater concentrationsof arsenic, Environmental Science and Technology 34, 3159-3166.

McRae, C.W.T., Blowes, D.W., and Ptacek, C.J. (1999), In situ removal of arsenic from groundwater using permeable reactive barriers: a laboratory study. Sudbury ’99 - Mining and the Environment II Conference, Sudbury, Ontario, 601-609.

Melitas, N., Wang, J., Conklin, M., O’Day, P., and Farrell, J. (2002), Understanding soluble arsenate removal kinetics by zero-valent iron media, Environmental Science and Technology, Vol. 36, pp. 2074-2081.

Newman, D.K., Kennedy, E.K., Coates, J.D., Ahmann, D, Ellis, D.J., Lovley, D.R., and Morel, F.M.M. (1997), Dissimilartory arseniate and sulfate reduction in Desulfotomaculum auripigmentum sp. nov., Archive of Microbiology, Vol. 168, pp. 380-388.

Pilarski, J., Waller, P., Pickering, W. (1995), Sorption of antimony species by humic acid, Water, Air, Soil Pollution, Vol. 84, pp. 51– 59.

Rochette, E.A., Bostick, B.C., Li, G., and Fendorf, S. (2000), Kinetics of arseniate reduction by dissolved sulfide, Environmental Science and Technology, Vol. 34, pp. 4714-4720.

Smedley, P.L. and Kinniburgh, D.G. (2002), A review of the source, behaviour and distribution of arsenic in natural waters, Applied Geochemistry, Vol. 17, pp. 517-568.

Spink, L.E. (2001), B.Sc. thesis, Department of Earth Sciences, University of Waterloo, 56p.

Stichbury M.L., Bain J.G., Blowes D.W. and Gould D., 2000. Microbially-mediated reductive dissolution of arsenic-bearing minerals in a gold mine tailings impoundment. ICARD 2000 (Proceedings from the Fifth International Conference on Acid Rock Drainage), Society for Mining, Metallurgy and Exploration, Littleton, CO, U.S.A., 97-103.

Stolz, J.F. and Oremland, R.S. (1999), Bacterial respiration of arsenic and selenium, FEMS Microbiology Reviews, Vol. 23, pp. 615-627.

Su, C. and Puls R.W. (2001), Arsenate and arsenite removal by zero-valent iron: kinetics, redox transformation, and implications for in situ groundwater remediation, Environmental Science and Technology, Vol. 35, pp. 1487-1492.

Su, C. and Puls R.W. (2003), In situ remediation of arsenic in simulated groundwater using zero-valent iron: laboratory columntests on combined effects of phosphate and silicate, Environmental Science and Technology, Vol. 37, pp. 2582-2587.

Takahashi, Y., Ohtaku, N., Mitsunobu, S, Yuita, K, and Nomura, M (2003), Determination of the As(III)/As(V) ratio in soil by X-ray absorption near-edge structure (XANES) and its application to the arsenic distribution between soil and water, Analytical Sciences, Vol. 19, pp. 891-896.

Thanabalasingam, P. and Pickering, W.F. (1986), Arsenic sorption by humic acids, Environmental Pollution (Series B), Vol. 12, pp. 233-246.

Thanabalasingam, P. and Pickering, W.F. (1990), Specific sorption of antimony(III) by the hydrous oxides of Mn, Fe, and Al, Water, Air, and Soil Pollution, Vol. 49, pp. 175-185.

United States Environmental Protection Agency (1979), Water Related Fate of the 129 Priority Pollutants, vol. 1, USEPA, Washington, DC, USA, EP-440r4-79-029A.

United States Environmental Protection Agency (1999), National Primary Drinking Water Standards, USEPA Office of Water, Washington, DC, USA, Doc. 810-F-94-001.

Waybrant, K.R., Blowes, D.W., and Ptacek, C.J. (1998), Selection of reactive mixtures for use in permeable reactive walls for treatment of mine drainage, Environmental Science and Technology, Vol. 32, pp. 1972-1979

Waybrant, K.R., Ptacek, C.J., and Blowes, D.W. (2002), Treatment of Mine Drainage Using Permeable Reactive Barriers: Column Experiments, Environmental Science and Technology, Vol. 36, pp. 1346-1356

WHO (1993), Guidelines for drinking-water quality, Volume 1: Recommendations, 2nd ed, WHO, Geneva.

Zobrist J., Dowdle P.R., Davis J.A., and Oremland R.S. (2000), Mobilization of arsenite by dissimilatory reduction of adsorbed arsenate, Environmental Science and Technology 34, 4747-4753.

Table 4.1 Aqueous As speciation of OC column

Sample	As(III) (%)	As(V) (%)
Influent	1	99
OC P2	51	49
OC P6	84	16
OC P12	75	25
OC Ef	80	20

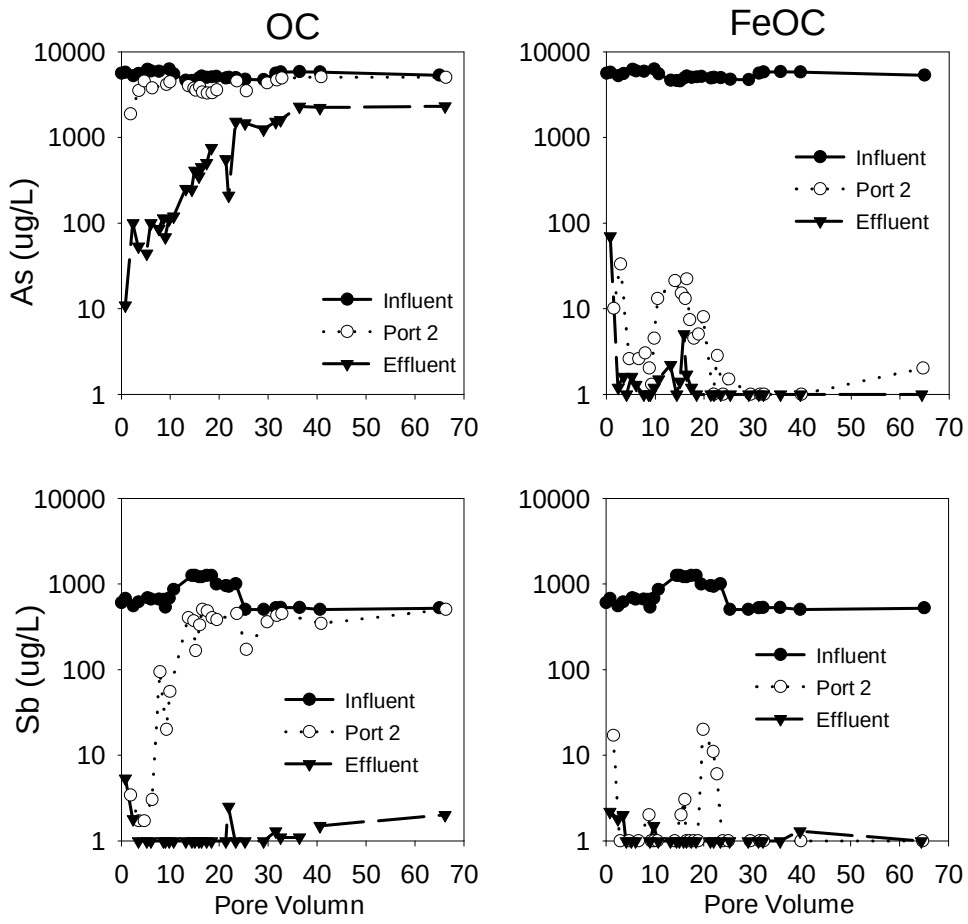

Figure 4.1 Temporal changes in As and Sb of OC and FeOC columns. Arsenic was removed fast and completely in the FeOC column, but only half of As was removed in the OC column after 35 PVs. Antimony was removed in both columns, but the FeOC was more efficient: all Sb was removed before Port 2.

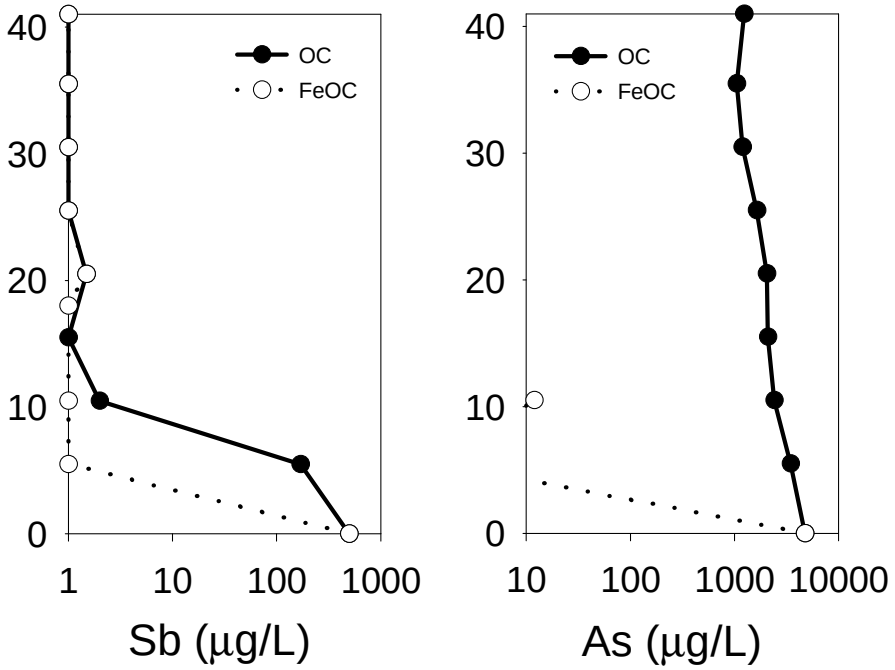

Figure 4.2 Profiles of Sb and As of OC and FeOC columns during PV 25-29. Both As and Sb were removed within first 5.5 cm in the FeOC column. In the OC column, only half of As was removed and Sb was detected after 15 to 20 cm.

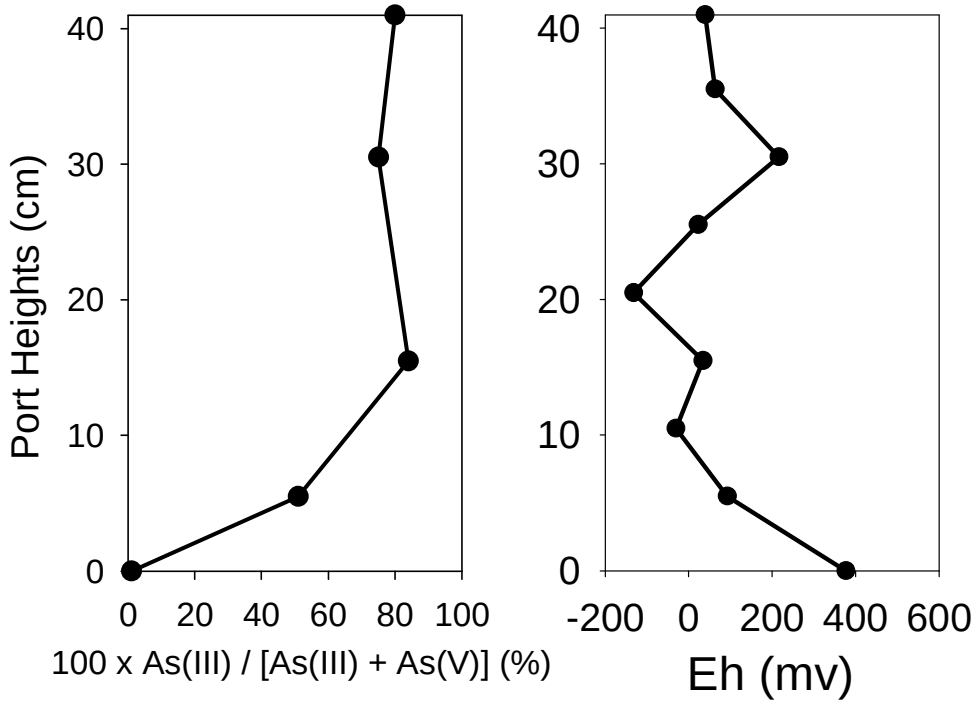

Figure 4.3 Profiles of arsenic aqueous speciation and Eh of OC column. As Eh values dropped from 400 to 0 to 100 mv, As(III) ratio increased from 0 to 80%.

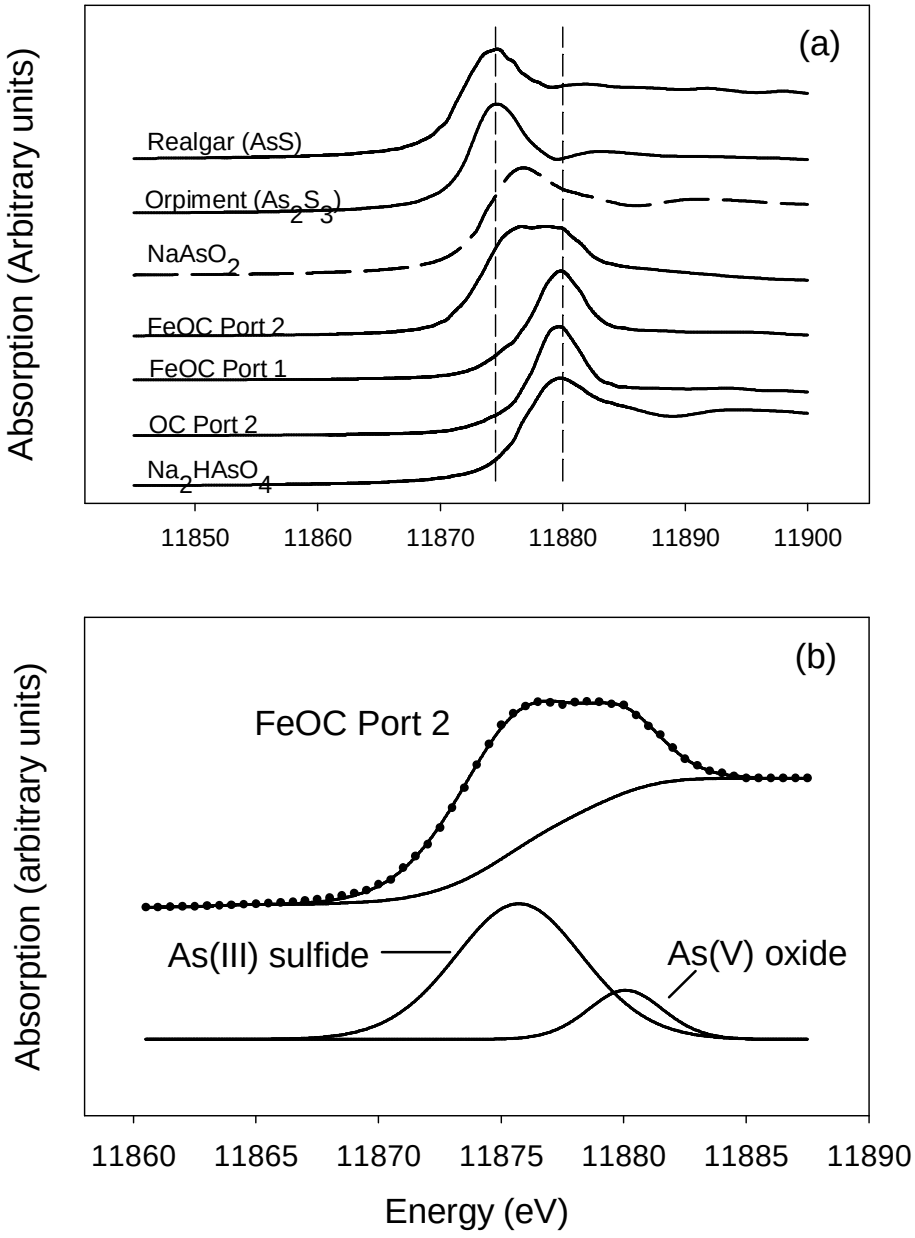

Figure 4.4 Arsenic XANES spectra. (a) Spectra of samples and reference materials and the spectra of $NaAsO_2$ is an approximation of the $NaAsO_2$ spectra in Figure 1 of Takahashi et al.(2003). (b) Interpretation of the spectra of FeOC Port 2. Only As(V) species was found in the sample of OC Port 2 and FeOC Port 1, which probably was caused by the As(III) oxidation by x-ray during analysis. As(III) sulfide is the dominant species in the sample of FeOC Port 2.

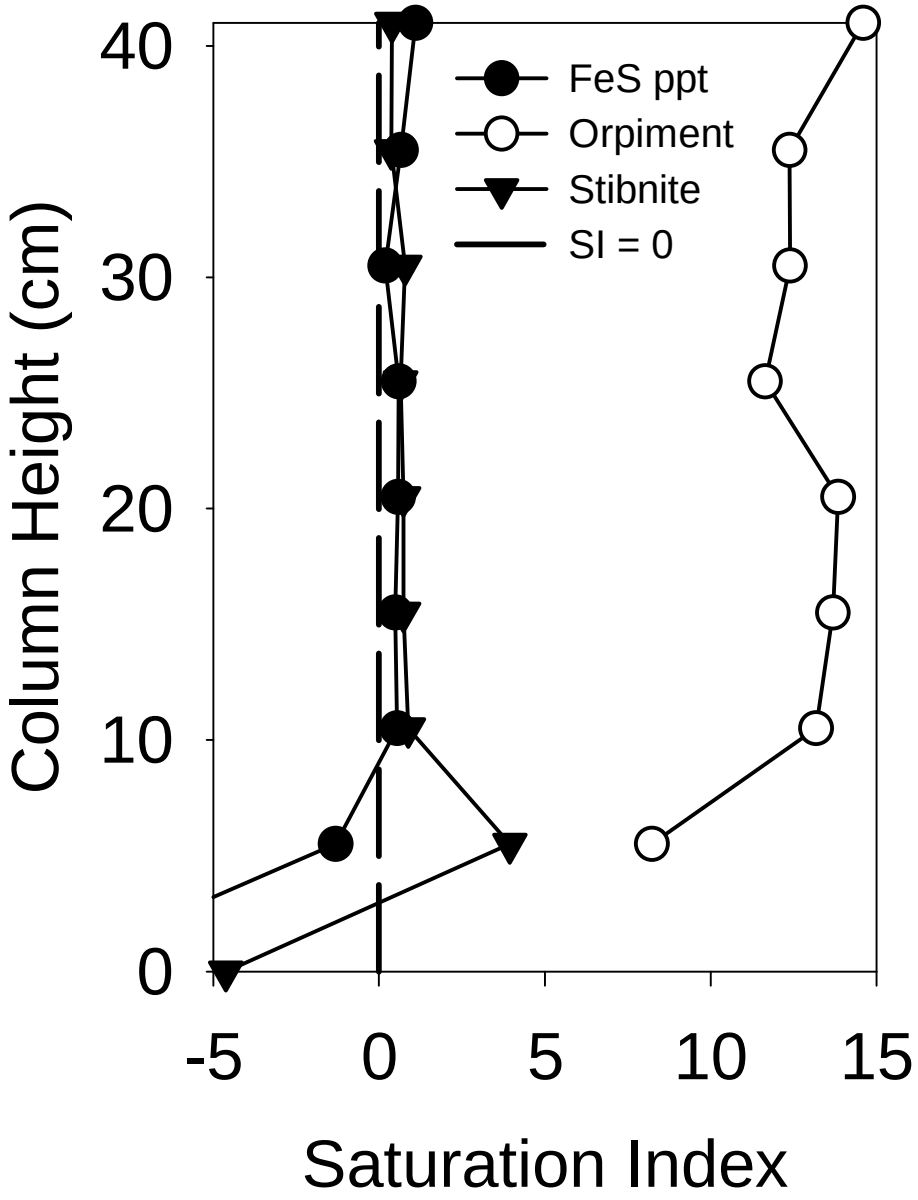

Figure 4.5 Saturation indices (SI) of selected sulfide minerals for the samples of the OC column at PV 25-29. SI values of stibnite were close to 0, indicating that Sb concentrations in pore water were controlled by stibnite. SI values of orpiment were much larger than 0, suggesting that As concentrations in pore water were not controlled by orpiment.

Chapter 5

Conclusions

5.1 Conclusions of the three studies

This study is the one of two experimental studies on the As and Sb partitioning at hydrothermal conditions. The other is Simon et al. (2007). It is the first As partitioning experiment which was conducted under the controlled oxygen fugacities, from reduced conditions to oxidized conditions (NNO – 3.2 to NNO + 7.8). These are also the first experiments which systematically study the effects of oxygen fugacity, SiO2 content, ASI on As and Sb partitioning, and the As concentration on As partitioning. The partition coefficients (± 1σ) of As and Sb between aqueous fluid and melt, $D_{As}^{f/m}$ and $D_{Sb}^{f/m}$, are 1.4 ± 0.5 and 0.8 ± 0.5, respectively, in the system SiO_2-Al_2O_3-Na_2O-K_2O-H_2O at 800 °C and 200 MPa. The partitioning of As is not affected by ASI or SiO_2 content of the melt, or by oxygen fugacity under oxidized conditions (f_{O_2} > NNO). However, under more reduced conditions (f_{O_2} ≤ NNO), an As mineral phase apparently crystallized and $D_{As}^{f/m}$ could not be determined. The partitioning of Sb is independent of f_{O_2} and SiO_2 content of the melt. However, ASI has a strong effect on Sb partitioning and $D_{Sb}^{f/m}$ for peralkaline melt (0.1 ± 0.01) is much smaller than that for metaluminous and peraluminous melts (0.8 ± 0.4). Thermodynamic calculations show that As(III) is dominant in aqueous fluid at 800 °C and 200 MPa and XPS analysis of run product glass indicate that only As(III) exists in melt, which confirms the finding that f_{O_2} does not affect As partitioning between fluid and melt. The peralkaline effect only occurs during Sb partitioning, not for As partitioning under oxidized conditions, which is consistent

with the XPS measurements that As(III) and Sb(V) are dominant oxidation states in melt under oxidized conditions, because the peralkaline effect is stronger for pentavalent than trivalent cations.

The biogeochemical study of the two types of reactive mixtures demonstrates that the Fe^0-bearing organic carbon reactive mixture sustained a higher sulfate reduction rate for a longer period of time than the organic carbon reactive mixture. The microbial enumerations and isotopic measurements indicate that the sulfate reduction was mediated by SRB. The cathodic production of H_2 by anaerobic corrosion of Fe probably is the cause of the difference in sulfate reduction rates between the two reactive mixtures. Zero-valent iron can be used to provide an electron donor in sulfate-reducing PRBs and Fe^0-bearing organic carbon reactive mixture has a potential to improve the performance of organic carbon PRBs. The $\delta^{34}S$ values can be used to determine the extent of sulfate reduction, but sulfur isotope fractionation is not consistent between reactive materials. The $\delta^{13}C$ values indicate that methanogenesis is occurring in the front part of both columns. This study shows a novel application of isotope tools for the study of permeable reactive barriers and the use of an innovative mixture of organic carbon and zero-valent iron for treatment for sulfate and heavy metal in mine drainage.

The results of the As and Sb remediation experiments demonstrate that the Fe-bearing organic carbon reactive mixture sustained higher removal rates and capacities for As and Sb in groundwater than organic carbon reactive mixture. As(V) was reduced to As(III) both in pore water and on the surface of the reactive material. As(V) reduction was mediated by bacterial activity. There were high levels of bacterial sulfate reduction in both reactive mixtures and As was immobilized through precipitation as arsenic sulfides or coprecipitation with iron sulfides. This study demonstrates the use of an innovative

mixture of organic carbon and zero-valent iron for treatment for As and Sb in mine drainage.

5.2 Relationships between the three studies

The partition coefficients of As and Sb determined in this study could explain why geothermal waters and hot springs have higher concentrations of As and Sb than river and lake waters. At high temperature, As and Sb concentrations in aqueous fluid are similar to those of the rocks, because $D_{As}^{f/m}$ and $D_{Sb}^{f/m}$ are 1.4 ± 0.5 and 0.8 ± 0.5 at 800 °C. At low temperature, As and Sb concentrations in natural waters (ppb level) are usually three orders of magnitude lower than those in sediments or rocks (ppm level).

Redox conditions affect the behavior of As and Sb in groundwater to greater extent compared to high temperature hydrothermal and geothermal fluids. The As and Sb remediation experiments demonstrate that the As(V) is reduced to As(III) and precipitates as arsenic sulfides or coprecipitate with iron sulfides in the reactive material. At 800 °C and 200 MPa, oxygen fugacity does not affect As or Sb partitioning at oxidized conditions (f_{O_2} > NNO), however, under more reduced conditions (f_{O_2} ≤ NNO), an As mineral phase apparently crystallized and $D_{As}^{f/m}$ could not be determined. Redox conditions also have different effects on As compared to Sb behavior. Mitsunobu et al. (2006) found that Sb(V) is very stable and Sb(III) is oxidized at more negative Eh than As in surface soil-water system. A similar trend was found at high pressure and temperature. The XPS measurements of the As and Sb partitioning experiments indicate

that As(III) and Sb(V) are dominant oxidation states in granitic melt at oxidized conditions.

Zero-valent iron is a key factor for both the sulfate reduction in the organic carbon PRB and the As and Sb remediation. The cathodic production of H_2 by anaerobic corrosion of Fe sustained a higher sulfate reduction rate for a longer period of time than the organic carbon only reactive mixture. Fe-bearing organic carbon reactive mixture also sustained higher removal rates and capacities for As and Sb in groundwater than the organic carbon-only reactive mixture. The two processes were closely coupled because sulfate reduction and As(V) reduction were both mediated by bacterial activity and As was immobilized through precipitation with sulfide or coprecipitation with iron sulfides.

5.3 Recommendation for future research

The recommended future research for As and Sb partitioning experiments includes:

- To determine the As mineral phase crystallized in the melt under neutral and reduced conditions (f_{O_2} ≤ NNO). An As mineral phase was suspected to have crystallized from either the melt or the aqueous fluid under these conditions, but was not be able to identify the mineral. The identity of the mineral would help to understand the As partitioning behavior under these conditions.
- To determine the oxidation state of Sb in the melt under neutral and reduced conditions (f_{O_2} ≤ NNO). XPS and XANES analysis of this study failed to determine the oxidation state of Sb in the melt under these conditions due to low

concentration of Sb in the glass samples. This information would elucidate the reactions occurring during partitioning.

- To determine the partition coefficients of As and Sb between the granitic melt and the low-salinity aqueous fluid at various oxygen fugacity conditions. Most natural hydrothermal fluids are low-salinity solutions. Partition data from the low-salinity aqueous fluid experiments would describe the real hydrothermal system more accurately.

The recommended future research for the biogeochemical study of the two types of reactive mixtures includes:

- To determine whether cathodic hydrogen enhances other anaerobic processes such as cellulolysis, cellobiohydrolysis, and fermentation besides sulfate reduction and methanogenesis. If cathodic hydrogen only affects sulfate reduction and methanogenesis, the life of the PRB system would be limited by the production of hydrogen. If cathodic hydrogen also increases the activity of the upstream microbial groups, then the PRB system would continue to be effective after the hydrogen production stops.
- To determine the relationship between hydrogen production or concentration and the relative activity of SRB, IRB, and methanogens. Lovley and Goodwin (1988) and Lovley et al. (1994) found that hydrogen concentrations indicated the predominant terminal electron-accepting processes (TEAPs) in both aquatic sediments and in anoxic groundwater. But it is unknown that whether TEAPs (sulfate reduction, iron reduction, methanogenesis, etc.) control the hydrogen concentration, or the hydrogen concentration determines the predominant TEAP. If the hydrogen concentration controls TEAPs, changing hydrogen concentration

(e.g. by using different size of zero-valent iron) can promote the desired TEAP such as sulfate reduction and suppress nonbeneficial TEAP such as methanogenesis.

- To determine long term performance of Fe^0-bearing organic carbon PRBs. The experiments of this study last 17 months, but PRB systems are designed to perform for decades. So long term data are needed to evaluate Fe^0-bearing organic carbon PRBs.

The recommended future research for As and Sb remediation experiments includes:

- The As and Sb removal capacities and the long term performance of Fe^0-bearing organic carbon PRBs. The experiments of this study performed well for 17 months, but PRB systems are designed to be effective for decades. So long term data are needed to evaluate the As and Sb removing abilities of Fe^0-bearing organic carbon PRBs.
- More detailed study on As- and Sb-bearing precipitates, such as As and Sb sulfides and As- and Sb-bearing iron oxides and iron sulfides. This study suggests that As and Sb was removed by coprecipitation with iron sulfides and oxides, precipitation as As and Sb sulfides. The identities of these minerals would help to understand the reactions occurring during removal.
- Antimony speciation in pore water of PRBs. This information would help to understand the Sb removal process.

5.5 References

Mitsunobu S., Harada T., and Takahashi Y. (2006), Comparison of Antimony Behavior with that of Arsenic under Various Soil Redox Conditions, Environmental Science and Technology 40, 7270-7276.

Appendix I

Water Chemistry Data

Water chemistry data

Sample	As umol/L	Sb umol/L	pH	Eh mv	Alkalinity mmol/L	SO4 mmol/L	S2- umol/L	Ca mmol/L	Fe umol/L	Mg mmol/L	Na mmol/L	K mmol/L
OC-P2-Nov23/04	24.69	0.028	6.85	209.8	19.90	2.09		3.34	44.05	0.45	13.14	0.080
OC-P2-Dec7/04	46.72	0.014	7.64	4.2	2.80	3.77		4.34	23.10	0.39	1.00	0.054
OC-P2-Dec17/04	60.06	0.014	7.63	-23.1	5.40	3.86	13.04	3.69	21.49	0.47	5.18	0.097
OC-P2-Jan3/05	50.05	0.025	7.03	-7.9	7.20	3.59	5.30	4.22	46.38	0.32	1.17	0.039
OC-P2-Jan12/05		0.772	7.23	38.2	4.30	3.83	1.28	4.77	18.09			
OC-P2-Jan26/05	54.86	0.164	7.28	-18.4	3.40	3.94	2.18	4.77	13.93	0.39	1.04	0.049
OC-P2-Feb3/05	59.13	0.452	7.49	-69.8	3.20	3.92	2.62	4.11	0.03	0.39	1.04	0.039
OC-P2-Mar10/05	53.08	3.285	7.54	122.6	2.40	3.93	1.22	4.15	0.03	0.41	1.01	0.050
OC-P2-Mar18/05	49.57	3.039	7.91	280.9	2.25	3.94	0.53	3.75	8.90	0.41	1.02	0.041
OC-P2-Mar25/05	47.12	1.355	6.9	118.3	2.10	3.77	10.61	3.94	0.03	0.40	1.02	0.037
OC-P2-Apr1/05	51.52	2.710	7.7	178.5	2.10	3.89	0.97	5.86	14.38	0.39	0.96	0.046
OC-P2-Apr6/05	44.85	4.107	7.04	115.7	6.30	3.88	0.72	5.59	29.90	0.53	0.94	0.054
OC-P2-Apr12/05	43.25	3.943	6.82	145.4	5.50	3.92	0.87	4.94	12.39	0.44	0.93	0.048
OC-P2-Apr19/05	43.78	3.285	7.12	143.9	4.50	3.95	0.72	4.54	0.03	0.38	0.88	0.053
OC-P2-May4/05	47.65	3.121	7.44	206.2	3.40	3.77	0.78	4.52	0.03	0.37	0.89	0.053
OC-P2-Jun8/05	60.02	3.696	8.29	181.9	2.80	3.67	0.12	4.35	0.03	0.39	1.02	0.049
OC-P2-Jun22/05	46.09	1.396	7.34	92.3	6.30	3.73	0.87	5.94	20.23	0.50	1.05	0.083
OC-P2-Jul28/05	56.97	2.932	7.56	239.6	4.00	3.90	0.56	5.27	0.03	0.44	1.08	0.082
OC-P2-Aug10/05	62.24	3.507	7.69	23.6	3.79	3.89	0.09	4.97	0.03	0.42	1.01	0.083
OC-P2-Aug18/05	64.88	3.671	7.41	83.6	3.37	3.89	0.12	5.16	0.03	0.44	1.09	0.086
OC-P2-Nov3/05	66.98	2.817	7.60	333.6	4.56	3.91	0.37	5.39	0.03	0.44	1.01	0.085
OC-P2-May10/06	66.74	4.107	7.83	283.6	3.37	3.93	0.03					
OC-EF-Nov12/04	0.15	0.044	6.54	54.8	36.40	1.97		3.64	188.01	1.58	66.99	0.289
OC-EF-Nov27/04	1.33	0.015	6.65		8.90	0.47		1.87	214.87	0.61	16.57	0.146
OC-EF-Dec6/04	0.71	0.004	6.84	42.8	15.10	1.37		1.97	239.94	0.66	14.09	0.120
OC-EF-Dec20/04	0.59	0.000	7.02	39.6	6.30	2.15	8.83	1.99	114.06	0.66	5.31	0.095

OC-EF-Dec31/04	1.33	0.000	6.87	7.1	7.30	2.56	9.98	3.34	178.88	1.12	1.97	0.115
OC-EF-Jan10/05	1.13	0.000	6.81	133.8	8.40	2.48	14.66	3.52	159.36	1.15	1.30	0.095
OC-EF-Jan18/05	1.51	0.008	6.7	37.5	6.30	2.96	17.06					
OC-EF-Jan24/05		0.008	6.94	-25.1	5.70	3.08	24.42	4.11	0.03			
OC-EF-Feb1/05		0.004	6.84	-74.5	5.20	3.17	15.47	4.07	130.18	0.81	1.06	0.075
OC-EF-Feb10/05	1.60	0.004	6.86	180.6	4.60	3.21	1.25	4.02	75.56	0.71	1.05	0.059
OC-EF-Mar4/05	3.34	0.005	6.92	146.7	3.80	3.28	19.18	3.78	81.44	0.47	0.99	0.060
OC-EF-Mar14/05	3.27	0.003	6.75	101.1	3.50	3.21	6.80	3.78	73.41	0.40	1.02	0.054
OC-EF-Mar22/05	5.47	0.004	7.12	82.5	3.40	3.24	3.24	3.76	75.38	0.39	1.01	0.054
OC-EF-Mar30/05	4.67	0.003	7.04	109.1	4.00	2.90	8.80	3.70	74.54	0.38	1.04	0.060
OC-EF-Apr5/05	6.01	0.006	7.09	52.3	3.10	3.20	10.01	3.77	54.08	0.35	0.97	0.048
OC-EF-Apr11/05	6.67	0.006	7.07	78.3	5.00	3.32	15.75	4.44	57.30	0.40	1.03	0.050
OC-EF-Apr18/05	10.01	0.007	7.05	70.8	8.00	3.51	18.25	6.06	69.12	0.54	0.97	0.048
OC-EF-May18/05	7.38	0.007	7.08	169.3	5.60	3.39	0.50	5.31	30.08	0.48	0.90	0.038
OC-EF-May24/05	2.78	0.021	7.22	195.1	4.10	3.50	0.69	4.34	4.39	0.39	0.90	0.034
OC-EF-Jun6/05	20.15	0.008	7.15	139.6	3.40	3.54	0.53	4.12	93.11	0.35	0.88	0.031
OC-EF-Jun21/05	19.38	0.007	7.1	-18.3	3.70	3.57	1.75	4.44	76.51	0.39	0.98	0.034
OC-EF-Jul22/05	16.48	0.007	7.11	39.6	6.20	3.71	7.83	5.48	84.89	0.49	0.94	0.045
OC-EF-Aug9/05	20.18	0.011	6.85		4.36	3.89	1.00	4.87	63.85	0.39	0.99	0.053
OC-EF-Aug16/05	21.34	0.009	7.15	63.6	4.14	3.87	1.22	4.77	65.23	0.39	0.97	0.061
OC-EF-Sep13/05	30.50	0.009	7.26	-46.4	3.96	3.77	0.59	4.53	62.96	0.38	1.02	0.063
OC-EF-Nov02/05	29.64	0.012	7.64	93.6	4.18	3.81	0.81	4.84	61.10	0.41	1.09	0.072
OC-EF-May8/06	30.70	0.008	7.41	153.6	3.50	3.93	0.97					
FeOC-P2-Nov17/04	0.13	0.140	7.46	-40.6	22.00	2.62		1.59	1359.07	0.70	16.57	0.235
FeOC-P2-Nov30/04	0.44	0.008	7.51	-28.7	3.10	3.45		3.74	368.86		1.50	
FeOC-P2-Dec17/04	0.03	0.000	7.7	49.1	8.50	3.68	0.69	2.74	77.00	0.83	3.65	0.103
FeOC-P2-Jan5/05	0.03	0.000	7.44	6.0	3.70	3.53	1.06	3.89	304.40	0.23	1.09	0.050
FeOC-P2-Jan12/05	0.04	0.000	7.43	43.1	3.80	3.55	1.28					
FeOC-P2-Jan20/05	0.03	0.016	7.34	29.8	3.10	3.66	1.56					
FeOC-P2-Jan26/05	0.02	0.004	7.53	-11.4	2.90	3.71	2.06	4.27	0.01	0.38	1.03	0.054
FeOC-P2-Jan28/05	0.06	0.004	7.49	-9.8	2.00	3.72	1.56	4.19	0.09	0.38	1.03	0.056

FeOC-P2-Feb3/05	0.17	0.008	7.58	-23.4	3.10	3.72	1.25	4.12	0.11	0.38	1.03	0.039
FeOC-P2-Mar10/05	0.28	0.000	7.48	98.6	1.70	3.70	0.87	3.51	45.89	0.39	1.00	0.054
FeOC-P2-Mar18/05	0.20	0.016	7.71	149.3	1.60	3.70	0.22	3.43	4.05	0.40	0.99	0.061
FeOC-P2-Mar23/05	0.17	0.025	7.59	58.5	1.50	3.71	0.19	3.31	24.66	0.39	1.00	0.058
FeOC-P2-Apr1/05	0.29	0.008	7.69	74.8	1.50	3.56	0.84	3.27	7.82	0.36	0.91	0.049
FeOC-P2-Apr6/05	0.10	0.005	7.33	-5.6	4.30	3.45	1.81	4.32	96.87	0.50	0.92	0.059
FeOC-P2-Apr12/05	0.06	0.005	7.24	8.0	4.10	3.42	1.62	4.34	265.01	0.40	0.96	0.046
FeOC-P2-Apr19/05	0.07	0.000	7.14	82.0	2.20	3.39	1.06	3.67	81.29	0.36	0.95	0.042
FeOC-P2-May4/05	0.11	0.164	7.34	253.9	1.60	3.36	0.41	3.24	0.03	0.36	0.93	0.051
FeOC-P2-May20/05	0.01	0.090	7.16	282.9	0.90	3.33	0.75	2.97	0.03	0.36	0.94	
FeOC-P2-May26/05	0.04	0.049	7.32	125.5	1.20	3.32	0.90	2.97	16.15	0.37		
FeOC-P2-Jun8/05	0.01	0.008	7.59	174.1	0.90	2.66	0.12	2.37	4.96	0.32	1.02	0.051
FeOC-P2-Jun22/05	0.02	0.000	7.54	-5.1	1.50	3.11	0.90	2.87	85.48	0.46	0.79	0.082
FeOC-P2-Jul28/05	0.01	0.004	7.47	318.6	0.82	3.26	0.31	2.54	0.03	0.40	1.01	0.084
FeOC-P2-Aug10/05	0.01	0.007	8.04	43.6	0.65	3.30		2.63	0.03	0.41	1.03	0.074
FeOC-P2-Aug18/05	0.01	0.007	7.70	23.6	0.55	3.34	0.00	2.62	6.27	0.40	1.06	0.075
FeOC-P2-Nov3/05	0.01	0.002	7.48	433.6	0.64	3.44	0.12	2.69	0.03	0.44	1.06	0.077
FeOC-P2-May10/06	0.11	0.008	7.20	293.6	0.53	3.16	0.12					
FeOC EF-Nov12/04	0.93	0.018	8.29	110.6	76.30	0.48		3.29	13.04	3.45	173.55	1.701
FeOC EF-Nov27/04	0.02	0.015	8.68		10.00	1.88		0.66	354.54	0.81	26.92	0.246
FeOC-EF-Dec6/04	0.02	0.016	8.9	19.7	7.90	1.51		0.45	7.00	0.44	17.92	0.176
FeOC-EF-Dec10/04	0.00	0.000	9.09	-31.8	10.20	1.50	46.89	0.29	11.53		11.31	
FeOC-EF-Dec20/04	0.02	0.000	9.25	-7.4	6.40	2.10	65.48	0.38	14.20	0.29	7.96	0.138
FeOC-EF-Dec31/04	0.02	0.000	9.1	-30.9	2.50	2.75	85.74	0.56	14.47	0.56	4.74	0.183
FeOC-EF-Jan10/05	0.01	0.000	8.38	129.3	1.60	2.72	84.92	1.26	27.40	1.44	1.44	0.163
FeOC-EF-Jan18/05	0.01	0.000	7.74	41.0	1.40	2.83	88.20					
FeOC-EF-Jan24/05	0.01	0.008	7.83	-26.4	1.30	2.88	89.91					
FeOC-EF-Feb1/05	0.02	0.012	8.07	-64.8	1.30	2.70	84.07	1.73	26.32	1.12	1.37	0.103
FeOC-EF-Feb10/05	0.02	0.007	8.48	157.1	1.60	2.33	72.71	1.63	15.56	0.93	1.22	0.092
FeOC-EF-Mar4/05	0.03	0.000	8.73	265.4	1.90	2.10	65.61	1.73	11.84	0.73	1.06	0.072
FeOC-EF-Mar14/05	0.01	0.000	8.75	266.0		1.87	58.18	1.78	0.71	0.49	1.02	0.062

FeOC-EF-Mar22/05	0.02	0.000	8.86	82.0	1.70	1.56	48.53	1.54	0.42	0.38	1.01	0.061
FeOC-EF-Mar30/05	0.07	0.000	9.04	273.7	1.80	1.12		1.23	0.03	0.30	1.00	0.056
FeOC-EF-Apr5/05	0.02	0.000	9.03	34.7	1.90	0.68	34.96	0.90	0.86	0.21	0.90	0.033
FeOC-EF-Apr11/05	0.02	0.000	9.11	122.9	1.50	0.83	21.11	0.93	0.98	0.19	1.01	0.030
FeOC-EF-Apr18/05	0.01	0.000	8.98	118.3	1.50	1.34	25.98	1.27	0.03	0.23	1.07	0.038
FeOC-EF-May18/05	0.00	0.000	8.83	178.2	0.90	1.74	41.89	1.54	0.03	0.23	1.00	0.043
FeOC-EF-May24/05	0.00	0.000	8.75	233.9	1.10	1.68	54.20	1.52	0.03	0.23	0.97	0.043
FeOC-EF-Jun6/05	0.00	0.000	9.04	-194.4	1.30	1.54	52.30	1.42	0.03	0.22	0.97	0.043
FeOC-EF-Jun21/05	0.01	0.000	8.74	-134.4	1.00	1.80	48.03	1.57	0.03	0.25	1.13	0.058
FeOC-EF-Jul22/05	0.01	0.000	9.07	240.6	1.10	1.93	56.02	1.59	0.03	0.26	1.04	0.063
FeOC-EF-Aug9/05	0.00	0.007	8.80	273.6	0.76	2.26	60.12	1.81	0.03	0.29	1.06	0.075
FeOC-EF-Aug16/05	0.01	0.007	8.97	273.6	0.85	2.26	70.49	1.77	0.03	0.29	1.00	0.077
FeOC-EF-Sep13/05	0.01	0.004	9.05	-196.4	0.85	2.60	70.56	2.03	0.03	0.33	1.03	0.076
FeOC-EF-Nov02/05	0.01	0.011	9.05	336.6	0.84	2.17	81.24	1.63	0.03	0.29	1.10	0.075
FeOC-EF-May8/06	0.01	0.008	8.65	233.6	0.81	2.44	67.57					
IN-Nov3/04	74.34	0.61	6.22		3.30	3.82	0.00	4.54	0.00	0.38	1.04	0.036
IN-Nov12/04	76.21	0.63	5.47		1.90	3.80	0.00	4.67	0.00	0.37	0.97	0.036
IN-Nov27/04	69.27	0.57	6.07		3.10	3.88	0.00	4.57	0.00	0.38	0.96	0.030
IN-Dec6/05	73.68	0.61	8	71.6	3.80	3.81	0.00	4.57	0.00	0.41	0.97	0.053
IN-Dec22/04	82.49	0.68	5.93	119.0	3.50	3.81	0.00	4.27	0.00	0.38	0.97	0.021
IN-Dec31/04	78.88	0.65	6.19	79.2	5.00	3.70	0.00	4.37	0.00	0.21	1.16	0.032
IN-Jan10/05	78.35	0.64	6.44	80.8	3.60	3.90	0.00	4.34	0.00	0.35	0.97	0.039
IN-Jan18/05		0.68	6.85	91.8	3.40	3.94	0.00		0.00			
IN-Jan24/05		0.60	7.19	10.9	3.60	3.98	0.00		0.00			
IN Feb1/05	82.89	0.50	7.74	-18.7	1.30	3.96	0.00	4.87	0.00	0.40	1.02	0.041
IN Feb10/05	73.01	0.50	8.19	404.9	3.40	3.96	0.00	4.94	0.00	0.40	0.99	0.060
IN-Mar4/05	61.22		8.13	351.4	2.30	3.96	0.00	4.08	0.00	0.39	1.00	0.034
IN-Mar14/05	60.80	0.49	8.2	319.6	2.20	3.98	0.00	4.02	0.00	0.40	0.99	0.039
IN-Mar22/05	60.14	0.53	8.25	313.1	2.50	3.97	0.00	3.99	0.00	0.39	0.97	0.036
IN-Mar30/05	65.00	0.56	8.25	368.6	2.10	3.98	0.00	3.94	0.00	0.39	0.87	0.058
IN-Apr5/05	68.47	0.55	5.94	373.6	2.50	3.80	0.00	4.24	0.00	0.39	0.91	0.050

IN-Apr11/05	66.47	0.55	6.23	406.2	3.60	3.84	0.00	4.77	0.00	0.38	0.90	0.052
IN-Apr18/05	67.14	0.56	6.9	355.1	4.20	3.84	0.00	5.01	0.00	0.39	0.91	0.050
IN-May3/05	68.07	0.54				3.73	0.00		0.00			
IN-May18/05	65.27	0.54	8.16	388.7	3.20	3.68	0.00	4.42	0.00	0.38	0.93	0.054
IN-May24/05	66.20	0.54	8.25	328.1	3.20	3.67	0.00	4.42	0.00	0.38	0.88	0.053
IN-Jun6/05	65.94	0.52	8.21	453.6	3.30	3.68	0.00	4.34	0.00	0.38	0.87	0.057
IN-Jun21/05	63.53	0.51	5.93	376.8	4.00	3.75	0.00	4.94	0.00	0.44	1.08	0.000
IN-Jul22/05	62.32	0.61	6.51	355.6	3.93	3.72	0.00	4.71	0.00	0.39	0.99	0.063
IN-Aug9/05	74.42	0.63	7.12	383.6	3.88	3.89	0.00	5.01	0.00	0.42	0.98	0.084
IN-Aug16/05	76.51	0.64	7.13	403.6	4.01	3.88	0.00	5.08	0.00	0.42	0.99	0.087
IN-Sep13/05	77.37	0.63	7.95	183.6	4.38	3.89	0.00	5.11	0.00	0.43	1.00	0.095
IN-Nov2/05	76.83	0.58	7.11	377.6	4.36	3.91	0.00	5.45	0.00	0.43	0.97	0.093
IN-May06/06	70.47	0.00	8.10	543.6	3.39	3.92	0.00		0.00			

Appendix II

Isotope, Microbiology, and Saturation Index Data

DIC isotope data

	Delta (34S)	Delta (18O)
OC-In-Jan27/06	4.37	9.27
OC-P2-Dec2/05	4.76	10.47
OC-P4-Dec7/05	4.3	9.37
OC-P6-Dec10/05	4.83	9.61
OC-P8-Dec16/05	4.91	9.56
OC-P10-Jan6/06	4.01	10.95
OC-P12-Jan16/06	3.82	10.56
OC-P14-Jan19/06	3.9	11.4
OC-Ef-Nov28/05	5.73	11.65
FeOC-In-Jan27/06	4.37	9.27
FeOC-P2-Dec1/05	6.39	9.72
FeOC-P4-Dec7/05	8.21	9.61
FeOC-P6-Dec10/05	9.32	9.44
FeOC-P8-Dec16/05	10.66	9.33
FeOC-P10-Jan6/06	13.09	9.97
FeOC-P12-Jan16/06	18.31	9.7
FeOC-P14-Jan19/06	20.33	10.84
FeOC-Ef-Nov28/05	14.81	12.34

Microbiology data

	Height	SRB	IRB	APB	FDA
	cm	cell/g	cell/g	cell/g	nmol / h / g
FeOC-P2	5.5	4.9E+07	1.7E+04	2.3E+01	5.92E-04
FeOC-P4	10.5	5.4E+03	3.3E+04	2.3E+01	1.77E-03
FeOC-P6	15.5	1.7E+05	3.3E+04	2.3E+01	2.21E-03
FeOC-P8	20.5	3.3E+04	1.1E+04	7.8E+00	2.23E-03
FeOC-P10	25.5	4.6E+07	1.1E+05	2.3E+01	1.61E-03
FeOC-P12	30.5	1.1E+05	3.3E+04	1.3E+01	2.15E-03
FeOC-P14	35.5	3.3E+04	1.7E+04	2.3E+01	1.84E-03
Average		1.4E+07	3.6E+04	1.9E+01	1.8E-03
OC-P2	5.5	5.2E+03	1.7E+05	1.0E-01	3.09E-03
OC-P4	10.5	3.9E+04	1.7E+05	2.3E+01	3.27E-03
OC-P6	15.5	3.6E+04	4.9E+04	1.0E-01	4.23E-03
OC-P8	20.5	2.7E+05	1.7E+05	2.3E+01	4.18E-03
OC-P10	25.5	3.2E+04	3.3E+04	1.3E+01	4.16E-03
OC-P12	30.5	2.5E+05	1.3E+05	2.0E+00	6.11E-03
OC-P14	35.5	3.2E+05	3.3E+04	1.0E-01	5.10E-03
Average		1.4E+05	1.1E+05	8.8E+00	4.3E-03

Saturation Index Data

Sample Name	Calcite CaCO3	Dolomite CaMg(CO3)2	FeS Ppt FeS	Gypsum CaSO4	Siderite FeCO3	Stibnite Sb2S3	Orpiment As2S3
IN-Feb10/05	1.089	1.174	-6.985	-0.791	-1.881	-7.859	
OC-P2-Feb3/05	0.373	-0.255	0.245	-0.801	0.194	2.362	
OC-P4-Feb8/05	0.224	-0.548	0.615	-0.819	0.206	0.877	
OC-P6-Feb11/05	-0.461	-1.759	-2.549	-0.928	-3.165	0.533	
OC-P8-Feb15/05	-0.262	-1.154	0.293	-0.851	-0.027	0.880	
OC-P10-Feb18/05	0.300	-0.350	0.779	-0.889	0.784	0.605	
OC-P12-Feb23/05	0.171	-0.523	0.936	-0.922	0.795	0.664	
OC-P15-Feb28/05	0.121	-0.568	0.919	-0.942	0.826	0.759	
OC-EF-Mar4/05	-0.199	-1.127	0.365	-0.939	0.490	1.069	
IN-Jun21/05	-1.070	-3.103	-10.197	-0.810	-3.974	-4.621	
OC-P2-Jun22/05	0.601	0.214	-1.302	-0.773	0.438	3.945	8.231
OC-P4-Jun27/05	0.711	0.428	0.555	-0.768	0.737	0.887	13.182
OC-P6-Jul3/05	0.505	0.018	0.500	-0.782	0.643	0.740	13.684
OC-P8-Jul6/05	0.527	0.055	0.580	-0.780	0.563	0.738	13.852
OC-P10-Jul11/05	0.831	0.711	0.599	-0.784	0.995	0.651	11.638
OC-P12-Jul14/05	0.649	-0.014	0.182	-0.791	0.569	0.777	12.393
OC-P14-Jul19/05	0.634	0.309	0.661	-0.800	0.697	0.379	12.381
OC-EF-Jul22/05	0.329	-0.305	1.101	-0.797	0.836	0.397	14.597
IN Feb10/05	1.089	1.174	-6.985	-0.791	-1.881	-7.859	
FeOC-P2-Feb3/05	0.393	-0.163	1.110	-0.864	1.189	0.646	
FeOC-P4-Feb8/05	0.179	-0.527	0.072	-0.926	0.443	0.973	
FeOC-P6-Feb11/05	0.714	0.442	0.094	-0.885	0.861	-6.946	
FeOC-P8-Feb15/05	0.995	1.185	-1.552	-1.109	-0.895	-7.820	
FeOC-P10-Feb18/05	-0.638	-2.028	-1.911	-1.099	-1.165	1.001	
FeOC-P12-Feb23/05	-0.162	-0.946	-0.872	-1.195	-0.419	-4.581	
FeOC-P14-Feb27/05	0.521	0.527	-0.018	-1.249	0.070	-5.543	
FeOC-EF-Mar4/05	0.977	1.671	1.566	-1.360	1.029	-5.087	
IN-Jun21/05	-1.070	1.174	-6.985	-0.791	-1.881	-7.859	
FeOC-P2-Jun22/05	-0.081	-1.031	0.875	-1.031	0.777	-1.430	
FeOC-P4-Jun27/05	1.162	1.685	-2.315	-1.164	-1.632	-10.791	
FeOC-P7-Jul4/05	0.002	-0.713	-1.341	-1.194	-2.548	-6.114	
FeOC-P8-Jul6/05	0.715	0.693	-2.701	-1.291	-1.839	-4.923	
FeOC-P10-Jul11/05	0.891	1.053	-2.119	-1.289	-1.710	-7.325	
FeOC-P12-Jul14/05	0.834	0.962	-2.746	-1.362	-1.723	-9.019	
FeOC-P14-Jul18/05	0.711	0.715	-2.472	-1.305	-1.840	-7.940	
FeOC-EF-Jul22/05	1.013	1.332	-0.056	-1.392	-1.603	-3.813	
OC-P2-Nov23/04	0.333	-0.124	-0.499	-1.281	0.621	2.123	

OC-P2-Dec7/04	0.430	-0.103	1.478	-0.841	0.502	-0.157
OC-P2-Jan3/05	0.209	-0.617	0.573	-0.889	0.554	1.239
OC-P2-Feb3/05	0.373	-0.251	0.246	-0.801	0.195	2.362
OC-P2-Mar10/05	0.241	-0.431	-3.986	-0.842	-2.573	4.001
OC-P2-Apr1/05	0.326	-0.261	3.712	-0.856	-2.469	3.644
OC-P2-May4/05	0.332	-0.334	-4.190	-0.830	-2.541	4.004
OC-P2-Jun8/05	1.059	1.162	-3.268	-0.852	-1.855	2.088
OC-P2-Jul28/05	0.575	0.160	-4.068	-0.779	-2.380	3.696
OC-P2-Aug10/05	0.658	0.329	-4.147	-0.796	-2.247	2.914
OC-P2-Nov3/05	0.677	0.351	-4.069	-0.774	-2.299	3.491
OC-EF-Nov12/04	0.182	0.083	0.287	-1.506	0.998	1.900
OC-EF-Dec6/04	0.013	-0.363	1.133	-1.626	1.300	0.493
OC-EF-Jan10/05	-0.001	-0.402	1.166	-1.112	0.937	0.403
OC-EF-Feb1/05	-0.120	-0.855	1.190	-0.948	0.715	0.337
OC-EF-Mar4/05	-0.199	-1.127	1.226	-0.939	0.482	0.208
OC-EF-Apr5/05	-0.112	-1.169	1.069	-0.940	0.406	0.277
OC-EF-May18/05	0.254	-0.449	-0.531	-0.833	0.333	1.497
OC-EF-Jun6/05	0.012	-0.961	0.124	-0.881	0.726	1.505
OC-EF-Jul22/05	0.329	-0.305	1.104	-0.797	0.836	0.391
OC-EF-Aug9/05	-0.125	-1.261	-0.226	-0.803	0.344	1.838
OC-EF-Sep13/05	0.217	-0.557	0.130	-0.834	0.709	1.358
OC-EF-Nov02/05	0.639	0.293	0.696	-0.813	1.071	0.906
FeOC-P2-Nov17/04	0.623	0.972	1.093	-1.521	2.683	2.551
FeOC-P2-Dec17/04	0.747	1.061	0.708	-1.063	1.446	-3.758
FeOC-P2-Jan5/05	0.307	-0.534	1.279	-0.903	1.547	-2.780
FeOC-P2-Feb3/05	0.393	-0.163	1.110	-0.864	1.189	0.646
FeOC-P2-Mar10/05	-0.023	-0.907	0.504	-0.908	0.481	-2.962
FeOC-P2-Apr1/05	0.108	-0.652	-0.019	-0.940	-0.119	0.656
FeOC-P2-May4/05	-0.207	-1.283	-3.555	-0.961	-2.899	2.921
FeOC-P2-Jun8/05	-0.309	-1.398	-1.108	-1.137	-0.587	0.166
FeOC-P2-Jul28/05	-0.462	-1.638	-3.144	-1.050	-3.033	0.671
FeOC-P2-Aug10/05	0.011	-0.701	-6.995	-1.033	-2.585	-13.470
FeOC-P2-Nov3/05	-0.542	-1.784	-3.524	-1.103	-3.132	-0.967
FeOC EF-Nov12/04	1.972	4.061	-0.406	-2.467	1.327	0.076
FeOC-EF-Dec6/04	1.077	2.250	1.106	-2.197	1.143	-0.807
FeOC-EF-Jan10/05	0.422	0.992	1.491	-1.417	1.079	-4.561
FeOC-EF-Feb1/05	0.176	0.252	1.348	-1.283	0.724	0.057
FeOC-EF-Mar4/05	0.976	1.671	1.566	-1.360	1.029	-5.087
FeOC-EF-Apr5/05	1.050	1.565	0.487	-1.994	0.091	-1.191
FeOC-EF-May18/05	0.730	0.725	-0.745	-1.430	-1.729	0.294
FeOC-EF-Jun6/05	1.035	1.354	-0.257	-1.511	-1.461	-1.570
FeOC-EF-Jul22/05	1.013	1.332	-0.056	-1.392	-1.603	-3.813
FeOC-EF-Aug9/05	0.671	0.637	-0.483	-1.285	-1.865	-1.405
FeOC-EF-Sep13/05	0.905	1.111	-0.464	-1.202	-1.731	-1.752
FeOC-EF-Nov02/05	0.882	1.106	-0.606	-1.341	-1.678	-1.196

FeOC column flow data

					PV=556.0 ml		Empty Jar=161.8 g	
Column	Date	Duration	Sample Volume	Total Volume Through	Cumulative Volume	Flow Rate	Flow Rate	Cumulative Pore Vol
		day	ml	ml	ml	ml/day	PV	
FeOC	03-Nov-04	0	0	0.0	0.0			
FeOC	12-Nov-04	9	65	248.4	248.4	1.2	28.3	0.4
FeOC	16-Nov-04	13	0	498.5	746.9	5.0	120.0	1.3
FeOC	17-Nov-04	14	65	65.7	812.5	3.2	76.3	1.5
FeOC	19-Nov-04	16	20	99.5	912.1	2.0	48.2	1.6
FeOC	22-Nov-04	19	0	169.7	1081.8	2.4	56.6	1.9
FeOC	24-Nov-04	21	80	126.4	1208.2	2.6	63.2	2.2
FeOC	27-Nov-04	24	65	288.3	1496.5	4.1	97.9	2.7
FeOC	29-Nov-04	26	65	65.0	1561.5	1.4	32.5	2.8
FeOC	30-Nov-04	27	50	50.0	1611.5	2.1	50.0	2.9
FeOC	01-Dec-04	28	60	60.0	1671.5	2.5	60.0	3.0
FeOC	06-Dec-04	33	60	346.9	2018.4	2.9	69.4	3.6
FeOC	08-Dec-04	35	85	85.0	2103.4	1.8	42.5	3.8
FeOC	10-Dec-04	37	90	162.9	2266.3	3.4	81.4	4.1
FeOC	15-Dec-04	42	0	236.4	2502.6	2.0	47.3	4.5
FeOC	17-Dec-04	44	105	105.0	2607.6	2.1	51.4	4.7
FeOC	20-Dec-04	47	80	295.6	2903.3	4.1	98.5	5.2
FeOC	22-Dec-04	49	120	120.0	3023.3	2.5	60.0	5.4
FeOC	24-Dec-04	51	0	92.0	3115.2	1.8	42.0	5.6
FeOC	26-Dec-04	53	0	75.5	3190.7	1.7	41.6	5.7
FeOC	28-Dec-04	55	0	137.7	3328.4	2.9	68.9	6.0
FeOC	31-Dec-04	58	85	85.0	3413.4	1.2	28.3	6.1
FeOC	03-Jan-05	61	120	120.0	3533.4	1.7	40.0	6.4
FeOC	05-Jan-05	63	120	120.0	3653.4	2.5	60.0	6.6
FeOC	07-Jan-05	65	0	329.0	3982.4	6.9	164.5	7.2
FeOC	10-Jan-05	68	85	312.4	4294.8	4.3	104.1	7.7
FeOC	12-Jan-05	70	120	120.0	4414.8	2.5	60.0	7.9
FeOC	14-Jan-05	72	0	55.6	4470.4	1.2	27.8	8.0
FeOC	18-Jan-05	76	85	361.0	4831.4	3.8	90.2	8.7
FeOC	20-Jan-05	78	85	85.0	4916.4	1.8	42.5	8.8
FeOC	24-Jan-05	82	115	115.0	5031.4	1.2	28.8	9.0
FeOC	26-Jan-05	83	85	85.0	5116.4	2.3	55.9	9.2
FeOC	27-Jan-05	84	0	232.5	5348.9	9.7	232.5	9.6
FeOC	28-Jan-05	85	115	115.0	5463.9	4.8	115.0	9.8
FeOC	31-Jan-05	88	0	172.3	5636.2	2.4	57.4	10.1
FeOC	01-Feb-05	89	85	85.0	5721.2	3.5	85.0	10.3
FeOC	03-Feb-05	91	102	102.0	5823.2	2.1	51.0	10.5
FeOC	04-Feb-05	92	0	67.0	5890.2	2.8	67.0	10.6
FeOC	07-Feb-05	95	0	142.0	6032.2	2.0	47.3	10.8
FeOC	08-Feb-05	96	103	103.0	6135.2	4.3	103.0	11.0

FeOC	10-Feb-05	98	90	90.0	6225.2	1.9	45.0	11.2
FeOC	11-Feb-05	99	90	90.0	6315.2	3.8	90.0	11.4
FeOC	14-Feb-05	102	0	183.1	6498.2	2.5	61.0	11.7
FeOC	15-Feb-05	103	102	102.0	6600.2	4.3	102.0	11.9
FeOC	18-Feb-05	106	100	100.0	6700.2	1.4	33.3	12.1
FeOC	22-Feb-05	110	0	276.3	6976.5	2.9	69.1	12.5
FeOC	23-Feb-05	111	100	100.0	7076.5	4.2	100.0	12.7
FeOC	25-Feb-05	113	0	134.6	7211.1	2.8	67.3	13.0
FeOC	27-Feb-05	115	110	110.0	7321.1	2.3	55.0	13.2
FeOC	04-Mar-05	120	90	190.0	7511.1	1.6	38.0	13.5
FeOC	09-Mar-05	125	0	184.0	7695.1	1.5	36.8	13.8
FeOC	10-Mar-05	126	110	110.0	7805.1	4.6	110.0	14.0
FeOC	14-Mar-05	130	90	290.0	8095.1	3.0	72.5	14.6
FeOC	16-Mar-05	132	0	256.8	8351.9	5.3	128.4	15.0
FeOC	18-Mar-05	134	130	130.0	8481.9	2.7	65.0	15.3
FeOC	22-Mar-05	138	90	343.4	8825.3	3.6	85.9	15.9
FeOC	23-Mar-05	139	130	130.0	8955.3	5.4	130.0	16.1
FeOC	30-Mar-05	146	90	92.6	9047.9	0.6	13.2	16.3
FeOC	01-Apr-05	148	90	92.0	9139.9	1.9	46.0	16.4
FeOC	04-Apr-05	151	0	70.0	9209.9	1.0	23.3	16.6
FeOC	05-Apr-05	152	90	141.8	9351.7	5.9	141.8	16.8
FeOC	06-Apr-05	153	110	110.0	9461.7	4.6	110.0	17.0
FeOC	08-Apr-05	155	0	95.0	9556.7	2.0	47.5	17.2
FeOC	11-Apr-05	158	90	274.2	9830.9	3.8	91.4	17.7
FeOC	12-Apr-05	159	110	110.0	9940.9	4.6	110.0	17.9
FeOC	14-Apr-05	161	0	36.5	9977.3	0.8	18.2	17.9
FeOC	15-Apr-05	162	0	101.7	10079.0	4.2	101.7	18.1
FeOC	18-Apr-05	165	90	289.7	10368.7	4.0	96.6	18.6
FeOC	19-Apr-05	166	90	90.0	10458.7	3.8	90.0	18.8
FeOC	21-Apr-05	168	0	12.2	10470.9	0.3	6.1	18.8
FeOC	03-May-05	180	0	414.5	10885.4	1.4	34.5	19.6
FeOC	04-May-05	181	100	100.0	10985.4	4.2	100.0	19.8
FeOC	05-May-05	182	0	68.3	11053.7	2.8	68.3	19.9
FeOC	09-May-05	186	0	295.3	11349.0	3.1	73.8	20.4
FeOC	11-May-05	188	0	160.8	11509.8	3.3	80.4	20.7
FeOC	13-May-05	190	0	143.1	11652.8	3.0	71.5	21.0
FeOC	18-May-05	195	90	435.0	12087.8	3.6	87.0	21.7
FeOC	20-May-05	197	100	100.0	12187.8	2.1	50.0	21.9
FeOC	24-May-05	201	90	319.7	12507.6	3.3	79.9	22.5
FeOC	26-May-05	203	120	120.0	12627.6	2.5	60.0	22.7
FeOC	30-May-05	207	0	187.2	12814.8	2.0	46.8	23.0
FeOC	06-Jun-05	214	90	318.4	13133.2	1.9	45.5	23.6
FeOC	08-Jun-05	216	110	110.0	13243.2	2.3	55.0	23.8
FeOC	13-Jun-05	221	0	237.4	13480.6	2.0	47.5	24.2
FeOC	14-Jun-05	222	0	62.7	13543.3	2.6	62.7	24.4
FeOC	15-Jun-05	223	0	79.1	13622.3	3.3	79.1	24.5

FeOC	16-Jun-05	224	0	68.8	13691.1	2.9	68.8	24.6
FeOC	17-Jun-05	225	0	90.3	13781.4	3.8	90.3	24.8
FeOC	21-Jun-05	229	90	90.0	13871.4	0.9	22.5	24.9
FeOC	22-Jun-05	230	95	95.0	13966.4	4.0	95.0	25.1
FeOC	24-Jun-05	232	0	325.5	14291.9	6.8	162.8	25.7
FeOC	27-Jun-05	235	110	110.0	14401.9	1.5	36.7	25.9
FeOC	28-Jun-05	236	0	120.4	14522.3	5.0	120.4	26.1
FeOC	29-Jun-05	237	0	96.3	14618.7	4.0	96.3	26.3
FeOC	05-Jul-05	243	200	224.0	14842.7	1.6	37.3	26.7
FeOC	06-Jul-05	244	110	110.0	14952.7	4.6	110.0	26.9
FeOC	07-Jul-05	245	0	36.1	14988.7	1.5	36.1	27.0
FeOC	08-Jul-05	246	0	63.3	15052.1	2.6	63.3	27.1
FeOC	11-Jul-05	249	110	110.0	15162.1	1.5	36.7	27.3
FeOC	12-Jul-05	250	0	93.0	15255.1	3.9	93.0	27.4
FeOC	14-Jul-05	252	120	120.0	15375.1	2.5	60.0	27.7
FeOC	15-Jul-05	253	0	50.9	15426.0	2.1	50.9	27.7
FeOC	17-Jul-05	255	0	139.7	15565.7	2.9	69.8	28.0
FeOC	19-Jul-05	257	110	110.0	15675.7	2.3	55.0	28.2
FeOC	20-Jul-05	258	0	131.9	15807.6	5.5	131.9	28.4
FeOC	21-Jul-05	259	0	68.4	15875.9	2.8	68.4	28.6
FeOC	22-Jul-05	260	90	165.1	16041.1	6.9	165.1	28.8
FeOC	26-Jul-05	264	0	198.6	16239.7	2.1	49.7	29.2
FeOC	28-Jul-05	266	100	137.6	16377.3	2.9	68.8	29.5
FeOC	04-Aug-05	273	0	504.5	16881.8	3.0	72.1	30.4
FeOC	05-Aug-05	274	0	84.3	16966.1	3.5	84.3	30.5
FeOC	08-Aug-05	277	0	217.3	17183.4	3.0	72.4	30.9
FeOC	09-Aug-05	278	90	159.3	17342.7	6.6	159.3	31.2
FeOC	10-Aug-05	279	90	90.0	17432.7	3.8	90.0	31.4
FeOC	11-Aug-05	280	0	26.6	17459.2	1.1	26.6	31.4
FeOC	15-Aug-05	284	0	212.9	17672.2	2.2	53.2	31.8
FeOC	16-Aug-05	285	90	169.2	17841.3	7.0	169.2	32.1
FeOC	18-Aug-05	287	90	90.0	17931.3	1.9	45.0	32.2
FeOC	24-Aug-05	293	0	342.0	18273.3	2.4	57.0	32.9
FeOC	01-Sep-05	301	0	577.3	18850.6	3.0	72.2	33.9
FeOC	09-Sep-05	309	0	551.3	19401.9	2.9	68.9	34.9
FeOC	13-Sep-05	313	90	374.6	19776.5	3.9	93.7	35.6
FeOC	21-Sep-05	321	0	47.0	19823.5	0.2	5.9	35.7
FeOC	26-Sep-05	326	0	354.0	20177.5	3.0	70.8	36.3
FeOC	30-Sep-05	330	0	263.4	20440.9	2.7	65.9	36.8
FeOC	05-Oct-05	335	0	314.1	20755.0	2.6	62.8	37.3
FeOC	20-Oct-05	350	0	486.5	21241.5	1.4	32.4	38.2
FeOC	27-Oct-05	357	0	271.1	21512.6	1.6	38.7	38.7
FeOC	02-Nov-05	363	90	535.9	22048.5	3.7	89.3	39.7
FeOC	03-Nov-05	364	90	90.0	22138.5	3.8	90.0	39.8
FeOC	17-Nov-05	378	0	752.2	22890.7	2.2	53.7	41.2
FeOC	25-Nov-05	386	130	801.2	23691.9	4.2	100.2	42.6

FeOC	28-Nov-05	389	108	228.4	23920.3	3.2	76.1	43.0
FeOC	29-Nov-05	390	120	120.0	24040.3	5.0	120.0	43.2
FeOC	06-Dec-05	397	200	540.4	24580.7	3.2	77.2	44.2
FeOC	13-Dec-05	404	200	353.5	24934.2	2.1	50.5	44.8
FeOC	15-Dec-05	406	200	277.5	25211.7	5.8	138.8	45.3
FeOC	21-Dec-05	412	200	424.1	25635.8	2.9	70.7	46.1
FeOC	30-Dec-05	421	0	699.5	26335.3	3.2	77.7	47.4
FeOC	11-Jan-06	433	200	624.1	26959.4	2.2	52.0	48.5
FeOC	18-Jan-06	440	200	492.9	27452.3	2.9	70.4	49.4
FeOC	25-Jan-06	447	0	303.8	27756.0	1.8	43.4	49.9
FeOC	02-Feb-06	455	0	697.2	28453.2	3.6	87.2	51.2
FeOC	14-Feb-06	467	0	898.2	29351.4	3.1	74.9	52.8
FeOC	02-Mar-06	483	0	1240.3	30591.7	3.2	77.5	55.0
FeOC	17-Mar-06	498	0	1150.9	31742.6	3.2	76.7	57.1
FeOC	22-Mar-06	503	0	399.6	32142.2	3.3	79.9	57.8
FeOC	03-Apr-06	515	0	933.3	33075.5	3.2	77.8	59.5
FeOC	12-Apr-06	524	0	675.7	33751.2	3.1	75.1	60.7
FeOC	26-Apr-06	538	0	1102.4	34853.6	3.3	78.7	62.7
FeOC	02-May-06	544	0	455.0	35308.6	3.2	75.8	63.5
FeOC	05-May-06	547	0	233.9	35542.5	3.2	78.0	63.9
FeOC	08-May-06	550	100	345.4	35887.9	4.8	115.1	64.5
FeOC	10-May-06	552	90	90.0	35977.9	1.9	45.0	64.7
FeOC	19-May-06	561	50	425.8	36403.7	2.0	47.3	65.5
FeOC	23-May-06	565	0	325.3	36729.0	3.4	81.3	66.1
FeOC	05-Jun-06	578	0	991.7	37720.7	3.2	76.3	67.8
FeOC	17-Jul-06	620	0	835.6	38556.3	0.8	19.9	69.3
FeOC	28-Jul-06	631	0	228.6	38784.9	0.9	20.8	69.8
FeOC	31-Jul-06	634	0	233.6	39018.5	3.2	77.9	70.2

Appendix III

Column Flow Data

OC column flow data

PV = 567.8 ml Empty Jar=160.1 g

Column	Date / Time	Duration	Sample Volume	Total Mass Through	Cumulative Mass	Flow Rate	Cumulative Pore Vol
		days	ml	ml	ml	ml/day	PV
OC	03-Nov-04	0	0	0.0	0.0		
OC	05-Nov-04	2	0	109.4	109.4	54.3	0.2
OC	12-Nov-04	9	70	323.7	433.1	47.9	0.8
OC	16-Nov-04	13	0	134.4	567.5	32.4	1.0
OC	17-Nov-04	14	10	35.0	602.5	40.7	1.1
OC	19-Nov-04	16	20	133.1	735.6	64.5	1.3
OC	22-Nov-04	19	0	162.5	898.1	54.2	1.6
OC	24-Nov-04	21	80	161.0	1059.0	80.5	1.9
OC	27-Nov-04	24	70	324.9	1383.9	110.3	2.4
OC	29-Nov-04	26	45	45.0	1428.9	22.5	2.5
OC	30-Nov-04	27	25	25.0	1453.9	25.0	2.6
OC	01-Dec-04	28	60	60.0	1513.9	60.0	2.7
OC	06-Dec-04	33	60	445.7	1959.6	89.1	3.5
OC	07-Dec-04	34	100	100.0	2059.6	100.0	3.6
OC	08-Dec-04	35	45	45.0	2104.6	45.0	3.7
OC	09-Dec-04	36	65	65.0	2169.6	65.0	3.8
OC	10-Dec-04	37	65	65.0	2234.6	65.0	3.9
OC	13-Dec-04	40	95	95.0	2329.6	31.7	4.1
OC	15-Dec-04	42	0	183.6	2513.2	91.8	4.4
OC	17-Dec-04	44	125	155.0	2668.2	75.9	4.7
OC	20-Dec-04	47	80	293.8	2961.9	97.9	5.2
OC	22-Dec-04	49	130	130.0	3091.9	65.0	5.4
OC	24-Dec-04	51	130	131.7	3223.7	60.2	5.7
OC	26-Dec-04	53	0	4.9	3228.5	2.7	5.7
OC	28-Dec-04	55	0	135.7	3364.3	67.9	5.9
OC	31-Dec-04	58	85	85.0	3449.3	28.3	6.1
OC	03-Jan-05	61	120	120.0	3569.3	40.0	6.3
OC	05-Jan-05	63	120	120.0	3689.3	60.0	6.5
OC	07-Jan-05	65	0	351.8	4041.0	175.9	7.1
OC	10-Jan-05	68	85	309.0	4350.0	103.0	7.7
OC	12-Jan-05	70	110	110.0	4460.0	55.0	7.9
OC	14-Jan-05	72	0	77.6	4537.6	38.8	8.0
OC	18-Jan-05	76	85	359.6	4897.3	89.9	8.6
OC	20-Jan-05	78	85	85.0	4982.3	42.5	8.8
OC	24-Jan-05	82	115	115.0	5097.3	28.8	9.0
OC	26-Jan-05	84	110	110.0	5207.3	55.0	9.2
OC	27-Jan-05	85	0	21.1	5228.4	21.1	9.2
OC	31-Jan-05	89	0	231.1	5459.5	57.8	9.6
OC	01-Feb-05	90	85	85.0	5544.5	85.0	9.8
OC	03-Feb-05	91	102	102.0	5646.5	68.0	9.9
OC	04-Feb-05	92	0	80.8	5727.3	80.8	10.1
OC	07-Feb-05	95	0	169.4	5896.7	56.5	10.4
OC	08-Feb-05	96	103	103.0	5999.7	103.0	10.6
OC	10-Feb-05	98	90	90.0	6089.7	45.0	10.7
OC	11-Feb-05	99	90	90.0	6179.7	90.0	10.9

OC	14-Feb-05	102	0	198.2	6377.9	66.1	11.2
OC	15-Feb-05	103	102	102.0	6479.9	102.0	11.4
OC	18-Feb-05	106	100	100.0	6579.9	33.3	11.6
OC	22-Feb-05	110	0	306.4	6886.3	76.6	12.1
OC	23-Feb-05	111	100	100.0	6986.3	100.0	12.3
OC	25-Feb-05	113	0	129.4	7115.7	64.7	12.5
OC	28-Feb-05	116	190	190.0	7305.7	63.3	12.9
OC	04-Mar-05	120	90	190.0	7495.7	47.5	13.2
OC	09-Mar-05	125	0	163.6	7659.3	32.7	13.5
OC	10-Mar-05	126	105	105.0	7764.3	105.0	13.7
OC	14-Mar-05	130	90	390.0	8154.3	97.5	14.4
OC	16-Mar-05	132	0	178.9	8333.1	89.4	14.7
OC	18-Mar-05	134	95	95.0	8428.1	47.5	14.8
OC	22-Mar-05	138	90	98.8	8526.9	24.7	15.0
OC	25-Mar-05	141	115	115.0	8641.9	38.3	15.2
OC	29-Mar-05	145	0	213.8	8855.7	53.5	15.6
OC	30-Mar-05	146	90	158.3	9014.0	158.3	15.9
OC	01-Apr-05	148	90	90.0	9104.0	45.0	16.0
OC	04-Apr-05	151	0	138.5	9242.5	46.2	16.3
OC	05-Apr-05	152	90	90.0	9332.5	90.0	16.4
OC	06-Apr-05	153	110	110.0	9442.5	110.0	16.6
OC	07-Apr-05	154	0	55.1	9497.6	55.1	16.7
OC	08-Apr-05	155	0	116.9	9614.5	116.9	16.9
OC	11-Apr-05	158	90	288.1	9902.5	96.0	17.4
OC	12-Apr-05	159	110	110.0	10012.5	110.0	17.6
OC	14-Apr-05	161	0	48.1	10060.6	24.0	17.7
OC	15-Apr-05	162	0	107.5	10168.1	107.5	17.9
OC	18-Apr-05	165	90	289.6	10457.6	96.5	18.4
OC	19-Apr-05	166	90	90.0	10547.6	90.0	18.6
OC	21-Apr-05	168	0	23.7	10571.3	11.9	18.6
OC	03-May-05	180	0	426.0	10997.3	35.5	19.4
OC	04-May-05	181	90	90.0	11087.3	90.0	19.5
OC	05-May-05	182	0	62.7	11150.0	62.7	19.6
OC	09-May-05	186	0	281.0	11431.0	70.3	20.1
OC	11-May-05	188	0	153.4	11584.4	76.7	20.4
OC	13-May-05	190	0	136.0	11720.4	68.0	20.6
OC	18-May-05	195	90	417.2	12137.6	83.4	21.4
OC	20-May-05	197	100	100.0	12237.5	50.0	21.6
OC	24-May-05	201	90	276.2	12513.7	69.1	22.0
OC	26-May-05	203	105	105.0	12618.7	52.5	22.2
OC	30-May-05	207	0	165.0	12783.7	41.2	22.5
OC	06-Jun-05	214	90	521.6	13305.3	74.5	23.4
OC	08-Jun-05	216	110	110.0	13415.3	55.0	23.6
OC	13-Jun-05	221	0	236.8	13652.1	47.4	24.0
OC	14-Jun-05	222	0	69.6	13721.7	69.6	24.2
OC	15-Jun-05	223	0	100.6	13822.3	100.6	24.3
OC	16-Jun-05	224	0	68.7	13891.0	68.7	24.5
OC	17-Jun-05	225	0	100.7	13991.7	100.7	24.6
OC	21-Jun-05	229	90	393.6	14385.3	98.4	25.3
OC	22-Jun-05	230	95	95.0	14480.3	95.0	25.5
OC	24-Jun-05	232	0	80.6	14560.9	40.3	25.6
OC	27-Jun-05	235	120	120.0	14680.9	40.0	25.9

OC	28-Jun-05	236	0	170.6	14851.5	170.6	26.2
OC	29-Jun-05	237	0	112.4	14963.9	112.4	26.4
OC	05-Jul-05	243	150	351.2	15315.0	58.5	27.0
OC	06-Jul-05	244	110	110.0	15425.0	110.0	27.2
OC	07-Jul-05	245	0	48.5	15473.5	48.5	27.3
OC	08-Jul-05	246	0	69.4	15542.9	69.4	27.4
OC	11-Jul-05	249	110	110.0	15652.9	36.7	27.6
OC	12-Jul-05	250	0	122.9	15775.8	122.9	27.8
OC	14-Jul-05	252	120	120.0	15895.8	60.0	28.0
OC	15-Jul-05	253	0	53.4	15949.2	53.4	28.1
OC	17-Jul-05	255	0	156.6	16105.8	78.3	28.4
OC	18-Jul-05	256	90	90.0	16195.8	90.0	28.5
OC	20-Jul-05	258	0	103.8	16299.6	51.9	28.7
OC	21-Jul-05	259	0	74.5	16374.2	74.5	28.8
OC	22-Jul-05	260	90	166.3	16540.5	166.3	29.1
OC	26-Jul-05	264	0	232.6	16773.0	58.1	29.5
OC	28-Jul-05	266	100	145.3	16918.3	72.7	29.8
OC	04-Aug-05	273	0	555.8	17474.1	79.4	30.8
OC	05-Aug-05	274	0	92.3	17566.4	92.3	30.9
OC	08-Aug-05	277	0	240.6	17807.0	80.2	31.4
OC	09-Aug-05	278	90	162.4	17969.4	162.4	31.6
OC	10-Aug-05	279	110	110.0	18079.4	110.0	31.8
OC	11-Aug-05	280	0	35.5	18115.0	35.5	31.9
OC	15-Aug-05	284	0	237.0	18351.9	59.2	32.3
OC	16-Aug-05	285	90	177.9	18529.8	177.9	32.6
OC	18-Aug-05	287	110	110.0	18639.8	55.0	32.8
OC	19-Aug-05	288	0	29.9	18669.6	29.9	32.9
OC	22-Aug-05	291	0	168.6	18838.3	56.2	33.2
OC	24-Aug-05	293	0	170.3	19008.6	85.2	33.5
OC	01-Sep-05	301	0	643.4	19652.0	80.4	34.6
OC	09-Sep-05	309	0	615.9	20267.9	77.0	35.7
OC	13-Sep-05	313	90	412.3	20680.2	103.1	36.4
OC	26-Sep-05	326	0	394.4	21074.6	30.3	37.1
OC	30-Sep-05	330	0	291.5	21366.1	72.9	37.6
OC	05-Oct-05	335	0	358.3	21724.4	71.7	38.3
OC	20-Oct-05	350	0	497.9	22222.3	33.2	39.1
OC	26-Oct-05	356	0	179.0	22401.3	29.8	39.5
OC	31-Oct-05	361	0	414.4	22815.7	82.9	40.2
OC	02-Nov-05	363	90	243.7	23059.4	121.9	40.6
OC	03-Nov-05	364	90	90.0	23149.4	90.0	40.8
OC	07-Nov-05	368	0	213.7	23363.1	53.4	41.1
OC	09-Nov-05	370	0	166.8	23529.9	83.4	41.4
OC	18-Nov-05	379	0	677.5	24207.4	75.3	42.6
OC	25-Nov-05	386	130	503.5	24710.9	71.9	43.5
OC	28-Nov-05	389	108	247.3	24958.2	82.4	44.0
OC	29-Nov-05	390	120	120.0	25078.2	120.0	44.2
OC	01-Dec-05	392	200	200.0	25278.2	100.0	44.5
OC	06-Dec-05	397	200	423.9	25702.1	84.8	45.3
OC	12-Dec-05	403	200	423.9	26126.0	70.6	46.0
OC	14-Dec-05	405	0	196.7	26322.7	98.4	46.4
OC	15-Dec-05	406	200	397.7	26720.4	397.7	47.1
OC	21-Dec-05	412	200	397.7	27118.2	66.3	47.8

OC	23-Dec-05	414	0	288.3	27406.4	144.1	48.3
OC	30-Dec-05	421	0	588.6	27995.0	84.1	49.3
OC	10-Jan-06	432	0	386.1	28381.1	35.1	50.0
OC	11-Jan-06	433	200	200.0	28581.1	200.0	50.3
OC	18-Jan-06	440	200	200.0	28781.1	28.6	50.7
OC	20-Jan-06	442	0	281.8	29062.9	140.9	51.2
OC	24-Jan-06	446	0	305.0	29367.9	76.2	51.7
OC	02-Feb-06	455	0	694.8	30062.7	77.2	52.9
OC	14-Feb-06	467	0	896.6	30959.3	74.7	54.5
OC	19-Feb-06	472	0	209.4	31168.7	41.9	54.9
OC	02-Mar-06	483	0	1069.9	32238.6	97.3	56.8
OC	17-Mar-06	498	0	1148.8	33387.4	76.6	58.8
OC	22-Mar-06	503	0	404.3	33791.7	80.9	59.5
OC	03-Apr-06	515	0	937.3	34729.0	78.1	61.2
OC	12-Apr-06	524	0	679.7	35408.7	75.5	62.4
OC	26-Apr-06	538	0	1109.4	36518.1	79.2	64.3
OC	02-May-06	544	0	461.0	36979.1	76.8	65.1
OC	05-May-06	547	0	237.0	37216.1	79.0	65.5
OC	08-May-06	550	100	350.2	37566.3	116.7	66.2
OC	10-May-06	552	90	90.0	37656.3	45.0	66.3
OC	19-May-06	561	120	590.5	38246.8	65.6	67.4
OC	05-Jun-06	578	0	989.3	39236.1	58.2	69.1
OC	17-Jul-06	620	0	954.6	40190.7	22.7	70.8
OC	28-Jul-06	631	0	238.2	40428.8	21.7	71.2
OC	31-Jul-06	634	0	237.1	40665.9	79.0	71.6

Appendix IV

Electron Microprobe Analysis (EMPA) Data

Major Ions EMPA Data

Sample	Si wt%	Al wt%	Na wt%	K wt%
As-1	31.42	5.73	5.48	3.04
As-1	31.56	5.87	5.66	3.20
As-1	31.55	5.66	5.80	3.03
As-1	31.54	5.77	5.22	3.16
As-1	31.54	5.79	5.54	3.04
As-2	29.44	5.66	6.36	2.72
As-2	29.59	5.67	6.89	2.75
As-2	29.39	5.63	6.82	2.72
As-3	28.65	10.37	5.70	5.19
As-3	28.22	10.57	5.80	5.31
As-3	28.14	10.62	5.89	5.23
As-4	34.13	6.36	3.24	3.31
As-4	33.64	6.27	3.04	3.34
As-4	34.35	6.46	3.05	3.31
As-4	34.16	6.49	3.27	3.32
As-5	32.58	6.05	4.60	3.00
As-5	32.81	6.10	4.76	3.19
As-5	32.75	6.11	4.43	3.18
As-6	31.64	6.09	5.02	3.02
As-6	31.29	5.75	4.69	2.86
As-6	31.44	5.94	5.10	3.07
As-6	31.56	6.03	4.77	3.06
As-7	32.15	6.22	5.59	3.02
As-7	31.77	6.04	5.72	2.95
As-7	32.03	6.08	5.79	3.03
As-8	33.74	5.91	4.10	3.63
As-8	33.67	5.92	4.18	3.62
As-8	34.01	5.84	4.32	3.57
As-9	34.16	6.39	3.82	3.33
As-9	33.62	6.43	3.71	3.43
As-9	34.49	6.18	3.90	3.61
As-9	34.14	6.29	4.00	3.46
As-10	30.97	5.85	4.91	2.98
As-10	31.30	5.98	4.77	3.04
As-10	31.14	5.87	4.99	2.88
As-11	28.55	8.1	5.85	4.38

As-11	28.5	8.05	5.64	4.37
As-11	28.68	8.23	5.66	4.31
As-11	28.69	8.09	5.59	4.49
As-11	28.8	8.11	5.50	4.34
As-12	33.85	7.23	2.95	2.75
As-12	33.57	7.07	3.19	2.85
As-12	33.86	7.14	2.80	2.81
As-12	33.79	7.11	3.03	2.83
As-13	34.50	4.88	3.98	3.85
As-13	33.75	4.81	4.71	3.93
As-13	33.57	4.83	4.08	3.89
As-13	33.52	5.07	4.51	3.96
As-14	32.27	7.2	4.07	3.82
As-14	32.11	7.41	3.98	3.92
As-14	32.37	7.17	3.49	3.84
As-14	31.94	7.29	3.88	3.78
As-14	32.08	7.66	3.65	3.80

Major Ions EMPA Data

Sample	Si wt%	Al wt%	Na wt%	K wt%
Sb-1	33.67	6.67	3.09	4.20
Sb-1	34.09	6.68	3.24	3.95
Sb-1	34.04	6.71	3.22	3.72
Sb-2	33.57	6.30	3.33	3.53
Sb-2	33.50	6.39	3.01	3.55
Sb-2	33.51	6.25	3.08	3.43
Sb-2	33.28	6.41	3.40	3.26
Sb-2	33.41	6.36	3.21	3.38
Sb-3	29.92	8.63	4.10	5.12
Sb-3	29.94	8.63	3.85	4.94
Sb-3	29.95	8.72	4.19	4.98
Sb-3	29.82	8.74	4.10	4.85
Sb-4	33.60	5.65	3.26	3.90
Sb-4	33.80	5.68	3.79	3.91
Sb-4	33.32	5.79	3.82	3.88
Sb-4	33.68	5.74	3.48	3.90
Sb-4	33.57	5.74	3.34	3.79
Sb-4	33.54	5.70	3.57	3.96
Sb-5	33.76	6.40	3.50	3.49
Sb-5	33.30	6.32	3.23	3.60
Sb-5	33.65	6.14	3.24	3.48
Sb-5	33.66	6.32	3.32	3.56
Sb-5	33.42	6.37	3.14	3.53
Sb-6	27.80	10.13	5.13	5.55
Sb-6	27.56	10.31	5.46	5.59
Sb-6	27.78	10.21	5.21	5.46
Sb-6	27.74	10.20	5.20	5.40
Sb-6	27.55	10.11	5.20	5.58
Sb-6	27.75	10.10	5.39	5.55
Sb-8	33.29	6.63	2.42	3.25
Sb-8	33.53	6.86	3.12	3.15
Sb-8	33.21	6.67	2.61	3.20
Sb-8	33.49	6.98	2.54	3.21
Sb-8	33.11	6.81	2.75	3.19
Sb-8	33.40	7.04	2.68	3.46
Sb-8	33.38	6.84	2.63	3.39
Sb-8	33.73	6.84	2.41	3.32
Sb-8	33.30	6.94	2.52	3.39
Sb-9	25.78	11.53	5.70	6.33

Sb-9	25.88	11.57	5.68	6.42
Sb-9	25.76	11.58	5.29	6.24
Sb-10	33.05	4.75	3.73	4.20
Sb-10	33.19	4.77	3.57	4.42
Sb-10	33.12	4.76	3.73	4.24
Sb-10	33.33	4.77	3.75	4.19
Sb-10	32.88	4.58	3.61	4.22
Sb-11	33.12	4.84	3.53	4.26
Sb-11	33.34	4.82	4.12	4.35
Sb-11	33.20	4.83	3.87	4.39
Sb-11	33.42	4.70	3.41	4.42
Sb-11	33.18	4.77	3.88	4.24
Sb-11	33.23	4.79	3.79	4.36
Sb-12	33.32	6.39	3.32	3.80
Sb-12	33.40	6.36	3.10	3.75
Sb-12	33.16	6.34	3.57	3.72
Sb-12	33.22	6.34	2.92	3.81
Sb-12	33.34	6.32	3.29	3.76
Sb-12	33.24	6.30	3.12	3.78

As EMPA Data

Label	Si wt%	Al wt%	Na wt%	K wt%	As wt%	Au wt%	O wt%	Total wt%
As-1	29.24	6.09	2.92	3.94	3.59	0.00	42.47	88.25
As-1	29.47	6.13	2.68	4.19	3.71	0.00	42.79	88.97
As-1	29.15	6.08	5.37	4.09	3.59	0.00	43.24	91.52
As-1	35.52	6.14	1.31	3.23	3.33	0.00	48.82	98.35
As-1	33.36	5.24	0.55	2.54	3.39	0.03	45.19	90.31
As-1	34.53	6.14	1.34	3.37	3.32	0.00	47.73	96.43
As-1	33.42	6.16	1.22	3.29	3.32	0.00	46.43	93.85
As-1	36.05	6.61	0.35	1.93	3.40	0.00	49.28	97.63
As-1	35.18	6.16	1.34	3.36	3.38	0.01	48.52	97.96
As-1	34.35	6.12	1.94	3.93	3.68	0.00	48.02	98.05
As-2	29.34	6.28	2.44	3.71	5.20	0.00	43.39	90.34
As-2	28.47	6.23	2.85	3.95	5.09	0.00	42.50	89.09
As-2	28.37	6.23	2.74	3.99	5.10	0.01	42.35	88.79
As-2	28.13	6.23	2.98	3.97	5.15	0.00	42.19	88.65
As-2	34.24	6.32	2.96	4.01	5.22	0.00	49.27	102.03
As-3	31.27	10.25	2.07	5.49	0.34	0.00	46.77	96.19
As-3	30.45	10.75	2.12	5.55	0.49	0.04	46.39	95.78
As-3	30.97	10.63	2.27	5.59	0.35	0.00	46.86	96.66
As-3	31.29	10.49	2.13	5.46	0.39	0.02	47.04	96.81
As-3	31.11	10.37	1.89	5.41	0.50	0.06	46.70	96.04
As-3	30.53	10.90	2.21	5.52	0.42	0.02	46.60	96.19
As-4	35.52	6.48	1.05	3.36	0.03	0.00	47.30	93.75
As-4	35.07	6.44	0.92	3.29	0.02	0.01	46.69	92.45
As-4	35.26	6.34	0.98	3.33	0.03	0.00	46.86	92.80
As-4	35.25	6.56	1.15	3.38	0.04	0.03	47.11	93.52
As-4	35.30	6.49	1.06	3.36	0.04	0.00	47.06	93.29
As-5	35.61	6.68	0.74	2.01	1.76	0.10	48.13	95.04
As-5	35.99	6.73	0.69	1.98	1.78	0.06	48.58	95.81
As-5	35.86	6.72	0.70	2.00	1.87	0.03	48.48	95.65
As-5	35.47	6.72	0.68	1.95	1.91	0.00	48.05	94.78
As-5	36.20	6.74	0.69	1.95	2.02	0.03	48.95	96.57
As-5	35.88	6.79	0.73	1.98	1.86	0.00	48.57	95.80
As-5	35.56	7.09	1.98	2.72	1.93	0.12	49.10	98.49
As-5	33.45	7.00	2.20	3.08	1.87	0.06	46.73	94.40
As-5	35.44	6.70	0.67	1.98	1.78	0.04	47.93	94.53
As-5	36.38	6.74	0.69	1.97	1.96	0.03	49.14	96.91
As-5	34.69	6.61	0.82	2.44	1.75	0.00	47.12	93.43
As-5	34.36	6.58	0.77	2.39	2.13	0.00	46.89	93.12
As-5	34.68	6.63	0.83	2.43	1.90	0.05	47.21	93.72
As-5	34.67	6.63	0.81	2.46	1.73	0.00	47.11	93.41
As-5	34.91	6.60	0.81	2.48	1.67	0.03	47.32	93.81
As-6	36.84	7.08	1.32	2.21	1.66	0.03	50.07	99.21
As-6	37.65	7.13	1.72	2.52	1.71	0.00	51.26	101.98
As-6	36.76	7.09	1.63	2.44	2.03	0.01	50.34	100.31
As-6	37.27	7.00	2.04	2.71	1.98	0.02	51.01	102.03
As-6	37.08	7.10	1.36	2.21	1.64	0.01	50.36	99.75
As-6	36.08	7.09	1.59	2.37	1.67	0.00	49.34	98.14

As-6	37.32	7.15	1.43	2.25	1.86	0.02	50.83	100.85
As-6	37.19	7.05	1.29	2.19	1.68	0.07	50.43	99.90
As-6	36.55	7.15	1.64	2.32	1.67	0.14	49.94	99.41
As-6	36.42	7.07	1.38	2.26	1.65	0.00	49.61	98.40
As-7	36.07	7.05	1.80	2.62	1.83	0.00	49.51	98.88
As-7	36.79	7.11	1.59	2.39	1.82	0.00	50.26	99.96
As-7	37.16	7.08	1.39	2.26	1.73	0.00	50.50	100.11
As-7	36.57	7.12	1.72	2.41	1.78	0.02	50.04	99.65
As-7	35.18	7.12	2.04	2.65	1.80	0.00	48.63	97.43
As-7	36.18	7.17	1.73	2.45	1.79	0.00	49.66	98.97
As-7	36.02	7.14	1.75	2.49	1.77	0.00	49.45	98.61
As-7	35.80	7.13	3.39	3.06	1.83	0.00	49.91	101.13
As-7	37.02	7.14	1.47	2.30	1.83	0.01	50.49	100.26
As-7	36.42	7.10	1.73	2.50	1.91	0.00	49.94	99.60
As-8	35.86	6.04	0.74	2.53	0.44	0.00	47.24	92.85
As-8	35.99	6.14	0.74	2.62	0.43	0.03	47.48	93.42
As-8	36.15	6.30	0.76	2.61	0.38	0.00	47.80	94.00
As-8	36.25	6.25	0.81	2.62	0.38	0.00	47.88	94.20
As-8	36.33	6.39	0.81	2.70	0.36	0.04	48.10	94.73
As-9	36.35	6.37	0.74	2.47	0.27	0.00	47.98	94.18
As-9	36.49	6.14	0.67	2.33	0.27	0.00	47.90	93.80
As-9	36.17	6.34	0.71	2.38	0.31	0.00	47.76	93.68
As-9	36.41	6.39	0.71	2.44	0.31	0.00	48.08	94.35
As-9	36.46	6.34	0.70	2.39	0.40	0.00	48.12	94.41
As-10	34.94	6.90	1.34	2.51	2.45	0.01	48.24	96.39
As-10	35.40	6.89	1.28	2.49	2.42	0.00	48.71	97.19
As-10	34.76	6.93	1.34	2.54	2.47	0.01	48.08	96.13
As-10	35.07	6.96	1.28	2.45	2.13	0.00	48.23	96.12
As-10	34.86	6.85	1.24	2.44	1.95	0.00	47.79	95.14
As-11	32.18	8.84	1.30	3.71	2.62	0.00	47.13	95.77
As-11	32.36	8.93	1.40	3.80	2.51	0.05	47.42	96.46
As-11	32.17	8.93	1.37	3.75	2.76	0.04	47.32	96.34
As-11	32.56	8.93	1.42	3.91	2.10	0.00	47.46	96.38
As-11	32.47	8.92	1.44	3.85	2.12	0.02	47.34	96.16
As-12	35.63	7.52	0.44	2.37	0.34	0.00	48.10	94.40
As-12	35.36	7.34	0.38	2.31	0.32	0.00	47.58	93.28
As-12	35.36	7.43	0.42	2.42	0.25	0.00	47.67	93.56
As-12	35.57	7.42	0.35	2.22	0.29	0.02	47.85	93.72
As-12	34.92	7.29	0.38	2.32	0.29	0.05	47.03	92.28
As-13	37.80	5.28	0.93	3.24	0.42	0.00	48.98	96.66
As-13	37.82	5.36	1.02	3.19	0.41	0.00	49.09	96.90
As-13	36.66	5.22	0.90	3.18	0.35	0.03	47.56	93.89
As-13	37.37	5.21	0.86	3.26	0.30	0.00	48.33	95.33
As-13	37.82	5.25	0.84	3.27	0.28	0.03	48.87	96.37
As-13	38.04	5.28	0.87	3.26	0.42	0.08	49.23	97.18
As-13	38.21	5.28	0.91	3.31	0.38	0.00	49.43	97.53
As-13	37.44	5.24	0.99	3.32	0.35	0.00	48.52	95.86
As-14	34.90	7.43	1.26	3.81	0.21	0.01	47.71	95.34
As-14	35.04	7.39	1.26	3.70	0.22	0.00	47.80	95.41
As-14	35.00	7.60	1.25	3.78	0.22	0.02	47.96	95.82
As-14	34.61	7.88	1.30	3.93	0.36	0.01	47.89	95.99
As-14	34.78	7.79	1.21	3.83	0.36	0.01	47.94	95.91

Sb EMPA Data

Label	Si wt%	Al wt%	Na wt%	K wt%	Sb wt%	Au wt%	O wt%	Total wt%
Sb-1	35.1400	6.7600	1.4452	4.0400	0.4466	0.0000	47.5300	95.3600
Sb-1	34.9200	6.7500	1.6604	4.0900	0.4937	0.0025	47.3600	95.2700
Sb-1	35.5700	6.8400	1.6978	4.1200	0.4547	0.0000	48.2000	96.8900
Sb-1	35.2900	6.7600	1.7341	3.9800	0.4843	0.0422	47.8000	96.0900
Sb-1	35.4700	6.8000	1.7377	3.7200	0.4568	0.0034	47.9800	96.1800
Sb-1	34.9400	6.6900	1.7469	4.1400	0.4713	0.0000	47.3700	95.3600
Sb-2	35.9700	6.8600	0.4637	2.5290	0.6456	0.0342	47.9700	94.4800
Sb-2	35.8400	6.8400	0.4169	2.4974	0.5403	0.0532	47.7600	93.9600
Sb-2	36.0500	6.8700	0.4496	2.5214	0.6343	0.0000	48.0600	94.5900
Sb-2	35.3800	6.8300	0.4398	2.3866	0.8365	0.0228	47.3000	93.1900
Sb-2	36.1100	6.7700	0.4575	2.4711	0.5222	0.0000	47.9900	94.3200
Sb-2	36.0700	6.7000	0.4255	2.5226	0.6328	0.0010	47.9300	94.2900
Sb-2	35.8600	6.8500	0.3933	2.4232	0.9021	0.0637	47.8800	94.3700
Sb-3	32.7000	9.4600	1.0545	4.5600	0.7496	0.0141	47.2100	95.7500
Sb-3	32.5700	9.4400	0.9903	4.5000	0.7591	0.0193	47.0100	95.2800
Sb-3	32.6900	9.4200	0.9371	4.5600	0.7535	0.0113	47.1300	95.5000
Sb-3	32.5500	9.4300	0.8533	4.4100	1.1159	0.0146	47.0300	95.4000
Sb-3	32.5400	9.3700	0.9623	4.4800	0.9146	0.0174	46.9500	95.2300
Sb-3	32.5700	9.3800	0.8934	4.4000	0.9476	0.0071	46.9700	95.1600
Sb-4	36.0300	6.1900	0.7201	3.3700	0.8313	0.0000	47.7700	94.9100
Sb-4	35.8700	6.1400	0.6998	3.3600	0.9328	0.0047	47.5700	94.5800
Sb-4	35.7400	6.0800	0.7026	3.3800	0.7930	0.0246	47.3200	94.0400
Sb-4	36.0800	6.2100	0.7058	3.3800	0.8024	0.0000	47.8300	95.0000
Sb-4	35.9500	6.2200	0.7263	3.4100	0.7744	0.0000	47.7000	94.7800
Sb-4	36.0600	6.1800	0.6982	3.2700	0.9441	0.0000	47.8100	94.9600
Sb-5	35.3100	6.6300	0.4798	2.6443	0.5765	0.0126	47.0300	92.6800
Sb-5	35.3900	6.7600	0.5653	2.6879	0.4640	0.0168	47.2300	93.1200
Sb-5	35.6300	6.7400	0.5656	2.6339	0.4571	0.0103	47.4700	93.5100
Sb-5	35.8700	6.7600	0.5200	2.6044	0.6461	0.0225	47.8000	94.2200
Sb-5	35.7600	6.8100	0.5704	2.6896	0.6535	0.0442	47.7700	94.3000
Sb-6	5.3502	5.5808	26.8128	10.3144	0.0213	0.7288	42.8778	91.6861
Sb-6	5.2718	5.6662	26.3703	10.3316	0.0000	0.7502	42.3766	90.7667
Sb-6	4.9259	5.5679	26.7802	10.2529	0.0000	0.8373	42.6503	91.0145
Sb-6	4.9291	5.6933	26.7281	10.3049	0.0446	0.9858	42.7075	91.3932
Sb-6	5.2521	5.7277	26.6959	10.3799	0.0000	0.7736	42.8008	91.6301
Sb-8	2.6911	3.3180	31.7505	7.0016	0.0000	0.6237	44.1412	89.5262
Sb-8	2.6821	3.2974	31.8454	6.8657	0.0008	0.7131	44.1389	89.5434
Sb-8	2.8389	3.2822	32.8542	6.9402	0.0000	0.6506	45.3936	91.9598
Sb-8	2.6889	3.3104	32.1104	6.8518	0.0000	0.8301	44.4564	90.2480

Sb-8	2.6678	3.2135	32.7105	6.8848	0.0000	0.6236	45.1016	91.2018
Sb-9	5.6448	6.3609	24.5362	11.6514	0.0090	0.8368	41.7527	90.7918
Sb-9	5.6485	6.5273	24.8136	11.7627	0.0000	0.8149	42.1959	91.7629
Sb-9	6.0055	6.5233	24.9957	11.4913	0.0000	0.8368	42.2897	92.1424
Sb-9	5.8812	6.4638	24.7045	11.6905	0.0057	0.8124	42.0767	91.6348
Sb-9	4.4726	6.5749	24.4036	11.5726	0.0000	0.8200	41.1612	89.0048
Sb-10	35.83	5.23	0.7386	3.1200	1.0436	0.062	46.71	92.72
Sb-10	35.92	5.21	0.7792	3.2000	1.0575	0.0047	46.83	93.00
Sb-10	36.03	5.22	0.739	2.9586	1.0409	0	46.89	92.88
Sb-10	35.56	5.29	0.6966	3.1000	1.0156	0	46.43	92.08
Sb-10	35.36	5.25	0.7171	3.1400	1.0252	0.0103	46.18	91.67
Sb-10	34.6100	5.2500	0.6693	3.2700	0.9617	0.0368	45.3200	90.12
Sb-10	35.2100	5.3900	0.7364	3.2400	1.0354	0.0259	46.1700	91.81
Sb-11	35.36	5.25	0.7124	3.2000	1.0502	0.0483	46.2	91.82
Sb-11	35.29	5.24	0.7328	3.1800	1.0375	0.0092	46.11	91.60
Sb-11	35.42	5.21	0.6931	3.1500	1.0700	0	46.22	91.77
Sb-11	35.31	5.35	0.7314	3.0300	1.0809	0.0376	46.22	91.76
Sb-11	35.04	5.27	0.7052	3.0000	1.0773	0.0227	45.83	90.96
Sb-11	34.4600	5.2900	0.6661	3.2400	1.0293	0.0113	45.1900	89.88
Sb-11	34.7000	5.2700	0.6799	3.2400	1.0034	0.0179	45.4500	90.36
Sb-12	1.4049	3.9085	36.3839	6.4720	0.0058	0.8048	48.6600	97.6399
Sb-12	1.6698	3.6849	36.4313	6.3843	0.0000	1.0560	48.7301	97.9564
Sb-12	1.6084	3.8753	36.1183	6.4319	0.0100	1.0042	48.4265	97.4745
Sb-12	1.5667	3.6360	37.0820	6.3294	0.0000	0.8781	49.3417	98.8338
Sb-12	1.9082	3.8334	36.9869	6.5034	0.0524	0.6626	49.5217	99.4687